High Strain Rate Characterization of Mechanical Properties by Low Temperature Testing for Polymeric Materials

M.B. Olde Dubbelink

September 2024

Mechanical Engineering

Department Production Technology (MS^3)

UNIVERSITY OF TWENTE.

Summary

The offshore wind energy sector is growing rapidly due to global climate concerns, driving the need for larger wind turbines to increase energy output and reduce costs. However, this growth introduces challenges, particularly the issue of rain erosion on turbine blades/ Current solutions, such as polymeric coatings, face challenges in weight and manufacturability for larger blades. A more sustainable approach involves using thermoplastic protective layers, specifically Leading Edge Protection (LEP) systems designed to reduce energy loss and maintenance needs. Despite the promise of LEP systems, limited research exists on rain erosion for these materials. Predicting the lifetime of wind turbine coatings remains challenging due to the need for expensive and lengthy testing methods. Therefore, developing a robust characterization method for LEP materials is essential, which was carried out in this research. Using Time-Temperature Superposition (TTS), based on the temperature and strain rate dependence of a polymer, in combination with tensile testing and Dynamical Mechanical Testing (DMA), a test framework that improves the modelling capabilities of wind turbine coatings at high strain rates with a focus on rain erosion was developed. The study showed that DMA testing is only relevant for materials in which the glass transition temperature (Tg) is close to the testing temperature range, while tensile testing can be used to characterize materials at high strain rates for all materials tested. Mimicking rain erosion using fatigue testing at specific strain rates and temperatures was found to be a promising way of predicting the lifetime of a material, albeit that some limitations need to be overcome. Furthermore, investigation of the break surface of a sample after fatigue failure shows cracks in the load direction. There seems to be a relation between the number of these cracks and the number of cycles until failure, which is a promising perspective to further predict rain erosion in the field with the use of mechanical testing.

Contents

1 Introduction **7**
- 1.1 Problem Introduction . . . 7
  - 1.1.1 Societal impact . . . 7
  - 1.1.2 Scientific Problem . . . 7
- 1.2 General Introduction to Polymers . . . 9
  - 1.2.1 Glass-Rubber Transition and Elastic Behaviour . . . 10
  - 1.2.2 Thermal history . . . 11

2 Mechanical Properties **13**
- 2.1 Stress-Strain Relation . . . 13
- 2.2 Yield Point . . . 14
  - 2.2.1 Determination of Yield Point . . . 14
  - 2.2.2 Yield behaviour . . . 16
- 2.3 Strain Rate and Temperature . . . 19
  - 2.3.1 Ree-Eyring . . . 20

3 Rheological Properties **23**
- 3.1 Viscoelasticity . . . 24
- 3.2 Time-Temperature Superposition . . . 26
- 3.3 Testing Methods DMA . . . 28

4 Fatigue **31**

5 Literature Overview **33**
- 5.1 Research Questions . . . 34

6 Experimental Setup **37**
- 6.1 Materials . . . 37
  - 6.1.1 PC . . . 38
  - 6.1.2 PVC . . . 38
  - 6.1.3 TPE . . . 39
- 6.2 Test setup . . . 40

7 Results & Discussion **43**
- 7.1 PC & PVC . . . 43
  - 7.1.1 DMA testing . . . 43
  - 7.1.2 Tensile testing . . . 44
  - 7.1.3 Discussion . . . 45
- 7.2 TPE . . . 46
  - 7.2.1 DMA testing . . . 46
  - 7.2.2 Tensile testing . . . 47
  - 7.2.3 Fatigue testing . . . 47
  - 7.2.4 SEM microscopy . . . 50
  - 7.2.5 Discussion . . . 51

8 Conclusions & Recommendations **57**
8.1 Conclusions 57
8.2 Test Framework 58
8.3 Recommendations 60

9 Bibliography **61**

10 Appendix **69**
10.1 SEM results 69

CHAPTER 1

Introduction

1.1 Problem Introduction

In order to establish the importance of this study, it will be discussed what the societal impact of the problem is. Furthermore, the scientific challenges connected to this problem will be discussed.

1.1.1 Societal impact

The offshore wind turbine energy sector has been witnessing remarkable growth, driven by global climate agreements addressing global climate concerns. This increasing demand for renewable energy necessitates the development of larger wind turbines, which in turn would lead to increased annual energy output and a corresponding reduction in the levelized cost of energy [1]. The development of these larger wind turbines has led to turbines approaching 200 meters in diameter, accompanied by blade tip speeds exceeding 100 ms^{-1}. When rain droplets hit these blades at such velocities, the consequence is a significant issue related to rain erosion damage caused by airborne rain droplets [2, 3]. The underlying cause of this problem is the degradation of aerodynamic efficiency, which in turn results in reduced annual energy production [4, 5]. The consequences of rain erosion damage on the blades have led to a significant increase in maintenance costs, contributing to a rise in the levelized cost of energy [6]. Currently, wind turbine blade coating relies primarily on polymeric material systems to mitigate rain erosion, often using thermosetting gel coats or elastomeric shells, but problems arise concerning weight and manufacturability when applied to blades of such considerable lengths [7]. A more sustainable alternative would be the use of a thermoplastic protective layer. More specifically, leading edge protection (LEP) systems have been developed, comprising erosion-resistant materials designed to minimize annual energy production loss and reduce maintenance requirements [8, 9].

1.1.2 Scientific Problem

Despite the potential benefits of these systems, literature reveals a limited number of studies focused on rain erosion for these materials [10, 11, 12]. The combination of high tip speeds and airborne particles with wind turbine blades necessitates the characterization of LEP systems at high strain rates in a feasible manner, in order to mimic the effects of rain erosion. The main challenge in accurately predicting the lifetime of wind turbine coatings lies in the need for costly and lengthy testing methods [13]. Although the Springer model [14] is widely used for predicting lifetime beyond the experimentally tested conditions, it lacks the capability to predict lifetimes under varying conditions, such as different strain rates or materials. To summarize the scientific challenge for characterizing materials with respect to their fatigue properties, it should be noted that either physical testing can be carried out, which is costly and lengthy, or modelling of the material behaviour can be performed, but important material parameters can not be accounted for.
To advance the development of materials for LEP systems, it is essential to establish a well-defined characterization method of their (visco-)elastic material properties. While moderate and low-speed testing has been extensively performed using tensile testers [15, 16, 17], high strain rate characterization remains a gap in the current understanding of these materials. To address this, a comprehensive investigation of high strain rates will be conducted using low-temperature testing so that the need for expensive and difficult testing methods is diminished. This will involve extensive mechanical testing of polymeric materials at multiple strain rates

and temperatures, followed by the application of time-temperature superposition to predict material properties beyond experimentally obtained data. This mechanical testing will use various approaches, including Dynamic Mechanical Analysis (DMA) to conduct frequency sweeps and temperature sweeps, which will be analyzed using time-temperature superposition and glass transition temperature determination. Additionally, tensile testing will be combined with the Ree-Eyring equation to describe and relate the applied strain rate and temperature to the plastic flow rate of a material [18]. The resulting data will be used to perform fatigue testing, hopefully enabling the prediction of the LEP system lifetime with respect to rain erosion impact. Ultimately, this research aims to establish a testing framework using low-temperature testing, which will facilitate the improvement of the modelling capabilities of current wind turbine coating technologies at high strain rates.

1.2 General Introduction to Polymers

To be able to carry out a proper study on polymeric materials, it should be understood what exactly a polymer is, and what are indispensable basic properties and characteristics of said polymers, with respect to this study. First and foremost, it is important to establish the main part of a polymer: the backbone structure. This backbone, or main structure, is realized by combining many monomers into a chain to result in a so-called chain structure by means of covalent bonding. Depending on the type of monomer, sidegroups may be present attached to the backbone, which causes the polymer to be branched. Regardless of the branching present, these chains can be characterized as macromolecular, as they can become enormous in length. When looking at these chain structures, the chains can be looked at as an individual chain system where there are linear chains. The conformation of these chains can be seen as random, much like a spaghetti string in a bowl of pasta. When many of these chains are put together, they become strongly entwined. This is how a polymer network arises. This causes the individual chains to create interactions between them, which are governed by relatively weak secondary bonds. This is one of the load-carrying abilities that a polymer produces, albeit a weak one.

A second, crucial, characteristic of a polymer that contributes to its strength and stiffness is entanglements. If the chain has sufficient length, a physical interaction between chains can be made. As stated, the polymer chains are strongly entwined. The ability of polymer chains to move, so-called chain segmental mobility, causes chains to entangle. In other words, one chain gets 'trapped' in another chain. This greatly improves the strength of the polymer network.

A third way of improving the strength of a polymer is by creating primary chemical bonds between chains. This can be done by a process called curing, where a bridge of material between chains is created using a chemical reaction. These bridges are so-called crosslinks. This leads to the formation of one, big network. A schematic overview of these interactions can be found in Figure 1.1.

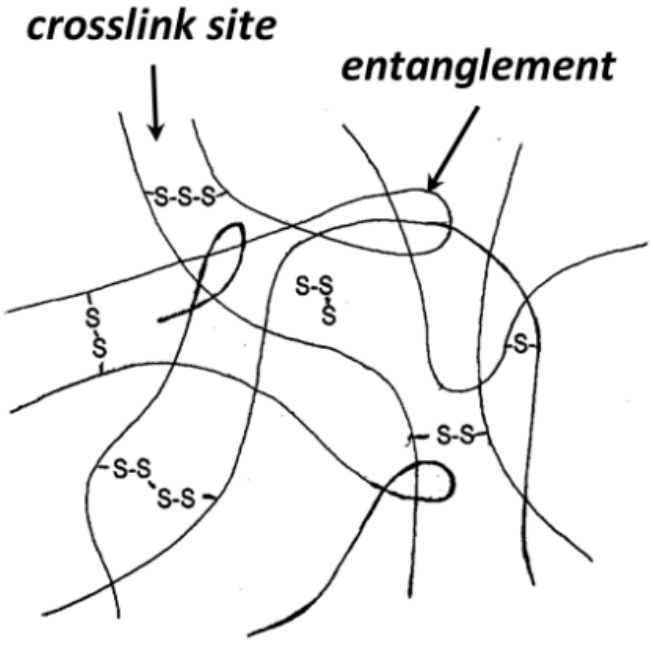

Figure 1.1: Representation of crosslinks and entanglements in polymeric materials.

After establishing the core properties of polymers, polymeric materials can be divided into three main categories:

- Thermoplastics: chain networks that have the ability to flow at elevated temperatures, and will go back to the solid state upon cooling. This is due to the fact that no chemical bonds are present. Furthermore, elevated temperature allows the chains to 'escape' the entanglements, creating the possibility to flow. When the material is cooled down, the mobility of the chains decreases up to the point that the material is solid, and a new configuration of chains is created. A drawback is that the thermoplastic material has limited use in environments with elevated temperatures due to their melting ability.

- Thermosets: a network is created at higher temperatures using a curing reaction, creating many crosslinks between chains. This high crosslink density causes the creation of one big network, that prevents the

material from flowing at elevated temperatures. Instead of flowing, the material will decompose at high temperatures. Furthermore, thermosets are very stiff and hard due to this network.

- Elastomers: a softened form of a thermoplastic with some crosslinks present. As the density of the crosslinks is far below that of thermosets, it has a combination of characteristics with respect to thermoplastics and thermosets. It will not flow upon heating the material, but it can absorb high deformations reversibly. Unfortunately, it has a relatively low modulus.

This study focuses on thermoplastic and elastomeric material and therefore, the remainder of this paper will leave out the consideration of thermosets.

When looking at thermoplastics - as elastomers are thermoplastics in a way - two categories can be distinguished within the thermoplastic polymer family. The first category is the amorphous polymer, in which the chains are orientated randomly, as shown in Figure 1.1. This configuration is 'frozen in' with this disordered arrangement, without any significant molecular motion. For many polymers, it is possible however to organize their molecules in a regular structure from the amorphous state. Within the more organized structures of the molecules, crystals can be found and hence, the crystalline structure. As there are still amorphous regions in between the organized structures, it is not possible to create a fully crystalline polymer. This can be seen in Figure 1.2. This is the reason why the term semi-crystalline polymers is used, which is the second category for thermoplastics.

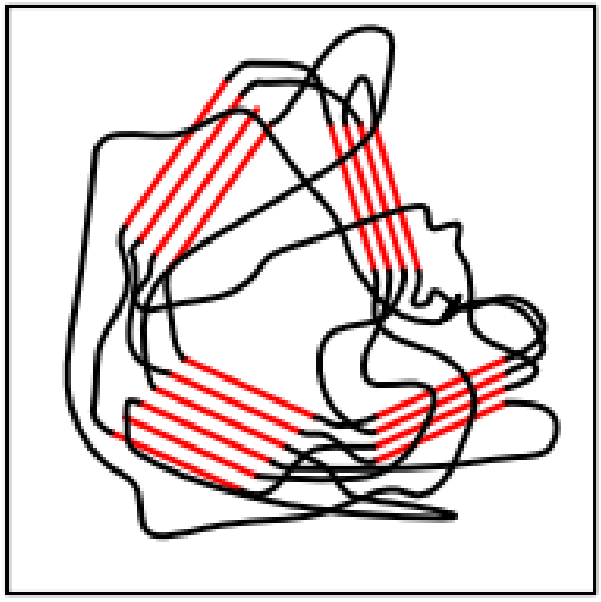

Figure 1.2: Schematic representation of a semi-crystalline polymer. Red represents a crystalline structure, black represents an amorphous structure [19].

1.2.1 Glass-Rubber Transition and Elastic Behaviour

The elastic response to heating varies significantly between amorphous and semi-crystalline materials. When the temperature exceeds the melting point T_m of a crystalline material, it undergoes melting. This transition is marked by a steep decrease in volume which indicates a quick transition from a crystalline material to a fluid. For amorphous materials, there is no such jump in volume, but rather a gradual increase. This gradual increase is not the instant melting of a material, but rather a transition from an amorphous state to a fluid state. This transition is referred to as the glass transition, and the temperature at which this happens is called the glass transition temperature, T_g. As stated previously, many polymers are semi-crystalline and will therefore exhibit both phenomena, resulting in having both a T_g and T_m.

The glass transition temperature is crucial in the behaviour of thermoplastic polymers. Above this T_g, the material will first soften gradually before melting. This soft state, between T_g and T_m, is referred to as the rubbery state. Temperatures below T_g are referred to as the glassy state. A good depiction of the influence of

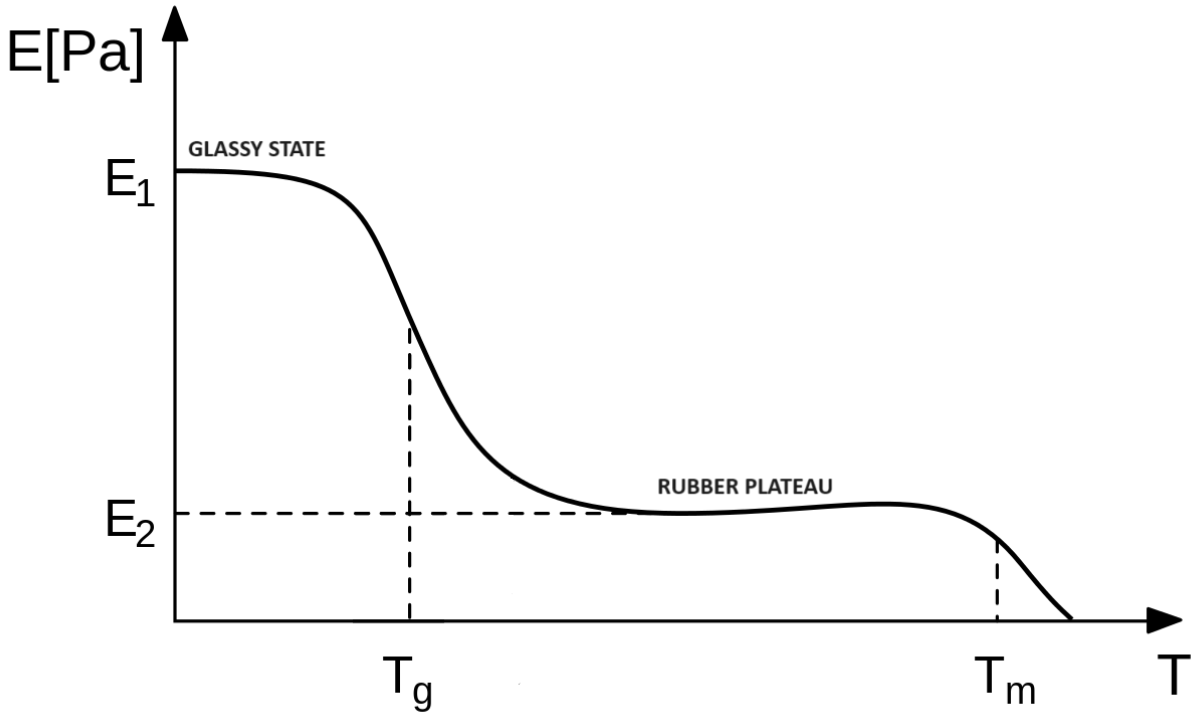

Figure 1.3: Elastic modulus as a function of temperature. Adapted from [20].

this glassy and rubbery state on the material behaviour of polymers is the elastic modulus of the material, E, as can be seen in Figure 1.3.
For temperatures below T_g, it can be seen that the E-modulus is high: this can be attributed to the fact that the mobility of the chains is nearly non-existent. This leads to the fact that the chains do not change their conformation as force is applied, they are only pulled apart from each other. As a consequence, chains can hardly move past each other, creating mechanical interlocking between the chains, and hindering displacement of the material due to the force. Furthermore, secondary interactions stay intact due to adjacent chains being connected. This leads to a high E-modulus. When the temperature rises to above T_g, a major change occurs within the polymer: full chain segmental mobility is created. The mechanical response of the polymer changes dramatically. Chains are no longer in a frozen state but can now move in the direction of the applied load. This means that there is almost no hindrance of chain movement with respect to each other, and the secondary interactions between chains are broken. This leads to a drop in E-modulus until a new plateau is found. This plateau is reached as a result of the entanglements that are present in the polymer, which prevent further displacement. This is the rubbery state as referred to above.

1.2.2 Thermal history

In the last part of the general introduction to polymers, the thermal history of polymers will be discussed. Although this might go beyond the basics of polymer materials, it is fundamental to take into account this phenomenon, and therefore it is discussed here.

Polymers are typically not in their thermodynamic equilibrium, a condition which is significantly influenced by the cooling rate during processing. As depicted in Figure 1.4, the transition from a rubbery to a glassy state is dependent on the rate of cooling. It can be seen that slower cooling rates allow the liquid lines to extend further downward, resulting in a decrease in the glass transition temperature and a corresponding lower specific volume. This phenomenon occurs because the polymer chains can dynamically adjust their conformation, facilitating the necessary shrinkage that is in accordance with the equilibrium volume line during cooling. However, as the temperature decreases, the mobility of the chains progressively decreases as well until it becomes insufficient to maintain equilibrium, causing the material to become "frozen in", unable to keep up with the required shrinkage. It can be seen that, even with infinitely low cooling rates, complete equilibrium can not be achieved. This indicates that the glass transition temperature is primarily governed by kinetics, or the "freezing-in phenomenon", rather than solely by thermodynamic transitions.

Closely related to this phenomenon is the volume retardation that is observed below T_g. After cooling down, a polymer enters a metastable state, as indicated by Point A in Figure 1.4. As the material is not in its thermodynamic equilibrium, the material will strive towards it. At a constant temperature, the volume will gradually decrease to point A'. This occurs because the repositioning of chains still occurs below T_g, albeit on a very limited scale, leading to a reduction in volume through changes in chain conformation. This reduction is referred to as volume retardation. The rate at which this happens is typically referred to as physical ageing [21]. It is a common phenomenon for materials that are stored or used below their T_g. Above T_g, the material will be in thermodynamic equilibrium and physical ageing will not occur.

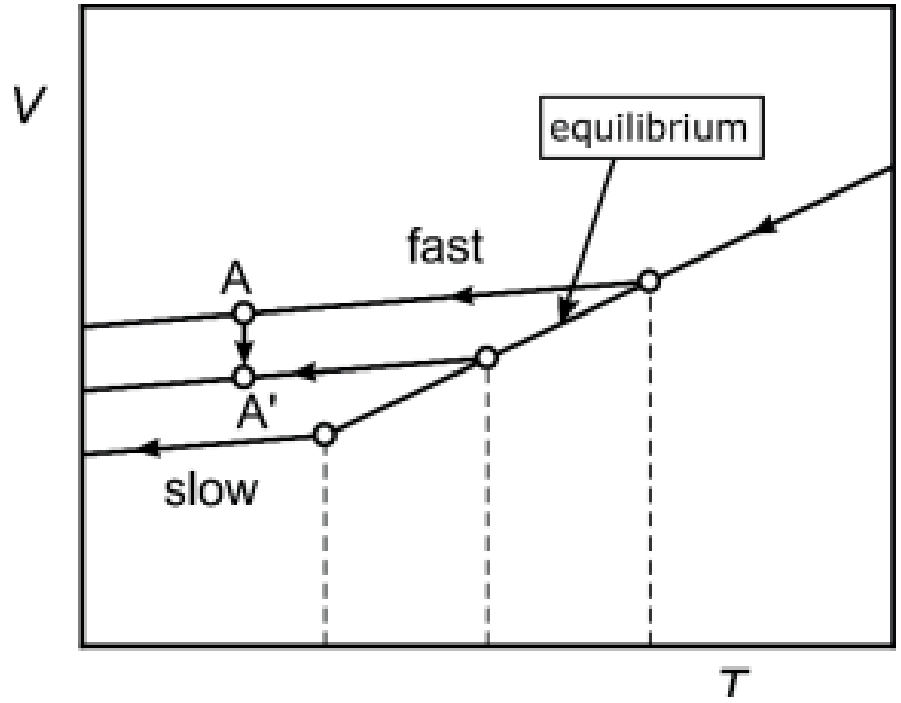

Figure 1.4: Effect of cooling on the glass transition [22]

Due to a decrease in volume, the material will undergo densification. As the polymer densifies, subsequent increases in modulus, relaxation times and yield stresses are observed [23, 24, 25, 26]. The rate at which these changes occur depends on the temperature and the applied stress, both of which accelerate physical ageing [27]. To develop a clear and consistent test setup, it is essential to ensure that the thermal history of all tested materials is similar, minimizing any effects of physical ageing that might have occurred. These effects can be minimized by heating the specimens to temperatures above T_g. As stated previously, this brings the material in its equilibrium state, eliminating any prior thermal history [28, 29].

CHAPTER 2

Mechanical Properties

With the general properties of polymers being discussed, this section will discuss the mechanical properties of polymeric materials. The focus of this study is on the elastic behaviour of polymers and therefore, relevant properties will be discussed. Firstly, the stress-strain relation of polymeric materials is discussed in general. Then, a closer look will be taken at different regions of the stress-strain curve, in combination with underlying phenomena. This approach allows for a thorough assessment of the data obtained from tensile tests, conducted in the climate chamber, and helps in identifying important modeling parameters.

2.1 Stress-Strain Relation

The evaluation of mechanical properties often involves tensile testing, wherein a material sample undergoes stretching under a constant strain rate. Essential parameters obtained from this are stress and strain, which are derived from this procedure by measuring force and subsequent displacement. The evaluation can give either true strain (ε_t) or engineering strain (ε_e), as well as true stress (σ_t) or engineering stress (σ_e). The distinction between true and engineering material characteristics lies in the consideration of changing geometries. For minor deformations, such as $\varepsilon < 0.01$, engineering strains and stresses suffice. These parameters are simplified due to assumptions of consistent cross-sectional area throughout the test. Essential to this determination is knowledge of the initial geometry of the sample, denoted by A_o and L_o:

$$\sigma_e = \frac{F}{A_o} \qquad \varepsilon_e = \frac{\Delta L}{L_o} \tag{2.1}$$

In reality, assuming a constant area in the test specimen is unreliable because the area changes when an applied load F is present. This deviation becomes particularly pronounced in polymer deformation, where larger deformations occur. This reliance on a constant area may result in notable differences between engineering strains and stresses and their actual values.

Therefore, true strains and stresses offer a more accurate description of material behaviour, including larger deformations. However, determining these parameters gives rise to the need for continuous monitoring of the length and area of the sample throughout the test. To simplify this process, an assumption of isochoric deformation is made, implying there is no volume loss. This eliminates the need for continuous monitoring of the cross-sectional area. As a result, the expressions for true stress and true strain [22], which account for these considerations, will be used in this study:

$$\sigma_t = \frac{F}{A_o}\frac{L}{L_o} \qquad \varepsilon_t = ln\frac{L}{L_o} \tag{2.2}$$

Now that a stress-strain response of a polymer can be set up, it is important to identify different phenomena occurring inside the polymers. For this, Figure 2.1 is used for reference. It shows the typical stress-strain behaviour of a polymer, including important modelling parameters.

From Figure 2.1a, the first important characteristic is the Young's modulus E, which is a measure of the stiffness

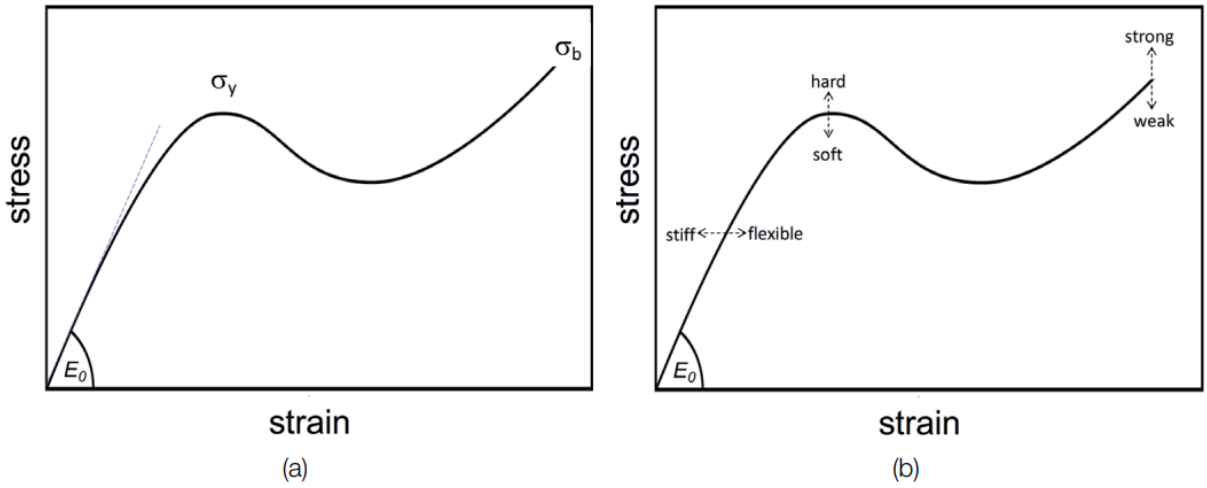

Figure 2.1: a) Schematic representation of stress-strain behaviour, b) Indicated changes in mechanical properties. From [22].

of the material. It is described by Hooke's Law as:

$$E_o = \frac{\sigma}{\varepsilon} \tag{2.3}$$

This equation above holds in the elastic region, where there is a linear increase in strain due to the applied stress. Beyond the elastic region, the slope gradually decreases until a maximum is reached. This is usually referred to as the yield stress σ_y [30]. In materials science, this yield point is used to determine whether plastic deformation occurs. Generally, stress levels below the yield stress result in reversible deformation; the material regains its original shape upon unloading the specimen. Stresses exceeding the yield point induce partly permanent deformation [31, 32]. However, this behaviour is not always true for polymers. After the yield point, stress may either increase slowly due to strain hardening or decrease as a result of strain softening. At higher stresses, the specimen ultimately undergoes actual fracture, known as the tensile strength σ_b.

The shape of the stress-strain curve in Figure 2.1b is typical for polymers. However, the trend that a part of this curve is following can be used to determine the characteristics of a specific material. First of all, the slope in the elastic region indicates whether the material is stiff (with a high E-modulus) or flexible. A material with a high yield stress is referred to as hard, while a lower yield stress indicates that the material is more soft. High tensile strength implies that the material is strong, in contrast to weak for lower material strength.

2.2 Yield Point

Now that the different regions of the stress-strain curve can be identified, and the Young's modulus can be determined, the next step is to look at the yield point. Typically, the yield stress or yield point is defined as the stress at which a material begins to deform plastically. Stresses below this stress induce completely reversible deformation, stresses above this level will cause irreversible or plastic deformation [31, 32]. Localization of deformation can be seen as the onset of necking behaviour and therefore is a measure for the yield point [33]. As these deformation mechanisms play a crucial role in material behaviour, it is important to be able to systematically determine the region where the elastic region ends and where plastic deformation starts. Therefore, Subsection 2.2.1 will discuss how the yield point can be determined, and Subsection 2.2.2 will discuss the yield deformation response upon uniaxial tension.

2.2.1 Determination of Yield Point

This study will use the Considère analysis to determine whether or not a yield point is present. It states that there is a localization of deformation if the true stress-strain response gives rise to a maximum in the engineering stress, which is stated as:

$$\frac{d\sigma_e}{d\lambda} = 0 \tag{2.4}$$

Where:

$$\lambda = \frac{L}{L_o} \tag{2.5}$$

This equation implies a maximum in the engineering stress, which states that there is a maximum in the applied force. When looking at the stress-strain behaviour of a polymeric material such as Figure 2.1, this maximum force can be attributed to the yield point as further deformation will occur under decreasing force. There are three possible outcomes to this Considère analysis [22]:

1. No tangent line: The Considère condition will not be met, resulting in homogeneous deformation of the material without any plastic strain.

2. One tangent line: In this case, the engineering stress reaches a maximum, followed by a continuous decline. Essentially, this implies that the localized zone will lack the capability to exert enough force to deform the remaining sample. Consequently, all deformation concentrates at a singular spot until failure occurs.

3. Two tangent lines: Here, a minimum can be established next to the previously mentioned maximum value of the engineering stress. This indicates a subsequent increase in the engineering stress, signifying the ability of the localization zone to plastically deform the rest of the sample.

Figure 2.2 shows an example of typical stress-strain curves corresponding with the possible outcomes for the Considère analysis.

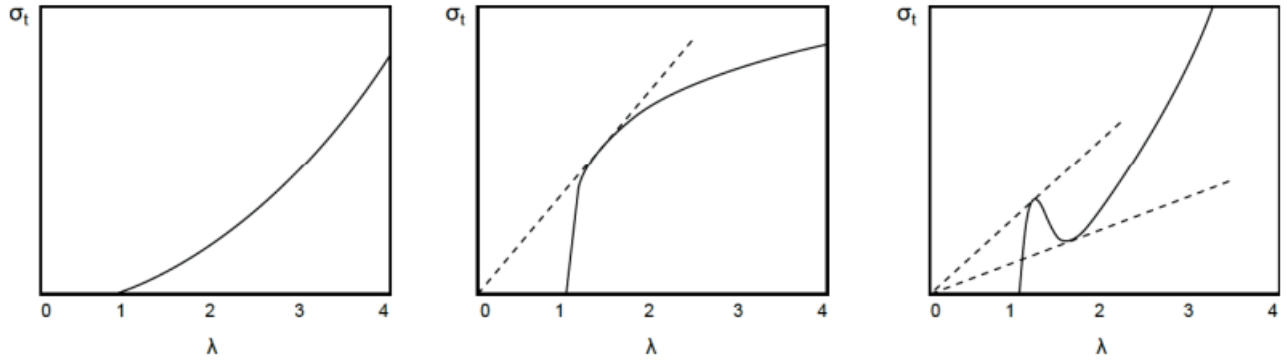

Figure 2.2: Possible outcomes for the Considère analysis. a) No tangent line; homogeneous deformation. b) One tangent line; localization up to failure. c) Two tangent lines; stable neck growth [22].

When determining whether or not a yield point is present, the outcome of the Considère analysis can be used. For the case where there is no tangent line, no yield point will occur and hence, determination thereof is obsolete. For the situation that two tangent lines can be constructed, a clear maximum value in true stress can be seen between $\lambda = 1$ and $\lambda = 2$. This directly gives the magnitude of the yield stress. For the situation where only one tangent line can be constructed, the determination of the yield stress requires a bit more work. Although the Considère analysis indicates that localization of deformation occurs, it can be seen that there is no clear yield point. Therefore, an estimation of the yield point should be used. Firstly, a line is constructed tangent to the true stress-strain curve at the inflection point. This inflection point is the point in which the slope of the stress-strain curve is the lowest. Then, a line tangent to the E-modulus at low strains is constructed. Typically, the E-modulus is determined between 0.05% and 0.25% strain and therefore, the determination of the slope of the second constructed line will be based on this range as well. The intersection point of both lines gives a good estimation of the yield stress, as shown by Figure 2.3.

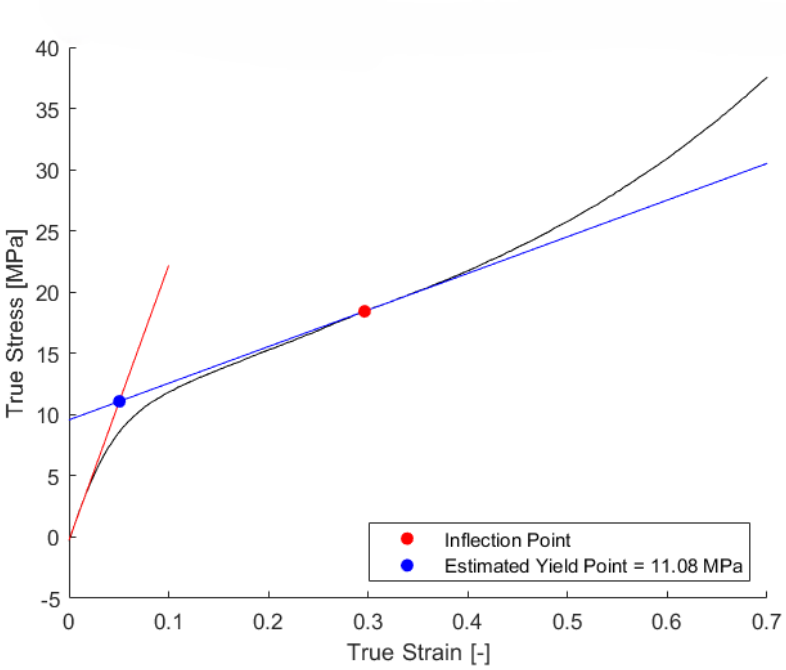

Figure 2.3: Stress-strain curve at -10 ^{o}C and 0.66 s^{-1} with yield point determination.

2.2.2 Yield behaviour

Now that the yield point of a material can be identified, a closer look at the working mechanisms of polymers at and around the yield point can be taken. As stated in the previous section, the yield stress or yield point is generally defined as the stress at which a material begins to plastically deform. Stress values below this stress induce completely reversible deformation, whereas stresses above this point will cause plastic deformation. However, it is important to note that for polymers, this statement is not applicable: plastic deformation starts before the yield point, and most of this deformation is recoverable [34, 35, 36]. To understand this rather unconventional behaviour, a closer look should be taken at the physical background of the yield point.
Glassy thermoplastics are amorphous polymers characterized by long, randomly intertwined and flexible macromolecules. Each macromolecule can change its spatial conformation through rotation along the covalent bonds forming the backbone of the main chain [27]. This dynamic behaviour leads to a random coil conformation as the most probable equilibrium state. The rate at which a chain undergoes conformational changes is highly dependent on temperature.

At elevated temperatures, conformational changes occur rapidly, allowing macromolecular chains to move freely and exhibit rubber-like and viscous behaviour. Conversely, at lower temperatures below the glass transition temperature, chain mobility significantly decreases, causing the polymer to adopt a glassy state. In this glassy state, contrary to the rubbery state, the material becomes more rigid and exhibits reduced molecular mobility, which affects the overall mechanical and thermal properties [37]. It is important to note that this great reduction in mobility does not completely eliminate the possibility of changes in chain conformation. While this mobility is often not observed within typical experimental timescales, it should still be considered.

For the determination of the yield point, it is important to establish the importance of applied stress as well. Much like the influence of elevated temperature discussed above, the application of stress enhances chain mobility as well. The influence of temperature and applied stress on chain mobility is particularly evident when examining the deformation characteristics of a polymer near its yield point. During the initial phase of a tensile test where stresses are still low, chain mobility is negligible, and the modulus is determined by intermolecular interactions between individual chains [38]. Upon the increase of stress, chain mobility increases as well, and localized chain conformation changes gradually contribute to material deformation. This contribution progressively grows until the applied stress reaches the yield stress, the point where the plastic strain rate resulting from chain mobility matches the experimentally applied strain rate [27]. This leads to permanent changes in chain conformation that accumulate as macroscopic plastic deformation [39, 40]. In other words, molecular mobility can be enhanced by the applied stress such that the rearrangement of molecular segments is stimulated, resulting in plastic flow. The magnitude of this plastic flow depends significantly on the applied stress [27].
Now that the importance of temperature and applied stress are established, it can be linked to the magnitude

of the yield stress. Any change in temperature or strain rate, so how fast the stress will accumulate, will cause the yield stress to change to accommodate a new equilibrium between the plastic rate of strain, and the experimentally applied strain rate [41, 42]. More specifically, it is observed that the yield stress tends to rise with higher strain rates and lower temperatures. This will be discussed more elaborately in Section 2.3.

With the dependence of the yield point on the strain rate and temperature being established, it is important to look at the deviating characteristics of the yield point for a polymer in comparison to conventional materials, like metals. As stated at the start of Section 2.2.2, plastic deformation starts before the yield point. In order to understand this behaviour, a study by Bauwens-Crowet et al. [43] is used.
It was discovered that there is an important relation between creep and constant strain rate. It was discovered that the steady state region, attributed to secondary creep, is identical to that obtained at the yield stress in a constant strain rate experiment. As stated previously, the yield stress increases with increasing strain rates. However, it was found as well that secondary creep in the creep tests, characterized by a steady flow region, was more prevalent for higher stress levels [44]. This is caused by secondary molecular processes, where there is a decrease in molecular mobility of the polymer chains [45, 46, 47]. As a result, the yield stress will increase. Using tensile tests at constant strain rate and creep tests under static load, steady-state values of stress and strain rates were obtained [27]. From both sets of tests, a linearly increasing line can be made, as can be seen in Figure 2.4. More specifically, this indicates that the yield point is the stress level at which the applied strain rate becomes equal to the macroscopically applied strain rate. This gives a good reason to argue that the polymer deviates from the conventional definition of yield stress as the transition from elastic to plastic deformation. Conversely, the initiation of plastic deformation occurs at stress levels considerably below the yield point, although it happens at a much lower rate compared to the applied strain rate.

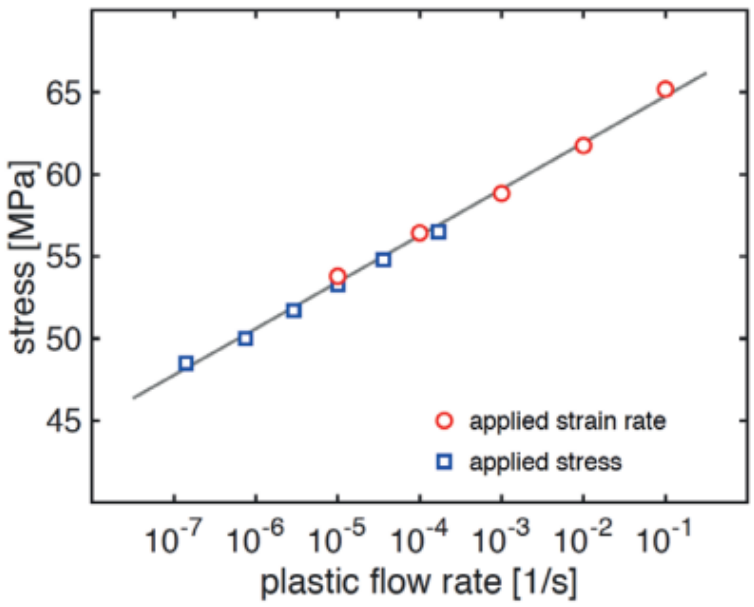

Figure 2.4: Yield stress dependence on strain rate (red circles) and the plastic flow rate's sensitivity to stress during secondary creep (blue squares) [22].

Another important and rather unconventional characteristic of the yield of polymers is their ability to - partially or fully - recover from plastic deformation, rather than the standard definition in material science of plastic deformation being irrecoverable. This can be explained by looking at the main deformation mechanism in polymers: the main-chain segmental motion. As a result, it can be argued that the yield point is a stress-induced glass-rubber transition [48]. At relatively low stress levels, relaxation times associated with main-chain segmental mobility are significantly longer compared to the experimental time scale, which results in elastic behaviour. For increasing stresses, the relaxation times decrease exponentially until they are similar to values in the range of the experimental timescale. This enables the material to undergo plastic flow within the relevant timescale, resembling the transition from a glassy to a rubbery state. When the applied stress is removed, this can be seen as the stress getting tremendously low, leading to the longest relaxation times returning to their enormously high values, preventing the recovery from the applied deformation as the timescale of immeasurable. However, relaxation times, rather than by applying stress, can also be lowered by an increase in temperature, such that raising the temperature to above the glass transition temperature can allow for partial or full recovery of the plastic deformation of the material [49, 50, 35]. Table 2.1 gives a summary of this rather complex behaviour and its effect on the mechanical properties.

Aspect	**Description**
Pre-Yield Plastic Deformation	Initiates before the yield point; most deformation is recoverable due to enhanced molecular mobility.
Molecular Conformation	Glassy thermoplastics have long, flexible macromolecules with rotation along covalent bonds, forming random coils.
Temperature Effects	High Temperature: Rapid conformational changes, macromolecules move freely, exhibiting rubber-like behaviour.
	Low Temperature: Decreased chain mobility, resulting in a glassy, rigid state with reduced molecular mobility.
Stress Effects	Applied stress increases chain mobility, contributing to material deformation and localized conformation changes.
Strain Rate Sensitivity	Yield stress rises with higher strain rates due to increased chain mobility and faster rearrangement of molecular segments.
Creep Behaviour	Secondary creep at high stress levels shows steady flow regions, correlating with yield stress at constant strain rates.
Recovery from Deformation	Partial or full recovery is possible through main-chain segmental motion.
	Elevated temperatures (above glass transition temperature) enhance recovery by increasing chain mobility.
Relaxation times	Decrease exponentially with increasing stress, enabling plastic flow.
	Increase significantly upon stress removal, hindering recovery within experimental timescales.
Equilibrium State	Yield stress changes with temperature and strain rate to balance plastic strain rate and applied strain rate.
Experimental Observations	Initial tensile test phases show negligible chain mobility; modulus determined by intermolecular interactions.
	Increased stress enhances chain mobility, leading to macroscopic plastic deformation at yield stress.

Table 2.1: Summarizing table for molecular behaviour and its effect on mechanical properties.

2.3 Strain Rate and Temperature

Most polymeric materials exhibit time-dependent material properties, such as the elastic modulus and yield strength. As discussed in Section 2.2.2, varying strain rate and temperature leads to a change in mechanical response. More specifically, changing the strain rate essentially means that the material is 'asked' to deform at a different rate. Changing the temperature has a serious impact on the behaviour of the material, where plastic deformation might occur more or less. Various studies showed that a polymer exhibits rubbery, ductile plastic or brittle behaviour [51, 52, 53], that is caused by changes in strain rate and temperature. This section will look at the change in yield behaviour upon changing the temperature and strain rate to establish the importance of these parameters in the context of high-strain rate characterization using low-temperature testing. The way these parameters are used to actually predict the behaviour of the material at strain rates beyond the experimental data is explicitly discussed in Subsection 2.3.1.

When conducting tensile tests on a polymeric material using different temperatures and strain rates, one can choose to vary the strain rate for a constant temperature and the temperature for a constant strain rate. As can be seen from Figure 2.5a, increasing the strain rate for a constant temperature will lead to an increase in yield point. This has to do with the segmental mobility of polymeric chains: at higher strain rates, the chains can not slide past each other upon loading as there is not enough time for this to happen: only very small molecular rearrangements are possible. Furthermore, due to the quick deformation, the chains have less time to disentangle. This leads to an increased number of chain entanglements, which resist further deformation. As a result, the material reacts more solid-like, leading to more resistance against plastic deformation and subsequently, an increase in yield point is observed. Similarly, decreasing the temperature for a constant strain rate leads to an increase in yield stress as well, as can be seen in Figure 2.5b. The decreasing temperature has a similar effect as the increased strain rate regarding the molecular motion to be decreased. Hence, for lower temperatures, it holds as well that chains can slide past each other with more difficulty and disentanglement is hindered more by this phenomenon as well.

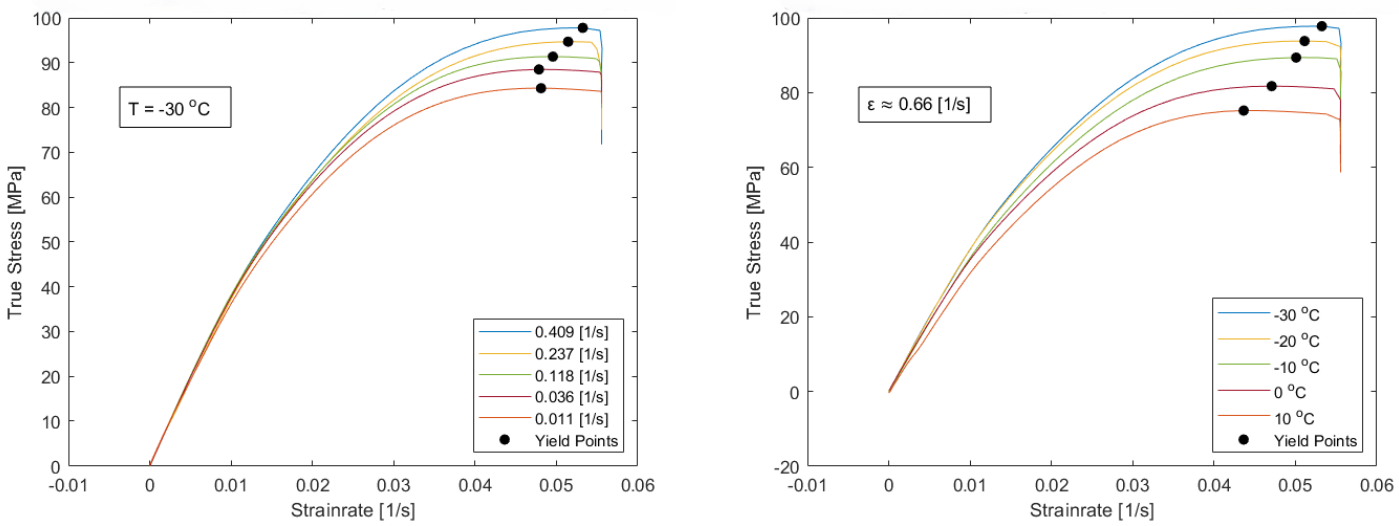

(a) (b)

Figure 2.5: Yield stress dependence on strain rate and temperature for PC.
a) Varying strain rate with constant temperature. b) Varying temperature with constant strain rate.

Now that it is found that the yield point increases for increasing strain rate and decreasing temperatures, one can take the yield points and plot this data in a semilog plot. As can be seen from Figure 2.6, plotting the true yield stress over the temperature versus the logarithmic value of the strain rate gives a linear relation. This establishes the direct relation between the strain rate and temperature with regard to the yield point. This behaviour comes in multiple forms on its own, with only one linear line through the data points for one active relaxation process, or multiple linear lines for more active relaxation processes. This behaviour is key to using low-temperature testing to obtain material behaviour at high strain rates, and therefore, Subsection 2.3.1 will elaborately explain how the observed behaviour can be used to predict the characteristics of a material beyond experimentally obtained data using this strain rate and temperature dependence.

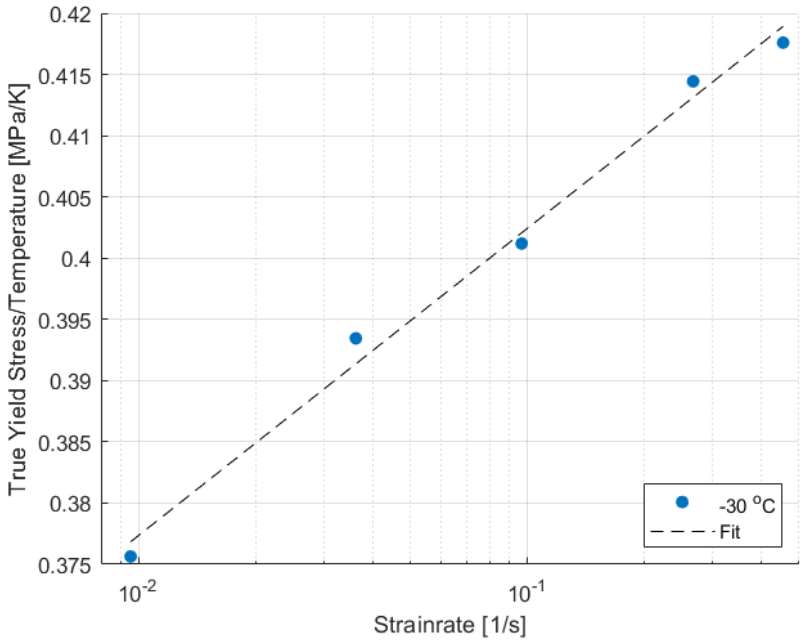

Figure 2.6: Strain rate and temperature dependence for PC with linear fit.

2.3.1 Ree-Eyring

With the material's mechanical response for stress-strain experiments being known and the dependence of strain rate and temperature being established, it can be argued that the applied stress induces a state of enhanced molecular mobility leading to plastic flow. A very effective way to describe temperature and applied stress dependence of plastic flow rate is the Ree-Eyring equation, which can be used to predict material beyond the experimentally obtained data. Eyring formulated a theory on viscous flow in materials, which has been widely utilized to describe the yield kinetics of solid polymers [54, 55]. It was based on the transition state theory, which stated that changes in chain conformation can only occur if a segment of this chain moves to an adjacent free position. This will only happen if the segment overcomes a free energy barrier, formed by intra- and intermolecular interactions [56]. With no stress applied, the potential energy in the chain is the same in each position and the potential free energy barrier is the same in each direction. This is schematically presented in Figure 2.7a, with ΔU being the potential barrier, or activation energy.

Eyring proposed that application of a stress σ increases the free energy in one position, whereas it decreases by the same amount in another direction [57]. These energy changes have a magnitude that is proportional to the applied stress: $\sigma\nu*$, with $\nu*$ being the so-called activation volume. It is the volume of a material involved in the process of overcoming the energy barrier.

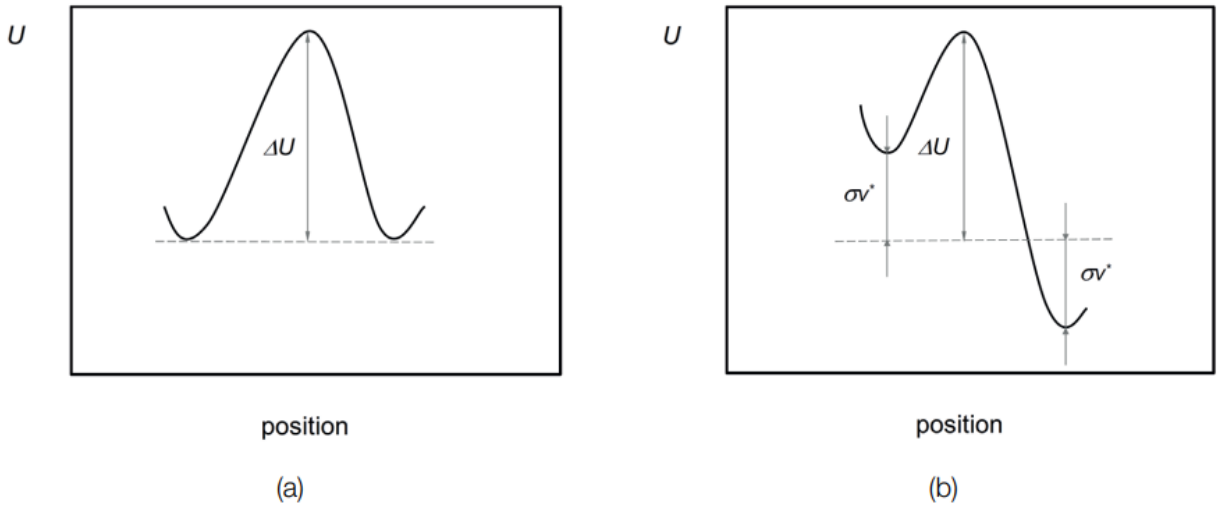

Figure 2.7: Illustration depicting the free energy barrier for segmental motion [58].

The frequency with which the segment jumps from one position and back is given by the jump frequency f_T at a certain temperature, as described by the Arrhenius equation, for an unstressed state [56]:

$$f_T = f_o \exp\left[\frac{-\Delta U}{kT}\right] \tag{2.6}$$

The barrier that needs to be overcome for the chains to move changes as stress is applied: Moving to a new location, referred to as a forward jump, the magnitude of the barrier is decreased by an amount of $\sigma\nu*$. Moving back to an original position, which is referred to as the backward direction, the magnitude is increased by the same amount. This can also be deducted from Figure 2.7b. Plastic strain accumulates as the material moves in a forward direction, and hence the resulting plastic strain is proportional to the difference between forward and backward jump frequency. Without going in-depth mathematically, Eyring used this expression to come up with a relation for the yield stress:

$$\sigma_y(\dot{\varepsilon}, T) = \frac{kT}{\nu^*} \sinh^{-1}\left[\frac{\dot{\varepsilon}}{\dot{\varepsilon}_0} \exp\left(\frac{\Delta U}{RT}\right)\right] \tag{2.7}$$

Here, k is the Boltzmann constant [$m^2\,kg\,s^{-2}\,K^{-1}$], ν^* the activation volume [m^3], $\dot{\varepsilon}$ the strain rate [s^{-1}], $\dot{\varepsilon}_0$ a strain rate constant [s^{-1}], ΔU the activation energy [$J\,mol^{-1}$], and T the temperature [K].
As explained in Section 2.3, at a constant temperature, this equation gives a linear relation between yield stress and the logarithmic value of the strain rate. Furthermore, keeping the strain rate constant gives a linear relation between yield stress and temperature. This gives multiple linear curves for different temperatures. By using the Eyring flow equation, a master curve can be constructed such that the material can be characterized at strain rates that were not experimentally tested [59]. This master curve is constructed using the fact that the Eyring flow equation holds for arbitrary temperature and strain rate for the tested yield strengths. The equation is valid for strain rates outside the tested domain and hence, the yield strength at these strain rates can be predicted without the need for additional testing. An example of this behaviour can be found in Figure 2.8, where PC samples were tested at various temperatures and strain rates, after which the Eyring flow equation was fitted through this data [43]. In this example, the Eyring fit is not extended beyond the experimentally used strain rates, but this can be easily done by extending the existing fit to higher strain rates.

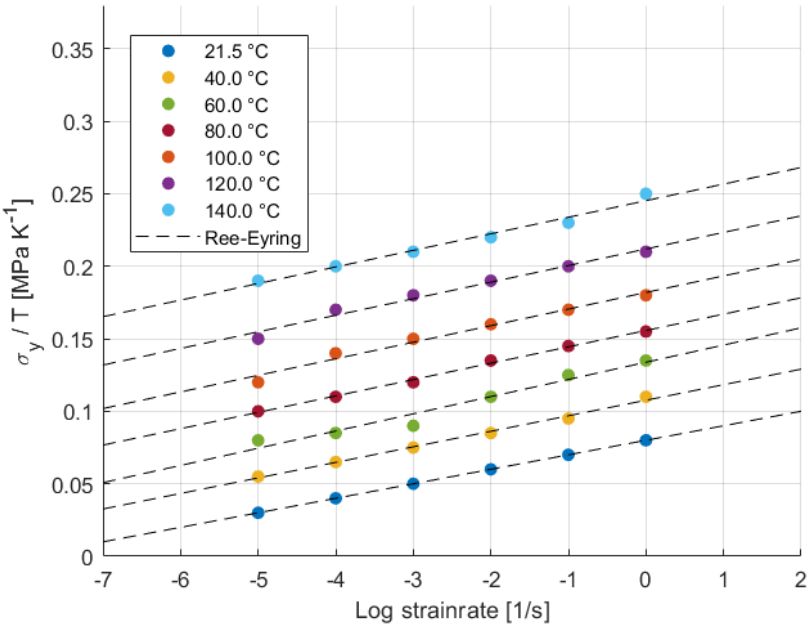

Figure 2.8: Yield stress of PC for various temperatures and strain rates. Data from Bauwens et al. [43].

However, there is a crucial limitation to this equation: only a single molecular relaxation process is considered, namely the main chain segmental motion. It is not uncommon that polymers possess different molecular relaxation mechanisms. This also applies to the yield stress, where more than one molecular process may contribute to it [60]. As can be seen from Figure 2.9a, there is a distinct increase in the slope of the linear relation with increasing strain rate, as other molecular processes are activated.
Hence, the Eyring equation would not suffice for lower or higher strain rates. More specifically, only a region where the yield stress is linearly dependent on temperature and strain rate can be effectively captured by the

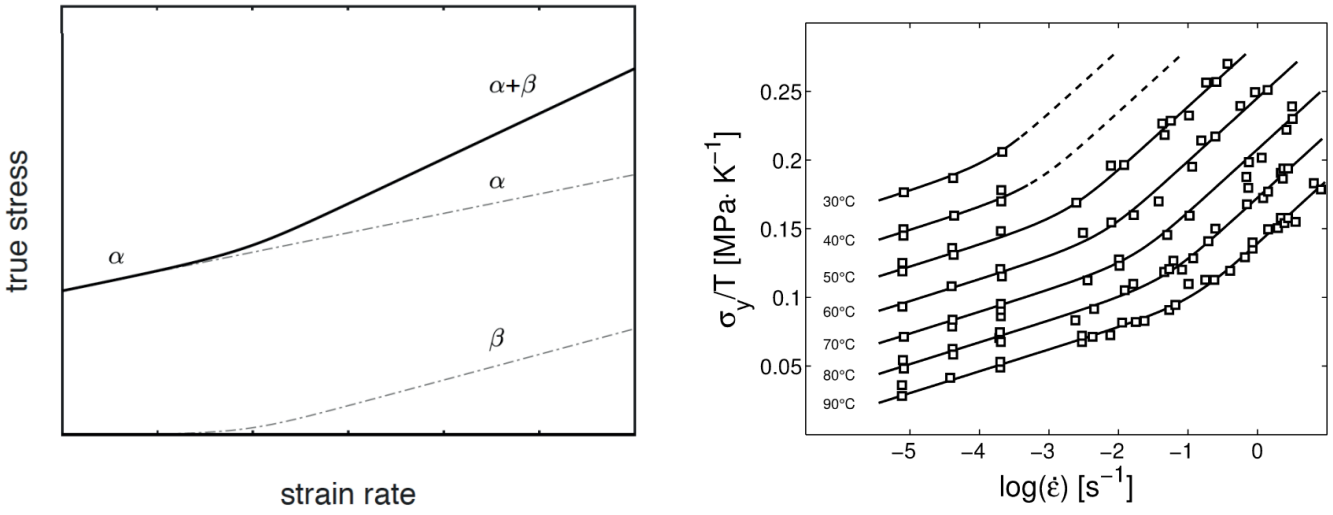

(a) (b)

Figure 2.9: a) Schematic representation of multiple molecular processes being active for increasing strain rate. b) Yield stress of PMMA for various temperatures and strain rates, adopted from [61].

Eyring equation. So, the transition region from one to multiple relaxation processes is not considered in the Eyring equation. The temperature dependence in the low-strain rate region is quite different from that in the high-strain rate region, which implies that no master curve can be constructed by shifting. This is because the different molecular processes induce different activation energies. Therefore, Ree and Eyring proposed an effective way of modelling the combined yield responses by assuming that the processes proceed at the same rate and that their stress contributions can be summed [62]. In this way, the total stress is decomposed into two individual stress-activated processes, each with its own kinetics and corresponding parameters. For the yield stress, this leads to the Ree-Eyring modification of the flow equation for i number of active processes:

$$\sigma_y(\dot{\varepsilon}, T) = \sum_i \frac{kT}{\nu_i^*} \sinh^{-1}\left[\frac{\dot{\varepsilon}}{\dot{\varepsilon}_{0,i}} \exp\left(\frac{\Delta U_i}{RT}\right)\right] \tag{2.8}$$

Here, multiple contributions of different molecular deformation processes are added. An example for polymers is the so-called α-process, which is related to the glass transition and main-chain segmental mobility, whereas the β-process relates to a secondary glass transition, partial main-chain mobility or side-chain mobility. This behaviour is found in PMMA for example, which can be seen in Figure 2.9b.
Furthermore, it is noteworthy that it is well-established that the contribution of the strain rate dependence is visible for both amorphous and semi-crystalline polymer systems, if the temperature is low enough or if the strain rate is high enough [43, 63, 64, 65]. However, it should be noted that the strain rate dependence is strongly influenced by the crystallinity of a semi-crystalline polymer [66, 67]. Therefore, the amorphous phase is crucial for the strain rate sensitivity of the material.

An important consideration is given by the fact that equation 2.8 only holds for temperatures that are below T_g. This limits the use of this equation in combination with the available test temperatures. To overcome this problem, an empirical relation for the stress response for temperatures above Tg was given by Richeton et al. [47] and can be found in Equation 2.9:

$$\sigma_y(\dot{\varepsilon}, T) = \sum_i \frac{kT}{\nu_i^*} \sinh^{-1}\left[\frac{\dot{\varepsilon}}{\dot{\varepsilon}_{0,i}} \frac{\exp\left(\frac{\Delta U_i}{RT_g}\right)}{\exp\left(\frac{ln(10)C_1^g(T-T_g)}{C_2^g+T-T_g}\right)}\right] \tag{2.9}$$

Many similarities can be found between equations 2.8 and 2.9. However, equation 2.9 yields additional parameters to account for the behaviour above Tg. It can be seen that the glass-transition temperature T_g is taken into consideration, as one would expect. Furthermore, parameters C_1^g and C_2^g can be seen. These are empirical constants that are used in the WLF equation to fit shift factor values using superposition. Section 3.2 gives an elaborate explanation of the WLF equation and its constants.
It should be noted that T_g occurs over a broad temperature range rather than a single point and that it is dependent on viscoelastic properties, meaning that it varies with the rate at which load is applied[68]. This equation neglects both effects by taking T_g constant.

CHAPTER 3

Rheological Properties

Throughout Chapter 2, it has been established that the characterization of mechanical properties is dependent on strain rate, temperature and the glass transition temperature. The elastic behaviour of a material is a critical aspect of this characterization, which is directly to these mechanical properties. Consequently, it is essential to investigate how the material's elasticity can be described. Furthermore, modelling parameters such as WLF parameters, might be needed if more complex material behaviour needs to be modelled. For example, The Ree-Eyring equation, presented in Section 2.3.1, demonstrated the dependence of the applied strain rate and temperature on material behaviour regarding yield, and additional parameters are needed to model complex behaviour, such as Equation 2.9. So, there is a pressing need to determine the glass transition temperature and WLF parameters of a material. In this Section, it will be elaborately explained how this information can be obtained using the elastic behaviour of the material. Rheology can be used as a theoretical framework, 'as it is 'the theory of deformation and flow of matter ' [69].

Firstly, it is necessary to consider the various states in which materials can exhibit elastic behaviour, and which states are of interest in the scope of rheology. For instance, materials can behave as linear elastic solids, where energy is fully stored and the stress-strain response is given by Hooke's law:

$$\sigma = E \cdot \varepsilon \qquad \tau = G \cdot \gamma \tag{3.1}$$

This implies that under constant strain rate $\dot{\varepsilon}$, loading and unloading of the material proceeds along the same stress-strain path without the need for additional work, implying there is no dissipation of stored energy: all energy gets stored by the material.

A second, quite different state that is important within rheology is referred to as a viscous material. The viscosity of a material is highly dependent on the applied strain rate and the stress-strain relation is given by Newton's law of viscosity:

$$\sigma = \dot{\varepsilon} \cdot \eta(T) \qquad \tau = \dot{\gamma} \cdot \eta(T) \tag{3.2}$$

As shown by Equation 3.2, the relationship between the applied strain rate and shear stress is clearly proportional to the viscosity η for a Newtonian fluid. More specifically, Newtonian fluids can be characterized by a single viscosity value at a given temperature, demonstrating temperature-dependent and strain-rate-independent viscosity.
Upon loading and unloading of the material with the same strain rate, comparable to the elastic solid, a stress-strain curve that does not follow the same path appears. Furthermore, to undo the applied strain, the same amount of work has to be performed compared to the loading stage. Hence, it can be stated that a viscous material completely dissipates all energy that is supplied.
When looking at the energy storage capabilities, the elastic solid state and the Newtonian fluids represent two extreme situations. Therefore, a third category of material was introduced in rheology: viscoelastic materials. These materials exhibit unique behaviour, where they partially store energy and partially dissipate it. Most polymeric materials exhibit non-Newtonian behaviour, characterized by viscoelastic behaviour and therefore, rheology primarily focuses on this class of materials. Section 3.1 will explain this type of material in more detail.

3.1 Viscoelasticity

When looking at the viscous contribution of a viscoelastic material, one can distinguish between Newtonian and non-Newtonian fluids. Newtonian fluids obey Newton's linear law of friction, as can be seen from equation 3.2. It was established that the viscosity varies for different temperatures, but it remains constant regardless of the applied strain rate. However, for Non-Newtonian fluids or Generalized Newtonian fluids, the viscosity is a function of the applied strain rate and therefore the stress in the material changes for varying strain rates as well:

$$\tau = \eta(T, \dot{\gamma})\dot{\gamma} \tag{3.3}$$

Within the study of rheology, the viscosity of a material is the most used qualitative property to define either a Newtonian or a non-Newtonian material [70]. It is defined as the flow resistance caused by internal friction. Changing viscosity for increasing strain rate can either lead to a decrease in viscosity when high strain rates are applied, which is referred to as shear thinning, or an increase in viscosity at high strain rates which is referred to as shear thickening. Figure 3.1 gives an illustrative example of the different behaviours of a material under increasing strain rate.

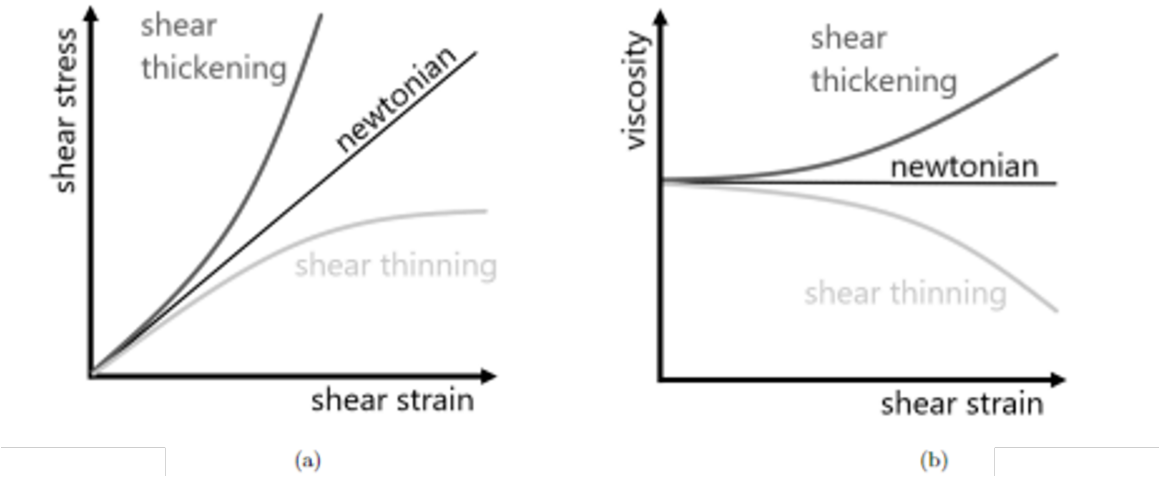

Figure 3.1: a) Linear relation between shear stress and applied strain rate. b) Dependence of viscosity on the applied strain rate. Adapted from [71].

The need to model viscoelasticity arises from the demand to bridge the gap between experimental conditions and real-world conditions. By employing constitutive equations to relate multiple physical quantities, it is possible to predict material properties under various loading conditions. As most LEP materials have viscoelastic behaviour, it is important to clearly understand viscoelastic behaviour to be able to characterize these materials. The modelling of viscoelastic material starts with the consideration that a material can behave as a pure elastic solid or a pure viscous fluid, as described in equation 3.1 and equation 3.2, respectively. One-dimensional models, such as the Maxwell model and the Kelvin-Voigt model, are commonly used in this context. Both models consist of a purely elastic spring, represented by the Hookan elasticity modulus E, and a purely viscous damper, represented by Newtonian viscosity η. The Maxwell model features both elements connected in series, whereas the Kelvin-Voigt model utilizes both elements in parallel. This is schematically represented in Figure 3.2.

Both relations can be used to describe constant and static tests qualitatively. Examples of these tests are the stress relaxation experiments, in which the stress response gradually decreases for a constant deformation, and a creep experiment, in which the strain response gradually increases for constant stress. When comparing both models, the Maxwell model gives a better qualitative description of the relaxation behaviour of polymers, due to the composition of the strain in two different elements. The elastic component, corresponding to the spring occurs instantaneously, while the viscous strain component grows with time. As the Maxwell model uses the Hookean law, this increase in strain leads to a decrease in stress, which describes the relaxation experiment. As the Kelvin-Voigt model uses both strain components in parallel, the stress relaxation modelling is not as accurate [73]. The Kelvin-Voigt model gives a better qualitative description of primary creep behaviour because in the infinite time limit the strain approaches a constant value, whereas the Maxwell model predicts a linear relation between strain and time which is often not the case [74].
However, it might be beneficial to perform dynamic testing on a material as well. This yields excitation that

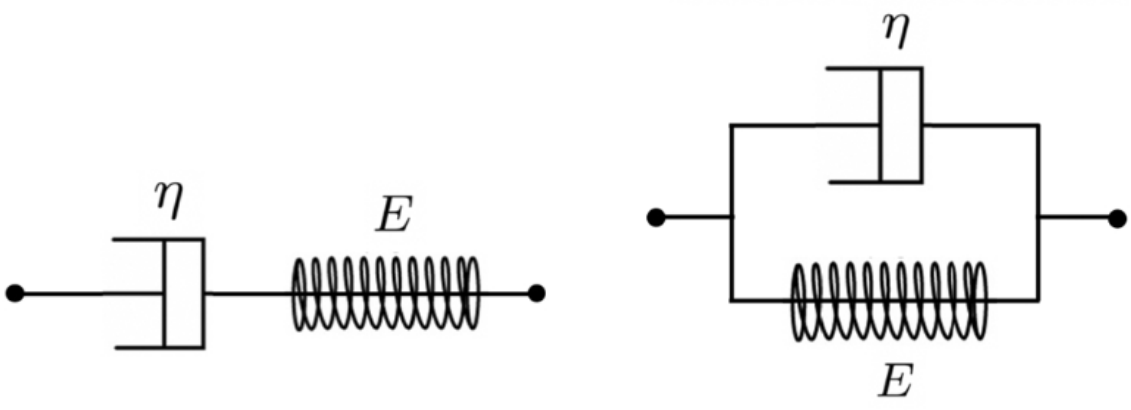

(a) (b)

Figure 3.2: Schematic representation of a) Maxwell model, b) Kelvin-Voigt model. Adapted from [72].

is oscillating using a sinusoidal strain excitation. Modelling this behaviour yields the benefit that elastic and viscous components are clearly recognizable. Furthermore, a wide range of frequencies can be measured, which can be linked to temperature. Three parameters are primarily used to describe the material behaviour over a large range of frequencies: the storage modulus E', loss modulus E" and tan δ. Before looking into the mathematical expressions of these parameters, it is important to understand the physical meaning thereof [75]:

- Storage Modulus: indicates how much energy is stored in the material during a cycle of deformation. It is associated with the elastic behaviour of the material.
- Loss Modulus: indicates how much energy is lost in the material during a cycle of deformation. It is associated with the liquid-like behaviour of the material.
- Tan δ: represents the material's damping capability, indicating the phase difference between the applied strain and resulting stress. A high value means that the material will dissipate more energy, whereas a low value indicates that the material behaves more elastic.

With the physical meaning known, the mathematical given by Meyers et al. [76] can be interpreted more easily, which will be given in the following part of this section.
Once again, material behaviour is characterized by elastic and viscous material. Hooke's law and Newton's law of viscosity are both defined for nominal and shear forces. This section will discuss material behaviour expressed in nominal strain and stresses. Looking at the elastic component of the response, it can be defined as:

$$\sigma = E \cdot \varepsilon \tag{3.4}$$

For an oscillatory strain, depending on frequency f, the resulting strain ε is defined as:

$$\varepsilon(t) = \varepsilon_0 \cdot \sin \cdot (\omega t) \text{ with } \omega = 2\pi \mathrm{f} \tag{3.5}$$

Which gives the following stress response for a pure elastic solid:

$$\sigma(t) = E \cdot \varepsilon_0 \cdot \sin(\omega t) \tag{3.6}$$

As this elastic component is based on a pure elastic solid, equation 3.6 can be rewritten to:

$$\sigma(t) = \sigma_0 \cdot \sin(\omega t) \tag{3.7}$$

Due to the fact that the strain and subsequent stress are in phase, it can be stated that they happen simultaneously and therefore, no energy is dissipated as one would expect from a purely elastic solid.

Looking at the viscous component of the response, it can be defined as:

$$\sigma = \dot{\varepsilon} \cdot \eta \tag{3.8}$$

Taking the time derivative of equation 3.5 gives the following relation:

$$\dot{\varepsilon}(t) = \varepsilon_0 \cdot \omega \cdot \cos(\omega t) = \varepsilon_0 \cdot \omega \cdot \sin(\omega t + \frac{\pi}{2}) \tag{3.9}$$

Subsequently leading to the stress response for a pure viscous liquid:

$$\sigma(t) = \eta \cdot \varepsilon_0 \cdot \omega \cdot \sin(\omega t + \frac{\pi}{2}) \tag{3.10}$$

Similarly to the elastic component relying on Hooke's law, this stress response of the viscous component is based on Newton's law of friction, and with the consideration that it holds that $\varepsilon_0 \cdot \omega = \dot{\varepsilon_0}$, and introducing a loss angle δ, equation 3.10 can be rewritten:

$$\sigma(t) = \sigma_0 \cdot \sin(\omega t + \delta) \text{ with } \delta = 90^o \tag{3.11}$$

Contrary to the elastic component, the strain and subsequent stress of the purely viscous component are 90^o out of phase. Therefore, it can be stated that all energy is dissipated.
The stress response for a pure elastic solid and a pure viscous liquid is now defined by equations 3.7 and 3.11 respectively. However, as stated previously, most materials exhibit material behaviour that is in between both material states. When closely comparing both equations, one final stress response can be given that can describe this behaviour:

$$\sigma(t) = \sigma_0 \cdot \sin(\omega t + \delta) = \sigma_0 \cdot \sin(\omega t) \cdot \cos(\delta) + \sigma_0 \cdot \cos(\omega t) \cdot \sin(\delta) \tag{3.12}$$

Here, the first segment is the elastic component that is in phase, and the second segment is the viscous component. The loss angle δ has a value between 0^o (fully elastic) and 90^o (fully viscous).
Using the applied strain given in equation 3.5 in combination with the stress response in equation 3.12, the storage modulus E', loss modulus E" and tan δ can be defined:

$$E' = \frac{\sigma_0}{\varepsilon_0}\cos(\delta) \qquad E" = \frac{\sigma_0}{\varepsilon_0}\sin(\delta) \qquad \tan\delta = \frac{E"}{E'} \tag{3.13}$$

These material characteristics are crucial for the characterization of the material. In Section 3.2, it will be explained how the storage modulus and loss modulus can be used to describe the elastic behaviour of the material. The determination of the glass transition temperature will be explained in Section 3.3.

3.2 Time-Temperature Superposition

A problem that arises in the characterization of viscoelastic problems is the timescale that is relevant for the application of polymers: it is too large to assess in a single experiment. However, time and temperature show interchangeability and therefore allow for short-term experiments at different temperatures to access the polymer's long-term mechanical response by shifting data to form a master curve. This technique is called time-temperature superposition (TTS) and this section will elaborately explain how this can be used.
As discussed in Section 2.3, the rate at which a deformation is applied and the temperature at which this occurs is of vital importance for the characterization and behaviour of a polymeric material. TTS uses these principles as well, and therefore, a small introduction to these topics will be repeated to be able to connect this behaviour to TTS.
Firstly, looking at the rate at which deformation is applied, it should be noted that TTS uses the fact that under a small deformation, the molecular mobility gives rise to a strong time dependence. More specifically, for relatively short times, only very small molecular rearrangements are possible and therefore, the material behaves as an elastic solid. When time increases, the changes in molecular conformation increase as well, eventually resulting in main-chain segmental motion. This leads to the material reacting more rubber-like. Substantially increasing time will even lead to the material behaving more fluid-like, due to chain slippage which is caused by reptation. Reptation is the movement of entangled polymers in the longitudinal direction relative to neighbouring chains, causing the material to exhibit flow-like behaviour [77].
The determination and recognition of the three events is difficult to observe in a single experiment, as the timescale at which this happens is too long. Therefore, the concept of varying temperature can be used, which is the second important changing variable of TTS. A solution to the enormous timescale is to carry out experiments in a suitable timescale, where isothermal experiments are carried out at elevated temperatures. It is now known that the increased temperature leads to increased molecular mobility. So, looking at the molecular mobility needed to describe the material in different states, increasing temperatures and higher times yield similar results compared to lower temperatures and lower times. This leads to the fact that all material states can be observed in a suitable experimental timescale using TTS if the temperatures at which the experiments are performed are chosen properly.
An example of how these experiments are carried out can be found in Figure 3.3. Here, the y-axis is chosen to be log E, which could both be the storage or the loss modulus, depending on the behaviour of interest. The obtained experimental data is represented by the 'Data' region. When a reference temperature is chosen, a mastercurve can be constructed by shifting the data of other temperatures using extrapolation. This extrapolation happens

according to a so-called shift factor a_T.
Two commonly used expressions to determine a_t are used to model this behaviour: the Arrhenius equation and the WLF equation. When the reference temperature is set to the glass-transition temperature, which is common practice for many polymers [78], two temperature ranges can be identified: Temperatures above T_g and temperatures below T_g. Both ranges show a significantly different behaviour, as explained in Section 1.2.1. For the determination of a_T for temperatures below T_g, the Arrhenius equation can be used to find the shift factor [79]:

$$a_T(T) = \exp\left[\frac{\Delta U}{R}(\frac{1}{T} - \frac{1}{T_g})\right] \tag{3.14}$$

Here, ΔU is the activation energy [J mol^{-1}], R is the ideal gas constant [J mol^{-1} K^{-1}] and T_g is the glass transition temperature [K].
The WLF equation is an empirical relation which describes the temperature dependence of a material above T_g. To find a_T in this range, the following equation can be found [78, 80]:

$$\log(a_T(T)) = \frac{-C_1(T - T_g)}{C_2 + (T - T_g)} \tag{3.15}$$

Here, C_1 [-] and C_2 [K] are the WLF parameters. With T_g being known and set as the reference temperature, these parameters can be used to construct a single mastercurve.

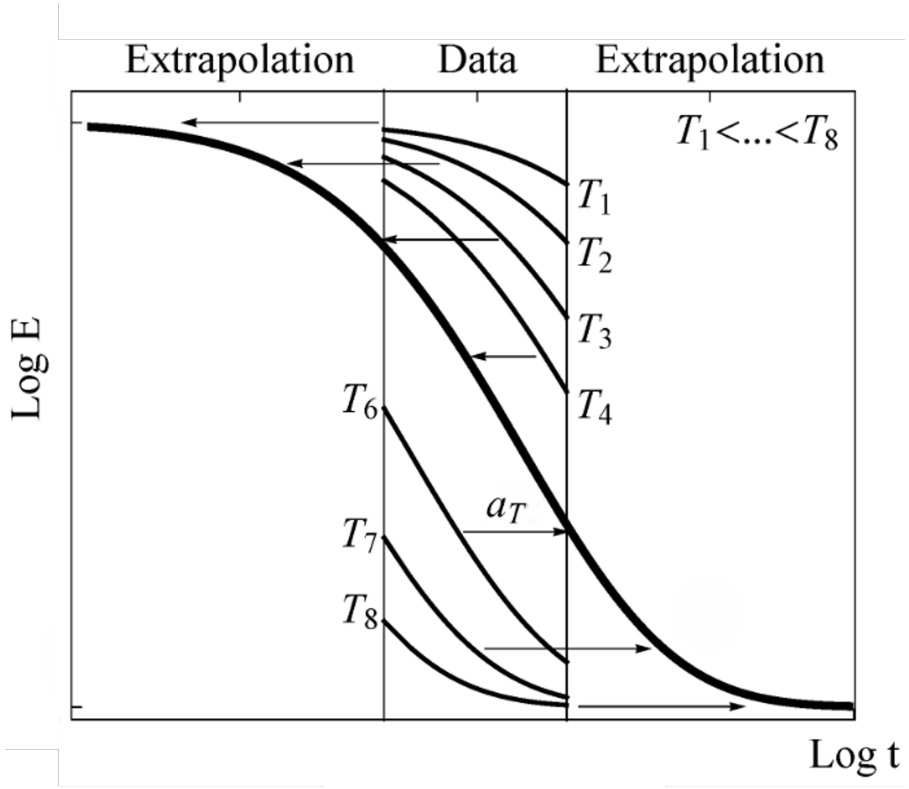

Figure 3.3: Schematic representation of the TTS principle for the construction of a master curve. Adapted from [81].

It should be noted that in some cases, the use of TTS yields is not applicable:

- TTS using this shift factor is only valid when all relaxation times are multiplied by the same factor. More specifically, all viscoelastic functions should be superposed with the same value of the shift factor [78]. For example, shifting the storage modulus from T_a to predict its behaviour at T_b should yield the same shift factor when shifting the loss modulus from T_a to T_b.
- There should be no structural changes within the material during the experiment. This means that only horizontal shifting is allowed on a log timescale [82]. In reality, this is only valid within certain temperature ranges.
- Physical ageing influence, as explained in Section 1.2.2, causes the linear viscoelastic response to deviate from the obtained mastercurve and should therefore be minimized.

3.3 Testing Methods DMA

This section will discuss different testing methods using Dynamical Mechanical Analysis (DMA) testing that might be relevant for this study, and discuss how and why the data obtained from these experiments can be used.

Analyzers
Within DMA, the most commonly used machines to perform temperature and frequency sweeps are so-called forced resonance analyzers. These types of machines cause the sample to oscillate at a fixed frequency. It can be chosen to use either stress control or strain control. In stress control, a predefined force is applied to the sample, after which the strain is measured. With this technique, longer relaxation times can be tested with more ease because the delicate control of force makes it easier to maintain constant force over longer periods. On the other hand, strain control displaces the sample with a certain strain, after which the force on the sample is measured. A better short-time response for materials of low viscosity is obtained and experiments of stress relaxation are performed more easily when using this method. This is because the displacement can be controlled precisely, allowing for quick and accurate measurements. Within the elastic region, the material response of both stress and strain control analyzers are very similar [83].
Both stress and strain can be applied using either torsional or axial analyzers. Torsional analyzers are mainly used for liquids and melts, but solid samples can be investigated as well. Axial analyzers are used for solid or viscous materials [83]. An advantage of axial testers is the ability to test higher modulus compared to torsional tests. Furthermore, it should be noted that small dimensional changes in the sample can lead to significant differences in results, such as inertia and shear heating of the samples [84].

Temperature Sweep
Temperature sweeps are often performed to describe the internal structure and configuration of macromolecules, by characterizing the polymer structure [85]. In particular, temperature-dependent behaviour is considered: melting or softening behaviour when samples are heated, or solidification or crystallization when the sample is cooled. Therefore, the test requires a pre-defined temperature profile, while a small-amplitude oscillation is applied to the sample with a constant frequency. The temperature is incremented and equilibrated for several minutes such that the material has time to reach the measurement temperature. From this test, the storage modulus E', loss modulus E" and tan δ can be measured. Two important material parameters can be evaluated from this important data: T_g and T_m. This subsection will focus on the determination of the glass transition temperature, as the materials melting behaviour is not discussed in this thesis.

Determination of T_g
Although T_g is usually reported as a single temperature, in reality, this glass transition happens over a range of temperatures rather than a single point [86]. Therefore, it is useful to define methods to unambiguously define points within this transition region to characterize the glass transition temperature and to be able to quantitatively compare materials. Although the glass transition is mainly governed by the type of polymer, many factors such as crystallinity, crosslinking and fillers can change this property significantly [87, 88], and therefore, there is a need for proper characterization of the glass transition. For a temperature sweep, it is important to acknowledge that T_g is sensitive to the frequency of the oscillation, but independent of the amplitude within the elastic region of the material [89].
Three methods to describe the glass transition temperature are commonly used with respect to DMA testing. The first method is based on the definition of a peak in the measured loss modulus. The peak of the loss modulus is related to molecular motion: as the material approaches the peak of the loss modulus, the dissipated energy increases due to the ability of large segments of polymers being able to move cooperatively [86]. Due to the larger segments moving as well, more internal friction leads to higher energy dissipation. On the other hand, the material as a whole becomes easier to deform. More specifically, the cooperative movement of the polymer chains, in addition to the movement of chains moving independently, requires more energy and hence, there is an increase in energy dissipation. As a consequence, there is more viscous-like behaviour due to the fact that the material is more likely to flow and dissipate energy. The movement of the sample as a whole, on the other hand, leads to less overall resistance to deformation which will reduce internal friction and therefore, will reduce the dissipated heat as well. As these materials have a competing effect, there will be a transition where one of the two motions is governing. At the peak, the rate of energy dissipation is optimal because the polymer chains are in a state of maximum cooperative motion. Beyond this point, at higher temperatures, the material will become too fluid-like and the polymer chains move too freely, reducing internal friction [86].
The second method is similar to the first method, but now a look is taken at the peak of tan δ. As explained in Section 3.1, this is defined by the ratio of the loss modulus to the storage modulus. Therefore, a peak in the tan δ indicates that the material has the most viscous material response in the transition region and subsequently, this peak can be used to determine T_g. An example of the determination of T_g using both methods can be found in Figure 3.4 The last method to determine the glass transition temperature is using the storage modulus. This

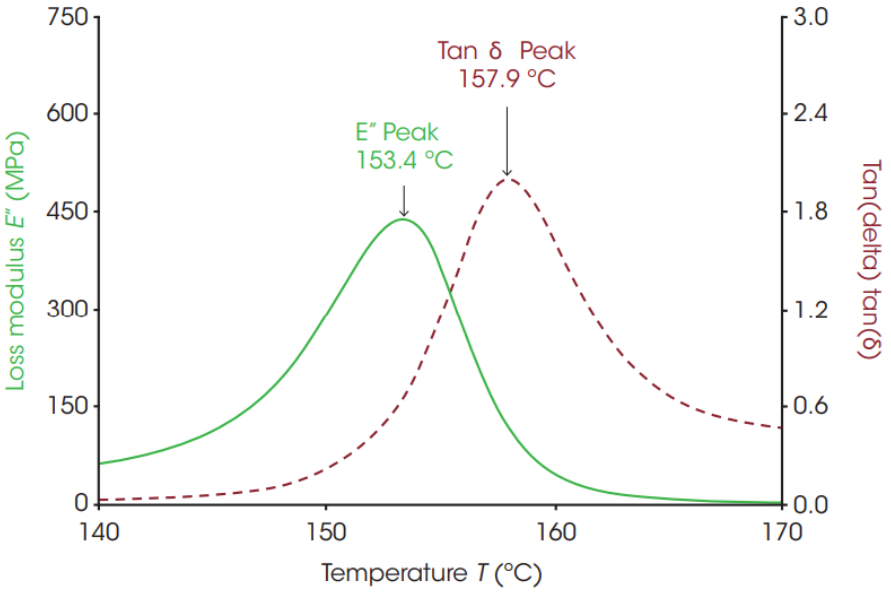

Figure 3.4: T_g determination of PC using a peak in loss modulus E" and tan δ [86].

method generally yields the lowest T_g. The method is relatively simple, which will be explained using Figure 3.5: the intersection of two lines gives an indication on the T_g. The first line is taken from the glassy plateau of the storage modulus, whereas the second line is taken in the transition region. Ideally, the first line should be constructed based on two data points that are sufficiently far away from the start of the decrease of the storage modulus, such that the glassy plateau is 'extended' horizontally. The second line, tangent to the transition region, is determined using the so-called inflection method [86]. The inflection point is the point on the storage modulus with the steepest slope. By taking the derivative of the storage modulus data, a minimum can be found that corresponds to this inflection point. From this minimum, the coordinates and slope of this point can be used to construct the second line such that it intersects the first line. The intersection of both lines indicates T_g.

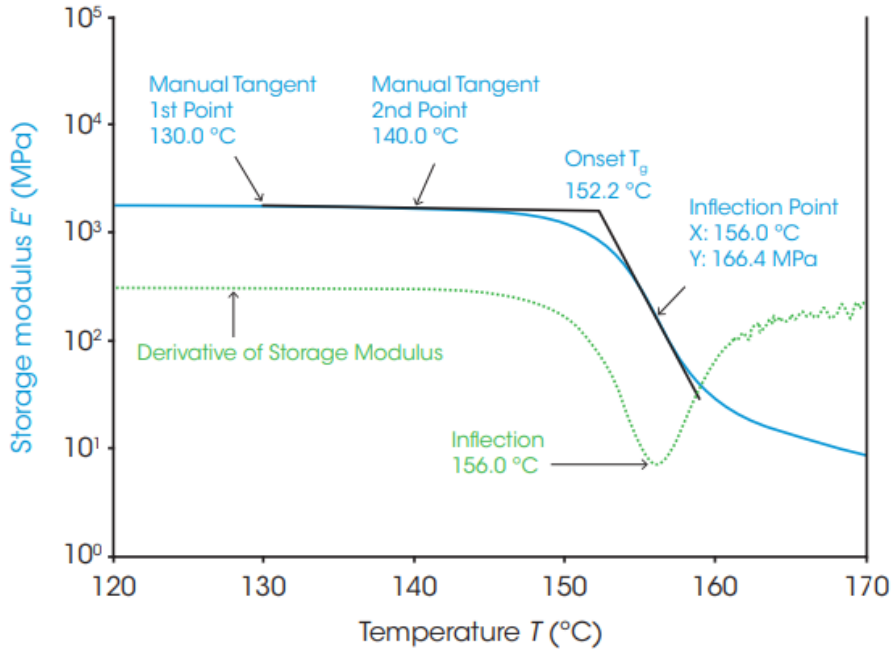

Figure 3.5: T_g determination of PC using the storage modulus E' [86].

Frequency Sweep

A second test to determine the viscoelastic properties of a material is a frequency sweep. In contrast to determining temperature-dependent properties using a temperature sweep, this method aims to describe the

time-dependent behaviour of a sample. Similar to the temperature sweep, the polymer's internal structure can be characterized. The test performs oscillatory small amplitude deformations in the elastic region of the material. The amount of deformation is constant, together with the temperature. The rate at which the deformation is applied, the frequency, varies throughout the experiment. Testing at high frequencies can be used to simulate fast motion on short timescales, whereas low frequencies simulate slow motion on long timescales [90]. Typically, the results of a frequency sweep yield the frequency on the x-axis, and the loss and storage modulus on a logarithmic y-axis. Using this data, elastic and viscous behaviour at frequencies beyond the testing domain can be characterized using TTS. An example of typical obtained data of this test can be found in Section 3.2, Figure 3.3, where the 'Data' region shows the obtained dataset.
It should be noted that the glass transition temperature can be determined from the frequency sweep as well, by observing a distinct peak in tan δ or the loss modulus. This implies that the glass transition is not only dependent on temperature but on strain rate as well.

CHAPTER 4

Fatigue

When discussing the mechanical properties of a material, only tensile testing was discussed at a constant rate. However, in any application, the polymers are exposed to varying loading cases. The applied stress is not constant but has a cyclic nature. In both situations, there is a certain maximum stress the material can endure, but in a cyclic loading, the material will often be exposed to lower stresses as well. The ratio between the maximum and minimum occurring stress is expressed as the stress ratio R:

$$R = \frac{\sigma_{min}}{\sigma_{max}} \tag{4.1}$$

Due to limitations of the available testing equipment, the machine will apply a zigzag-like pattern to the material, rather than a sinusoidal signal which is common practice in fatigue testing. Therefore, the static and cyclic loading can be expressed as given in Figure 4.1.

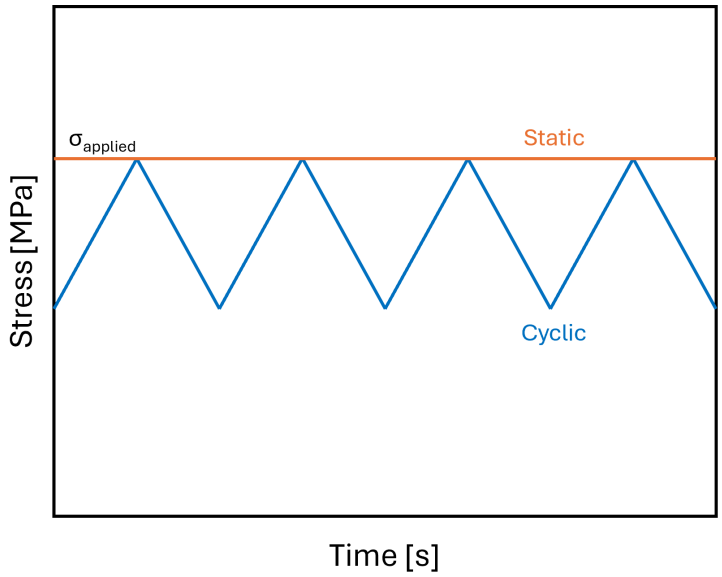

Figure 4.1: Stress output signal for static and cyclic loading for identical applied stress.

Looking at failure mechanisms in both cases, it can be stated that the accumulation of plastic deformation is the highest for a static load case. In the cyclic load case, the accumulation rate is much lower as the average stress is lower. Therefore, cyclic lifetime is expected to be higher for cyclic loading, if the failure of the sample is dominated by plasticity-controlled failure. This happens at relatively high stresses, where a plastic zone is formed, which usually causes ductile failure. However, failure can also be induced by cracks, or so-called crack-growth-controlled failure, at much lower stresses. This mechanism is reliant on the fact that microdefects initiate cracks which grow constantly over time when applying cyclic stress. This causes the ability of a polymer to fail even under its yield stress. Although the time to failure is influenced by both failure mechanisms for

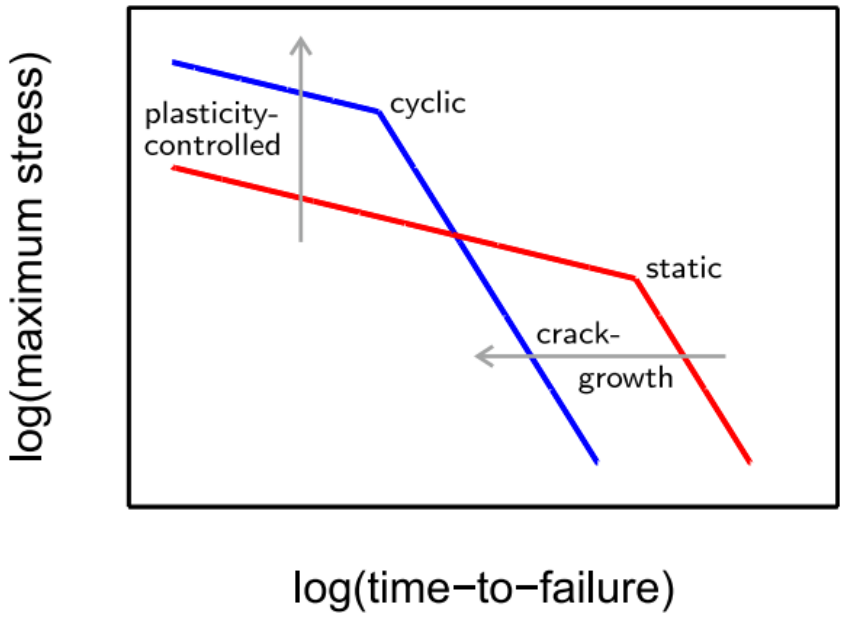

Figure 4.2: Schematic representation of the effect on cyclic and static loading on the dominant failure mechanism in polymers [92].

the cyclic loading, one mechanism is mostly dominant [91]. Typically, polymers show both mechanisms to be dominant, depending on the applied stress. As stated previously, fatigue testing at high stresses induces plasticity-controlled failure while lower stresses induce crack-growth-controlled failure. Typically, a change in slope can be recognized when there is a change in dominant failure mode. This phenomenon, together with the influence of static and cyclic loading, can be found in Figure 4.2.
It can be clearly seen that the plasticity-controlled region shows an increased lifetime in cyclic loading compared to the static loading case. This can be attributed to the fact that plastic deformation accumulates at a slower pace, as stated previously. On the other hand, cyclic loading induces a strong decrease in lifetime when crack growth is the dominant failure mode. This can be explained by looking at the tip of the crack. For static loading, this tip is stretched until it breaks and the load on the new crack tip is increased. This extra load causes the plastic deformation region behind the crack to increase, which is partly able to redistribute the new stress. In cyclic loading, this extra plastic zone is not formed as the force is unloaded before this can happen. Therefore, there is no redistribution of stress and therefore, this additional load significantly reduces the lifetime of a sample in crack-growth-controlled failure. Increasing the stress ratio R causes this effect to be more prevalent.
Both slopes of the cyclic tests can be fitted using the Basquin fit. The Basquin fit is a power law relation which can describe the linear slope between the applied stress and the number of cycles until failure. Typically, it is expressed in the form that can describe the number of cycles based on a reference value:

$$N = \frac{B}{S_r^m} \tag{4.2}$$

Here, N is the number of cycles up to failure, S_r is the reference value of the fatigue strength, m is the slope of the linear relation, and B is the stress at one cycle. Comparing the values of m and B at different temperatures, one can obtain valuable information on the number of failure modes present, and the temperature dependence of these failure modes.
Proper identification of the dominant failure mode is crucial when characterizing a material, such that the proper modelling considerations can be made and long-term performance can be improved.

CHAPTER 5

Literature Overview

Now that the different aspects that are relevant for high strain rate characterization of polymeric materials are clear, a look can be taken at what relevant studies have been conducted on this subject. First, a look is taken at high strain rate studies in general: what techniques are used to characterize high strain rate deformation response. As explained in the Introduction, extremely high strain rates can occur at tip speeds exceeding 100 ms^{-1}. Therefore, this study aims to reach strain rates of 10^4 s^{-1}, also known as the "High Rate" range [93]. Possible "well-established" methods to measure strain rates are discussed, that can measure these kinds of high strain rates.

Firstly, a split-Hopkinson bar is a commonly used apparatus for high strain rate characterization in either tension, compression or torsion, and it is well-described such that it can be used repeatedly [94, 95, 96]. Typically, strain rates of 10^2-10^4 s^{-1} can be obtained [97, 98]. Although this is in the range that the study desires, it should be taken into account that this way of testing induces many problems regarding the need for unconventional specimen sizes or inertia constraints [99, 100, 101]. These problems can be reduced using carefully controlled long-duration loading and pulse shaping in combination with high-speed imaging [102, 103, 104], leading to a complicated test setup.

Another widely applied method for measuring high strain rates is the Taylor impact test modified by Hutchings [105, 106]. This method uses the firing of material against a rigid target, after which the change of shape is measured [107, 108]. Typically, strain rates of 10^3 to 10^4 s^{-1} can be obtained [97]. The polymeric materials used in this study are subject to viscoelastic recovery after impact, such that the measurement of yield strengths is not accurate. However, materials can be tested fairly well to obtain ductile to brittle transformations and constitutive models can be covered using this test. However, this is outside the scope of this study. The inaccuracy of the results and the complexity of the setup make that this is not the best strategy for measuring high strain rates.
The last commonly used technique is the dynamic tensile extrusion experiment, which is a more recently used form of the Taylor series in the way that similar transitions in polymer responses are found. In this test, a polymer sphere is impacted into a converging nozzle at high speed, which can be observed by high-speed photography. Although strain rates of 10^5 s^{-1} can be reached with this method, studies show that this test is sensitive to the ductility of the specimen material [109, 110, 111].
With the most important mechanical test methods being discussed, it can be established that although it is possible to reach the required strain rates, it is often difficult to obtain repeatable results due to a complex setup, or due to the disadvantages of the particular tests. Therefore, a new testing method needs to be approached to diminish these drawbacks. A method to obtain similar data from polymeric materials is the use of time-temperature superposition. This induces the conduction of experiments over a range of strain rates at a single temperature and a range of temperatures at a single strain rate. Noting that the increase of the logarithm of the strain rate is equivalent to the decrease of temperature, the data collected at constant temperatures can be mapped on those obtained at constant rates, or conversely [97]. The rate sensitivity is an effect of underlying polymer transitions, which normally happen below room temperature, but now happen at elevated temperatures as strain rates increase. Using this technique, a master curve for different material properties of rate dependence can be constructed, extending data outside the range of experimentally accessible strain rates [46, 112, 113]. Although these studies date back more than 50 years, it is still a commonly used method. One example of this

data is the yield point of a polymer, which can be plotted using the Ree-Eyring equation. More information about this can be found in Section 2.3.1. More recently, this method has been applied to numerous well-known polymeric materials, such as PC, PVC, PMMA, PEI and PE. An overview of the maximum obtained strain rates in these experiments using time-temperature superposition can be found in Table 5.1.

Material	**Maximum strain rate** s^{-1}	**Reference**
PC	10^1 - 10^3	[43, 114]
PVC	10^1 - 10^3	[43, 115]
PMMA	10^3 - 10^6	[61, 115]
PEI	10^2	[116]
PE	10^3	[117]

Table 5.1: Maximum obtained strain rates for several polymers.

The problem with these test results is that they were mostly obtained using the complex testing methods that were described before using either extremely high strain rates or extremely low temperatures, which can cause difficulties when the tests have to be repeated many times for future modelling purposes. Furthermore, these materials are outdated as coatings for wind turbines, as there has been a shift towards more elastomeric LEP systems for rain erosion mitigation. Mostly thermoplastic elastomers based on polyurethane have been used [118]. Therefore, it is suggested to develop a test setup with a combination of low temperatures and high strain rates, which are available in most laboratory setups, all the while maintaining the aim to reach a strain rate of 10^4 s^{-1} with the use of Ree-Eyring and time-temperature superposition, that would enable the characterization of a larger domain of materials. However, some remarks regarding the use of Ree-Eyring and time-temperature superposition should be taken into account. Firstly, good thought should be given to the sample size used in the tensile tester: inertia problems may occur at higher strain rates for samples that are too large. This occurs because the stress generated by the specimen's inertia can reach a level that is significant to the intrinsic strength of the material [101, 119]. Secondly, strain rate sensitivity can be dependent on tensile testers that are hydraulic or screw driven [97]. Thirdly, specimen heating should be taken into account. The change from isothermal to adiabatic conditions for increasing strain rates is an important aspect of high strain rate deformation. Several authors showed that temperature rises are significant for high strain rates, which impact the yield behaviour due to the contribution of heat to plastic work [120, 16, 121]. At low strain rates, produced heat has time to conduct out of the specimen, keeping the temperature constant. However, at sufficiently high strains, the produced heat may remain in the specimen, depending on the material's thermal diffusivity. This heat might contribute to a part of the plastic work that the specimen will undergo [17]. On a log scale, this transition from isothermal to adiabatic conditions is proven to be relevant for the transition of multi-process transitions for a polymeric material [122, 123].
If this study can successfully characterize a material at high strain rates using reasonable strain rates and temperatures, fatigue testing for polymers can be carried out. This is needed to predict the lifetime of the LEP coating based on rain erosion, which causes impact fatigue. So, the low-temperature fatigue properties of a material should be characterized using the proposed testing method. From literature, it can be found that some low-temperature fatigue testing has been done, but these studies date back only include relatively standard polymers that are not used as LEP materials, such as PMMA, ABS, PC-ABS, PC and PVDF [124, 125, 126, 127, 128]. Consequently, there is a pressing need to obtain relevant material properties at high strain rates for modelling purposes of fatigue caused by rain erosion, while minimizing the reliance on expensive and time-consuming testing procedures.

5.1 Research Questions

With the problems of commonly used setups to obtain high strain rates and the challenges of using time-temperature in combination with the Ree-Eyring being known, the following objectives for this study can be stated:

1. Understanding the advantages and disadvantages of currently used methods to obtain high strain rate characterization of polymeric materials

2. Understanding the behaviour of polymeric materials at high strain rates, by means of low-temperature testing. This entails the research on PVC, PC and TPE at temperatures of -30 ^{o}C, -20 ^{o}C, -10 ^{o}C, 0 ^{o}C and 10 ^{o}C using strain rates of 0.66 s^{-1}, 0.209 s^{-1}, 0.066 s^{-1}, 0.0209 s^{-1} and 0.0066 s^{-1}.

3. Understand the fatigue behaviour of polymeric materials at high strain rates, including their failure mechanisms.

4. Apply the gained knowledge to wind turbine blade coating technologies and the relevance of said knowledge, such that future research goals can be identified.

With these objectives kept in mind, the final goal of this study can be stated as follows:

The development of a reliable and less complex test procedure to characterize material properties at high strain rates using low-temperature testing, including fatigue behaviour to model rain erosion of wind turbine blades.

If this can be done successfully, a simpler approach can be used to acquire high-strain material characteristics in terms of laboratory equipment. This will help current wind turbine coating technologies based on polymeric materials to be well-defined regarding the material properties, and therefore it can help tremendously at helping modelling material behaviour.

CHAPTER 6

Experimental Setup

6.1 Materials

For this study, different materials will be investigated such that a proper test procedure can be set up for characterizing polymeric (visco) elastic properties at high strain rates, using low-temperature testing. Polycarbonate (PC), Polyvinylchloride (PVC) and a thermoplastic elastomer (TPE) will all be tested using the experimental method discussed in Section 6.2, where a strain rate range and temperature range are specified that will be used. Within both these ranges, PC exhibits linear behaviour regarding the yield stress dependence on temperature and strain rate [43], whereas PVC exhibits multiple segmental motion processes that result in different behaviour [129]. More about this behaviour can be found in Section 2.3.1. Furthermore, a TPE is used such that a more elastomeric-like material is tested as well. These materials are more commonly used in LEP systems, and therefore give a better indication of how the testing method should look like. In this way, a variety of materials with different properties can be studied, such that an unambiguous test setup can be tested and validated, regardless of the material used.

The abovementioned materials were provided in sheets which were 2 mm thick for PC and PVC, and 0.7mm thick for the TPE. Dogbone samples were made according to NEN-ISO 37-S2, which is schematically shown in Figure 6.1. For DMA testing, rectangular samples were made, with dimensions of 50x5 mm, in length and width direction respectively. For the TPE, stamping was used to acquire the samples. The PVC and PC sheets were too hard to use this method and were therefore milled to get the required shape. The reason to choose these dimensions is that the effects of specimen inertia, discussed in Section 5, are tried to be minimized, while still having a sample that can be handled in terms of dimensions. Relevant dimensions for this dogbone are given in Table 6.1.

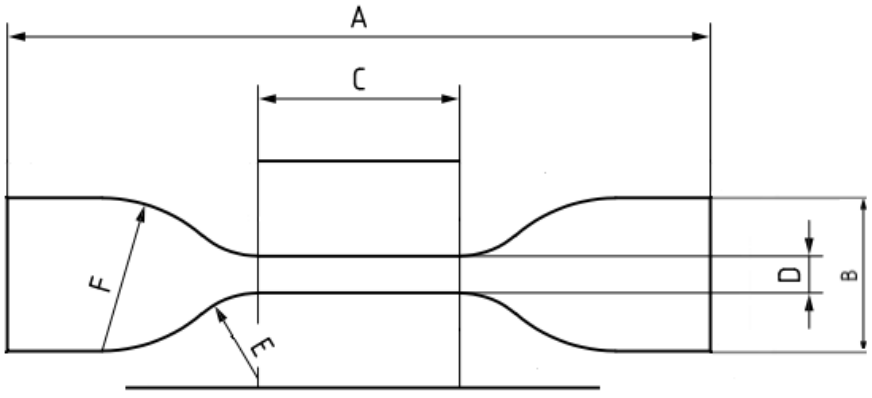

Figure 6.1: Typical dimensions for dogbone [130].

Dimension [mm]	Type S2
A - Overall length	75
B - Width of ends	12.5 ± 1
C - Length of narrow portion	25 ± 1
D - Width of narrow portion	4 ± 1
E - Transition radius outside	8 ± 0.5
F - Transition radius inside	12.5 ± 1

Table 6.1: Values for dimensions given in Figure 6.1 [130].

In order to be able to assess the material behaviour, it is important to look at how the three materials are composed. Therefore, a closer look will be taken at each material.

6.1.1 PC

Polycarbonate is a group of thermoplastic polymers containing carbonate groups in their chemical structures. Although there are multiple grades, the material typically is considered a strong and tough material that can be processed relatively easily. In this study, PC from SABIC Innovative Plastics is used. Most often, the material is formed using a condensation reaction with phenol and acetone, creating the following chemical structure:

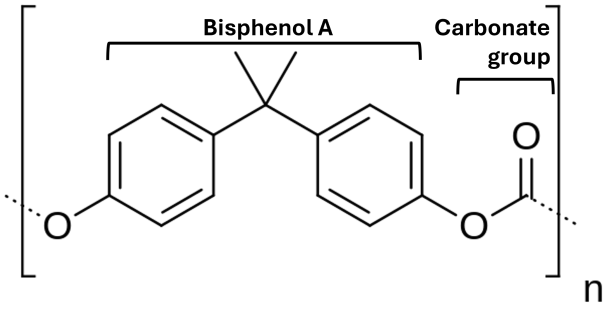

Figure 6.2: Chemical structure of PC, adapted from [131].

Due to the bisphenol A being in the side group, the main chain reacts relatively stiff, resulting in a high T_g for PC, being around 150 ^{o}C [132].

6.1.2 PVC

PVC is a rigid thermoplastic material that can be made softer and more flexible using plasticizers. Therefore, the material is often divided into rigid and flexible forms and therefore, many grades can be distinguished within this material. In this study, PVC-CAW provided by SIMONA is used, which is a rigid type of PVC. It is mostly produced by suspension polymerization of the monomer vinyl chloride, which gives the following chemical structure:

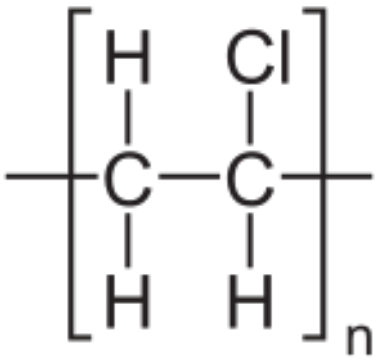

Figure 6.3: Chemical structure of PVC [133].

Compared to the structure of PC, it can be seen that the main chain is much more flexible due to the backbone having only single-bonded carbon atoms. However, the interaction of the Cl-group makes that the T_g increases

significantly compared to other materials with this 'simple' main chain. The T_g of PVC is around 60 ^{o}C [134].

6.1.3 TPE

A TPE is a thermoplastic elastomer, where a physical mix of polymers is formed into a copolymer. Using a TPE, one can use the advantage of the material having both thermoplastic and elastomeric properties. More specifically, it exhibits the elastic properties of rubber while being processable as a thermoplastic such that no vulcanization is needed, in contrast to elastomers. For the material used in this study, a specific configuration is used in which two 'building blocks' that form a block copolymer are used. A rigid, hard segment and a more soft segment. Both segments are being linked using a urethane bond. A schematic representation is given in Figure 6.4.

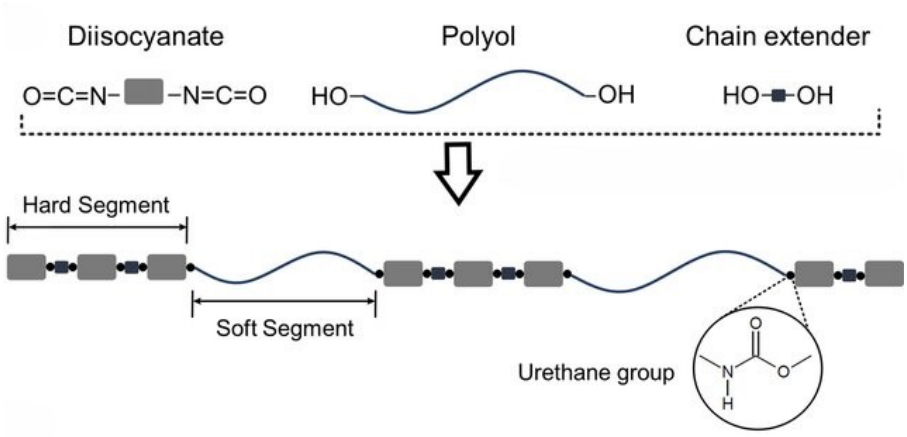

Figure 6.4: Schematic representation of a TPE using urethane bonds [135].

The chemical configuration is obtained using diisocyanates, short-chain diols (acting as chain extenders), polyols, and urethanes. Multiple segments of diisocyanates are bonded using urethane bonds, which create a rigid segment within the polymer chain. Alternating to this hard segment, a soft segment consisting of chain extenders is bonded using a urethane bond as well. The chain extenders usually consist of short-chain diols [136].
Although this type of TPE does not include crosslinks that can significantly change the mechanical properties of the material, there is a special trait that this material exhibits. The hard segments tend to align, creating a semi-ordered structure as a result. This is schematically depicted in Figure 6.5. This can be done as the chain extenders allow for flexible movement of the hard segments. Between the hard segments, hydrogen bonds can be formed. As they form throughout the entire group of segments, these hydrogen bonds act like a crosslink, albeit less strongly. When comparing a traditional crosslink and this group of hydrogen bonds when applying a load up to failure, one crucial difference should be noted. Upon increasing the load of a crosslinked material, more and more crosslinks are broken until the entire specimen is broken. Once a crosslink is broken, it will not contribute significantly anymore to withstand the applied force. For the set of hydrogen bonds, this is substantially different. Although a lower force is needed for the hydrogen bonds to break and for the hard segments to move relative to each other, new hydrogen bonds can be formed when a new set of hard segments aligns [137]. So, after the breakage of a hydrogen bond, it will still contribute to withstanding the applied force, in contrast to chemical bonds.

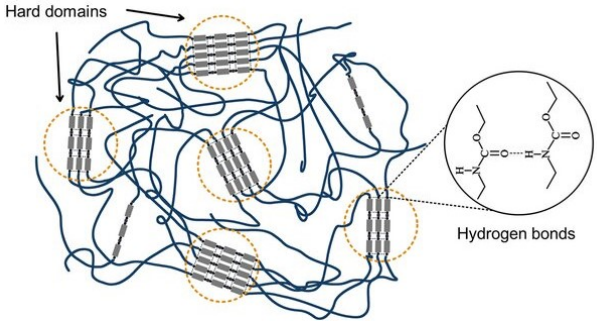

Figure 6.5: Alignment of hard segments within TPE [135].

6.2 Test setup

This section will discuss the different test setups for the tensile testing, the DMA testing and the fatigue testing.

Tensile testing
The tensile test setup consists of a ZwickRoell Retroline tensile tester, and an ESPEC SH-242 temperature and humidity chamber to regulate temperature. Furthermore, a clip-on extensometer was used to measure the displacement of the narrow portion of the dogbone during the test for PC and PC. The extensometer makes use of two small knives that move relative to each other upon loading the specimen. It uses strain gauges, and their high resolution allows for the measurement of small deformations. Furthermore, it excludes the machine displacement, as well as the displacement of the broader parts of the dogbones. In this way, a more accurate measurement of displacement was carried out, allowing for the calculation of more accurate strains and strain rates. However, the maximum displacement of this extensometer is 2 mm. For the TPE, the displacement of the samples is much higher and therefore, the clip-on extensometer can not be used. To mitigate the effect of the additional displacement of the broader part of the dogbone sample, rectangular samples are used for the TPE.
The clamps of the tensile tester are separated 45 mm, such that the length of the narrow portion of the dogbone (25 mm) can be positioned properly. This specific machine has a maximum testing speed of 30 mms^{-1}, which relates to a strain rate of 0.66 s^{-1} with a grip-to-grip separation of 45 mm. The Ree-Eyring relation uses a logarithmic scale for the strain rate, meaning that several decades should be covered by choosing the proper test speeds. Therefore, also testing speeds of 3 $\text{mm}\,\text{s}^{-1}$ (0.066 s^{-1}) and 0.3 $\text{mm}\,\text{s}^{-1}$ (0.0066 s^{-1}) to cover 3 decades, with also testing speeds of 9.3 $\text{mm}\,\text{s}^{-1}$ (0.207 s^{-1}) and 0.93 $\text{mm}\,\text{s}^{-1}$ (0.0207 s^{-1}) in between these decades will be used for this study. Another reason to choose these strain rates is the absence of specimen heating, which was discussed in Section 5. Studies have shown that these strain rates are sufficiently low to diminish the effect of this specimen heating. Furthermore, this study wants to focus on the use of low-temperature testing to obtain high-strain rate material characteristics. Therefore, the temperatures at which tests are performed should be as low as possible. The temperature chamber has the lowest operating temperature of -40^o C. However, this temperature may not always be reached due to external factors. To ensure the repeatability of the tests, it is therefore chosen to use -30^o C as the lowest temperature to be tested at. With increasing steps of 10^o C, tests will also be conducted at temperatures of -20^o C, -10^o C, 0^o C and 10^o C for constant strain rates. For PVC, an additional temperature of -25 ^{o}C was used to be able to better characterize the transition from one to multiple relaxation processes. PC and PVC samples are first heated above their respective T_g, which can be found in the previous section. TPE is stored above its T_g and therefore, there is no need to rejuvenate the samples first. This is done to reduce the effects of the physical ageing that might influence Young's modulus or the yield stress, as explained in section 1.2.2. After this procedure, the sample is placed in the tensile tester and the climate chamber cools the sample to the desired temperature. When this is done, the test can be executed. First, a sample is tested until failure such that the relevant parameters for the remaining tests can be determined. More specifically, the tensile test for PC and PVC can not be done up to failure as the displacement of the sample would exceed the maximum of 2 mm of the clip-on extensometer. Stopping the test just after the yield point of the material prevents damaging the clip-on extensometer while gathering relevant information. As the knives of the clip-on were originally spaced 11.79 mm, tests for PC were stopped at a machine displacement of 3.7 mm and tests for PVC were stopped at a machine displacement of 2.7 mm. These values make sure that the yield stress of the material is reached and that the test stops soon after while keeping the maximum displacement of the clip-on at around 1.5 mm.
For the tests of TPE samples, rectangular samples are used. Although this leads to the fact that there will be stress concentrations around the clamps, it allows for a better estimation of the strain rate during the test. If a dogbone sample were to be used, stresses would be directed towards the clamps more evenly but the gradual transition from the narrow to the broad part of the dogbone samples leads to the fact that there is no indication of the actual strain rate at the position where failure occurs. As this study is focussed on the use of the relation between temperature and strain rate, the tradeoff is made and therefore, the choice is made to test the TPE with rectangular samples. Although this eliminates the effect of the geometry of the sample, one should still consider machine displacement. As no clip-on can be used because of the high displacement, calculations on strain and strain rates need to be done using the output data from the tensile tester, which still includes the machine displacement. Therefore, close consideration should be given when analysing these results.
Combining the displacement results of the clip-on extensometer and the force data from the tensile tester, stress-strain diagrams can be obtained for PC and PVC samples. To allow for more practical applications and account for the geometry changes during testing, the true stress and true strains will be used for these diagrams. From this data, the true yield stress can be determined, which will be evaluated using the Ree-Eyring theory to predict the material behaviour at higher strain rates which are beyond the experimentally obtainable range.

DMA testing
For the DMA testing, a DMA Eplexor 2500 was used. First, a temperature sweep of all materials was performed using rectangular samples to see if T_g was in the relevant testing window. As the testing range of the tensile test was set to -30 ^{o}C to 10 ^{o}C, the choice was made to set the testing temperature range such that these temperatures were effectively measured. Therefore, the temperature was set at -80 ^{o}C to 30 ^{o}C, with an increasing time step of 2 ^{o}C, at 10Hz. Especially the lower bound of the temperature range was set significantly lower, to be able to detect a glassy plateau that is needed for the determination of T_g using the storage modulus method (See Section 3.3). Furthermore, the choice for a frequency of 10Hz is based on the fact that adiabatic effects will play a role if the frequency is too high. However, choosing the frequency too low will lead to excessive duration of the test. During the test, a static strain of 0.2 s^{-1} was applied for all materials, while a dynamic strain of 0.1 s^{-1} was applied. This makes sure that the material is being characterized in the linear elastic region of the material. With this test, relevant information for the storage modulus, loss modulus and tan δ were obtained. For the frequency sweep, only the TPE was considered. This is done to characterize the viscoelastic properties of the material. There is a need for this as the T_g of the TPE was found to be close to the testing temperatures, being around -28 ^{o}C As the T_g for PC and PVC were much higher, there was no need to carry out a frequency sweep for these materials. To effectively capture the viscoelastic behaviour below and above T_g, a temperature range of -60 ^{o}C to 20 ^{o}C was set, with a temperature step of 5 ^{o}C. Furthermore, a frequency range of 0.1 Hz to 10 Hz was set. Choosing 3 decades allows for the construction of a mastercurve. These relatively low values were chosen for the same reason as explained for the temperature sweep. In this frequency range, there was a frequency increment of 3/decade, leading to 7 frequencies for a single temperature. Furthermore, the static and dynamic strains were the same compared to the temperature sweep, being 0.2 s^{-1} and 0.1 s^{-1} respectively. Using this test, the relevant elastic behaviour of the material is characterized.

Fatigue testing
For the fatigue testing, only the TPE was considered as this is the material that is closest to the real-life application for wind turbine coating. The settings of the fatigue testing procedures are force-controlled and therefore, the testing procedure uses this as well. This is valid as the samples all have the same dimensions within the NEN-ISO 37-S2 tolerances [130]. The testing occurs at a maximum machine speed of 1800 mm/min with a clamp-to-clamp distance of 45 mm. The R-ratio for this test is 0.1, meaning that the minimum force is 10% of the force that is set for testing. The machine applies the maximum and minimal forces in a zigzag form, rather than a smooth sinusoidal form. Applying the maximum and minimum force once is considered to be one cycle and the machine continues to do this until the sample breaks. The number of cycles until failure is the important outcome here.
First, rectangular samples were used for this. The results of the tensile testing give valuable information. Firstly, the force at which the material breaks is important, such that this value is not exceeded in fatigue testing. Furthermore, the force at which yield occurs, or the estimation thereof using the inflection method (Section 2.2.1), is an important value. By characterizing both forces, a test can be conducted below and above the force at which yield occurs, as the characterization of the fatigue behaviour might differ in terms of crack-growth-controlled failure or plasticity-controlled failure. However, as was expected from the tensile testing, the samples all failed at a location close to the clamp, which indicates clamp failure due to localization of stresses. To minimize this effect, the same tests were performed using dogbone samples. So, a tradeoff is made between a more accurate strain rate at the point of failure, but stress localization occurs due to which lifetime prediction is less accurate, or strain rate is less accurate at the point of failure but the number of cycles until failure is more accurate. For this TPE, the important testing values are summarized in Table 6.2, together with the forces at which tests were performed.

Temperature	**Samples**	**F_t [N]**	**F_y [N]**	**Tests $\geq F_y$ [N]**	**Tests $< F_y$ [N]**
-30 ^{o}C	Rectangular	135	115	120, 115, 95	110, 105, 100, 90, 85, 80, 70, 60
-20 ^{o}C	Rectangular	120	80	100, 95, 90, 85, 80	75, 70, 60, 50, 40
-10 ^{o}C	Rectangular	105	45	105, 90, 85, 80, 75, 70, 65, 60, 55, 50	40
-30 ^{o}C	Dogbone	180	95	160, 140, 130, 120, 110, 100, 95	90, 85, 80
-20 ^{o}C	Dogbone	150	60	130, 120, 110, 100, 95, 80	-
-10 ^{o}C	Dogbone	145	35	130, 120, 110, 100, 90	-
0 ^{o}C	Dogbone	160	20	130, 120, 110, 100, 90	-

Table 6.2: Forces at which fatigue testing is conducted, with a strain rate of 0.66 s^{-1}

Lastly, SEM microscopy was used to determine the fracture behaviour of the materials. By coating the samples using gold, there is a conductive layer around the fracture surface that enables SEM microscopy. It gives

an indication on whether plasticity-controlled or crack growth-controlled failure is dominant for the samples. Furthermore, in the case of crack-growth dominance, the amount of cracks and the distance between cracks might be an indication for the temperature dependence of fatigue failure. Therefore, the portion of the sample that has crack-growth controlled failure will be examined by looking at the crack density in the middle 0.5 mm of the break surface. For fatigue testing, the following samples were examined: -30 ^{o}C with 95N (34.3 MPa), 80N (30.7 MPa) and 85N (29.9 MPa), and -20 ^{o}C with 100N (36.2 MPa) and 80N (29.9 MPa). The choice for these samples is based on the fact that this allows for testing at and below yield for -30 ^{o}C and for testing below and above yield for -20 ^{o}C.

CHAPTER 7

Results & Discussion

In this chapter, the results of the experimental works will be discussed. Firstly, the temperature sweep results of PC and PVC are discussed. Then, a look is taken at the yield stress dependence on strain rate and temperature for PC and PVC using the Ree-Eyring fits. Then, the remainder of the chapter will focus on the TPE, where the results of the temperature sweep and the frequency sweep will be discussed first. After this, the yield stress dependence on strain rate and temperature will be discussed. With this information, the relation between fatigue and high strain rate behaviour will be established.

7.1 PC & PVC

In this section, the results of the testing with the PC and PVC samples will be discussed.

7.1.1 DMA testing

In order to determine whether or not the thermal history of the material plays a role, temperature sweeps for both PC and PVC need to be studied. The results of both temperature sweeps can be found in Figure 7.1.

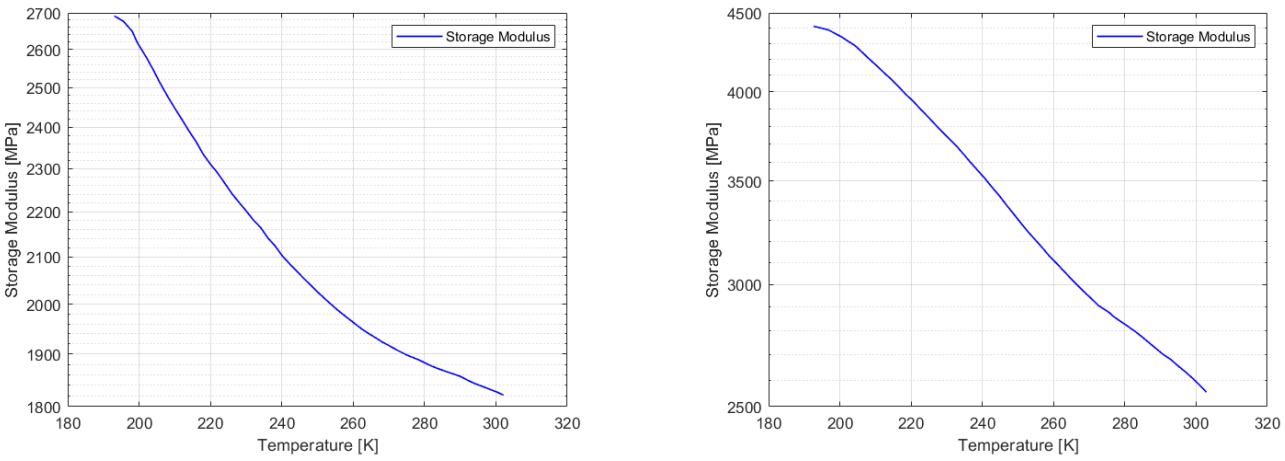

(a) (b)

Figure 7.1: Temperature sweep for storage modulus from -80 ^{o}C to 30 ^{o}C with a 2 ^{o}C temperature step at 10Hz. a) PC, b) PVC.

It can be seen that there is no drop in storage modulus on a logarithmic scale for both materials. This indicates that the temperature range in this test does not entail the T_g of both materials. However, the PVC results show a similar trend compared to the method of determining the T_g using the storage modulus. In Section 3.3, both a logarithmic decrease and a plateau should be present, but this is not the case. Although the storage modulus seems to drop significantly throughout the test, a logarithmic scale would reveal that the data is more

plateau-like as all data points are in the order of magnitude of thousands. Compared to the elastic modulus as a function of the temperature in Figure 1.3, the data is either completely in the glassy state or completely on the rubber plateau. One can determine in which state the material is by looking at the loss modulus and tan δ. The results from the temperature sweep showing both datasets for both materials can be found in Figure 7.2.

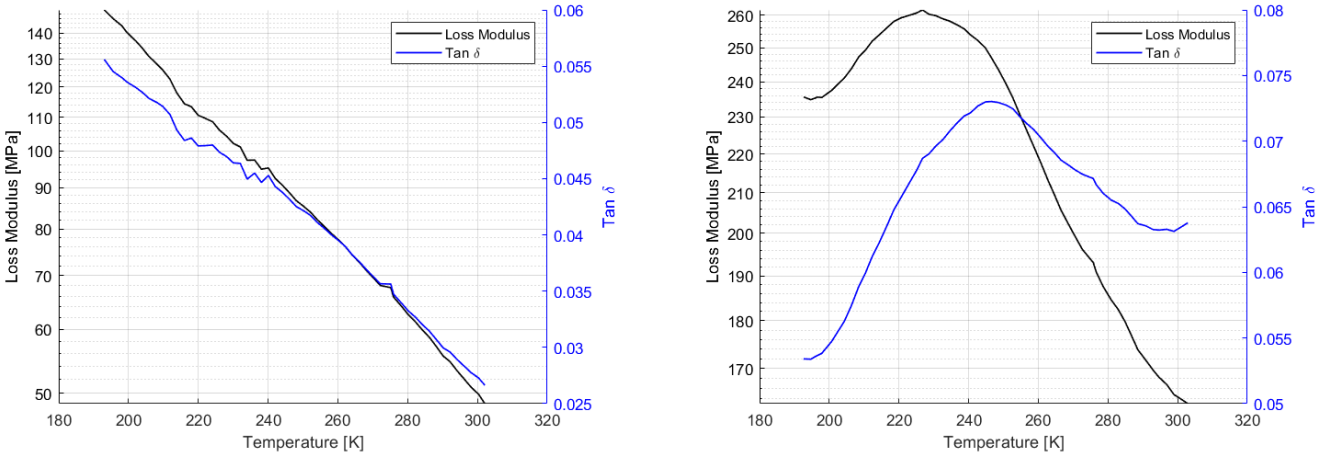

Figure 7.2: Temperature sweep for loss modulus and tan δ from -80 ^{o}C to 30 ^{o}C with a 2 ^{o}C temperature step at 10Hz. a) PC, b) PVC.

For PC in Figure 7.2, it can be seen that no peak in either the loss modulus or tan δ can be observed and therefore, there is no T_g in this temperature range according to the T_g determination methods using the loss modulus or tan δ, as explained in Section 3.3. Furthermore, it can be seen that values of tan δ are relatively low. This is because the loss modulus values are low compared to the storage modulus values. Where the storage modulus is in the order of thousands, the loss modulus is in the order of hundreds. This indicates that the material is behaving more elastically rather than viscous.
Looking at the loss modulus and tan δ for PVC, a distinct peak in both loss modulus and tan δ can be observed and one might argue that the T_g can be determined here. In fact, plasticized PVCs do indeed have T_g values around this temperature. However, the fact that the storage modulus does not give an indication for the T_g and the fact that similar to PC, the values of the loss modulus and tan δ are relatively low, it is believed that these peaks do not represent the T_g. This can be explained by the fact that there is only a minor difference between the lowest tan δ value of around 0.05 and the highest value of around 0.07, while peaks in tan δ are usually reported at a value of around 0.4-0.8, depending on the PVC blend [138, 139] From Section 6.1.1 and 6.1.2, it can be found that PC has a T_g of around 150 ^oC, and PVC has a T_g of around 60 ^oC. Using this information and the results of the temperature sweep, it can be stated that both materials are in a glassy state. More specifically, as the testing temperatures are well below the T_g of both materials and the fact that it is proven that the materials behave elastically, it can be stated that the materials exhibit glassy behaviour. Being in a glassy state means that thermal history, as explained in Section 1.2.2, does influence the material properties upon storing the samples at room temperature. Therefore, the samples should be heated above their respective T_g to minimize the effect of physical ageing.

7.1.2 Tensile testing

Now that the relevance of physical ageing is established, the results of the tensile testing that was done after heating the samples can be discussed. Figure 7.3 shows the result of the temperature and strain rate dependence of both PC and PVC. For PC, it can be seen that the slopes of every testing temperature are almost identical. This indicates that there is only a single relaxation process active, referred to as the α-process. Using the same slope for data of every temperature, which is a prerequisite for the single-relaxation process fit of Ree-Eyring, most data points can be captured. The Ree-Eyring fit describing a single relaxation process, using equation 2.3.1, fits the experimental data rather well. Only at lower strain rates and lower temperatures, some data points deviate from the Ree-Eyring fit.
For PVC, it can be seen that the data points at temperatures of 0 ^{o}C and 10 ^{o}C follow a single linear trend that is similar in slope. This indicates a single relaxation process, again referred to as the α-process. For the data points of -10 ^{o}C and -20 ^{o}C, a small increase in slope can be seen from a strain rate of around 0.1 s^{-1} and higher. This is an indication that the combination of these temperatures and strain rates is the onset of the activation of

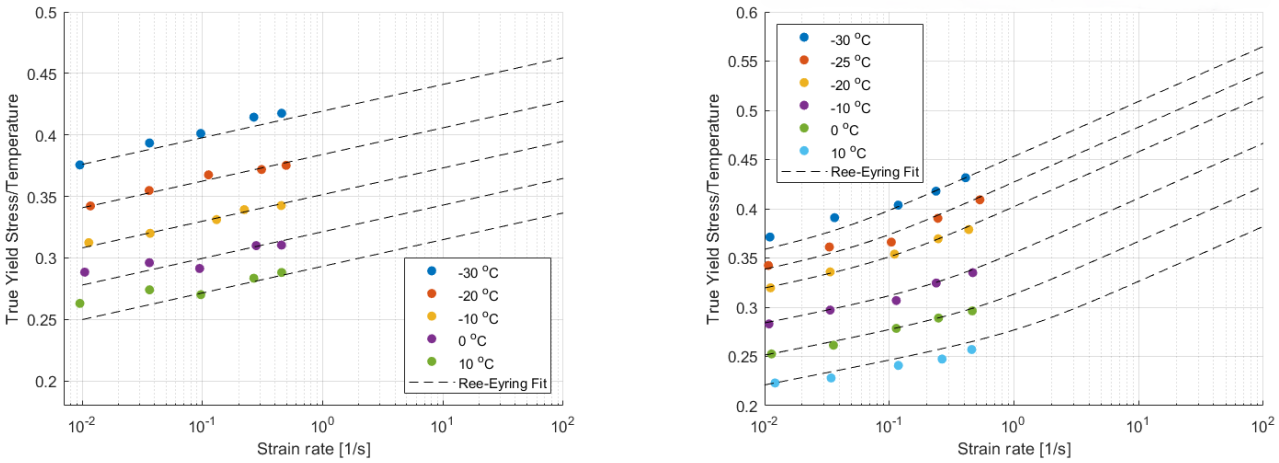

(a) (b)

Figure 7.3: True yield stress over temperature with Ree-Eyring fit. a) PC, b) PVC.

a second relaxation process. This is referred to as the β-process. For the data points at temperatures of -25 ^{o}C and -30 ^{o}C, the transition from a single relaxation process to multiple relaxation processes is more distinct at a strain rate of around 0.1 s^{-1} and higher, resulting in a significantly higher slope. Looking at the Ree-Eyring fit that incorporates multiple relaxation processes, as given by Equation 2.8, it can be seen that the α-process is considered fairly well, albeit that some data points deviate slightly from the fit. For higher temperatures, it can be seen that the accuracy of the fit shifts more towards the β-process and the combination of both processes at higher strain rates.
In Table 7.1, the relevant modelling parameters used in the Ree-Eyring fit are presented, together with values from literature, for both PC and PVC.

Material	**Relaxation Process**	$\dot{\varepsilon}_0$ [s^{-1}]	ν^* [nm^3]	ΔU [kJ mol^{-1}]	**Reference**
PC (tested)	α	$1.5{\cdot}10^{22}$	1.46	191	[-]
PC (literature)	α	10^{22} - 10^{31}	2.26 - 3.40	315	[43, 140]
PVC (tested)	α	$5.84{\cdot}10^{22}$	1.28	181	[-]
	β	$3.12{\cdot}10^{9}$	1.02	50	[-]
PVC (literature)	α	10^{38}	2.01	295	[43]
	β	10^{9}	1.40	60	[43]

Table 7.1: Obtained Ree-Eyring parameters compared to literature

It can be seen that the strain rate constant of the α-process of PVC in this study deviates significantly from the value in literature: this study obtains a strain rate constant in the order of magnitude of 10^{22}, while literature suggests it should be in the order of 10^{38}. Other Ree-Eyring parameters obtained in this study are in the same order of magnitude compared to values in literature. However, it should be noted that all three parameters are interrelated: changing one parameter slightly might have a significant impact on the other two parameters. This might explain the significant difference in values for the strain rate constants for the α-process for PVC. More in-depth thought about this will be given in the discussion.

7.1.3 Discussion

Firstly looking at the results of the temperature sweep of the materials, it can be concluded that the main takeaway of this test is that the materials both have a T_g that is substantially above room temperature. This is in accordance with values found in literature. Furthermore, the establishment of the fact that the materials are in a glassy state makes sure that there is no need to go in-depth into these results. Even if the test can be carried out in a more precise way, the new results would not affect the outcome of the test. The conclusion is that there is a need to minimize the effect of the thermal history before carrying out the test.
Looking at the results of the tensile testing of PC, given in Figure 7.3a, it was established that most data is mostly captured by the fit: the data points that are not on the Ree-Eyring fit have some experimental scatter. As stated in the results section, this was prevalent for lower temperatures and lower strain rates. In order to minimize this effect, more tests can be performed at a combination of temperature and strain rates that do not fit the Ree-Eyring in the current result. This would lead to the fact that the experimental scatter is

minimized and subsequently, the Ree-Eyring parameters are optimized. This might yield different results for the parameters but these are not necessarily better: as stated in the final part of Section 7.1.2, all three parameters are very much dependent on each other and subsequently, optimizing one parameter might not necessarily yield a better fit. Therefore, it is most important to obtain the parameters in the same order of magnitude rather than getting the exact same values. This was indeed the case for the tested PC that was compared to literature values.
For the evaluation of the fit of the PVC testing, given in Figure 7.3, some more consideration is required. As the Ree-Eyring fit at relatively high temperatures, say 10 ^{o}C and 0 ^{o}C, only applies to a single relaxation temperature, the fit captures the data points fairly decent as it is based on these two temperatures. Some deviation is found due to experimental scatter caused by a lack of data points, similar to PC. At -10 ^{o}C and -20 ^{o}C, the data points are captured pretty well with only some deviation occasionally. At the lowest temperatures, it can be seen that the fit is less accurate in capturing the α-process. This can be attributed to the fact that the α-process is fitted for the temperatures of 10 ^{o}C and 0 ^{o}C. Furthermore, the transition point from a single relaxation process to multiple processes shifts to lower strain rates for lower temperatures [43]. This leads to the accuracy of the α-process being compromised. However, fit results yield a very accurate fit at the lowest temperatures for the β-process. As this process is fitted on these two temperatures, this is a logical consequence. To summarize the behaviour of the fit, it should be noted that the α-process at higher temperatures is more accurate. For lower temperatures, the accuracy of the fit needs to compromise between both relaxation processes, where the choice is made to fit the situation with multiple relaxation processes as these temperatures show this behaviour most prevalent. Lastly, the observation that there is a distinct difference between ε_0 obtained in this study and found in literature should be discussed. This can be attributed to the fact that there might be a difference in the type of PVC material. The value obtained from literature does not specify a specific type, and therefore it is not known whether a flexible or rigid PVC was used.

7.2 TPE

The remainder of this chapter will discuss the results of all tests that have been performed using the TPE material. These include DMA testing, tensile testing, fatigue testing and the evaluation thereof using a SEM-microscope.

7.2.1 DMA testing

For the DMA testing of the TPE, a similar temperature sweep was carried out compared to the test of PC and PVC. The result can be found in Figure 7.4. Using the storage modulus data in combination with the

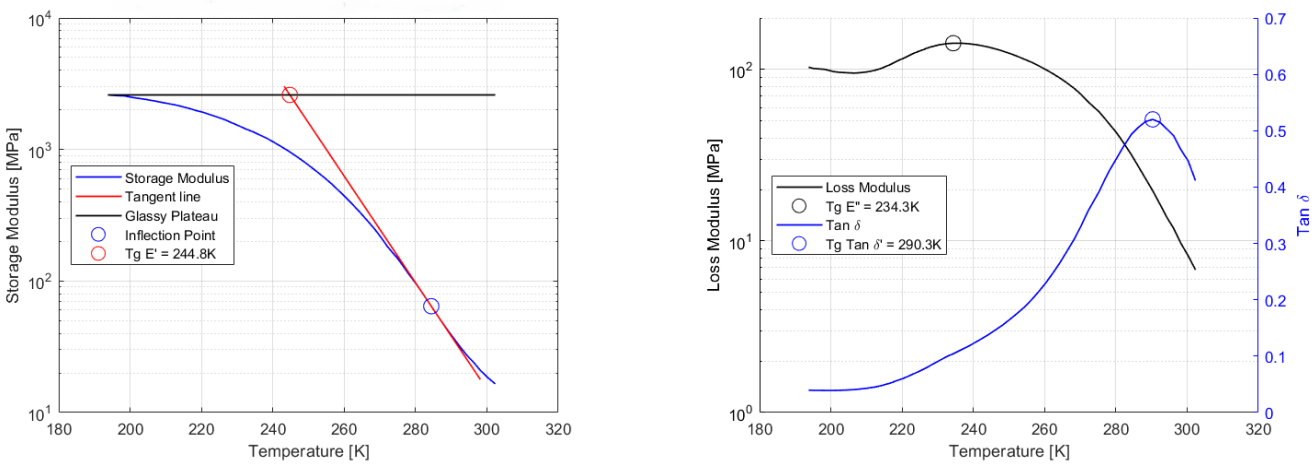

(a) (b)

Figure 7.4: Temperature sweep from -80 ^{o}C to 30 ^{o}C with a 2 ^{o}C temperature step at 10Hz with T_g determination. a) using storage modulus, b) using loss modulus and tan δ. See Section 3.3 for more information.

inflection method, the TPE appears to have T_g of around -28 ^{o}C. As this study is mainly focussed on the elastic behaviour of the material, the value of T_g from this method is used for further characterization of the TPE. However, it should be noted that when looking at the T_g obtained from the loss modulus and tan δ, there is a significant difference between the lowest and highest obtained values. More specifically, the temperature at which the peak of the loss modulus occurs is around -39 ^{o}C and the temperature corresponding to the peak in

tan δ is at around 17 ^{o}C. Another important aspect that needs to be considered is the broadness of the peaks. Although the peak in tan δ is relatively sharp and smooth, indicating a less ambiguous T_g determination, it can be seen that the peak in the loss modulus is significantly broader. The last insight in these results that should be noted is the fact that the T_g from the loss modulus is lower than the one from the storage modulus, which is uncommon for a large range of polymers [86]. The fact that the T_g determined from the tan δ is the highest is common for a large range of polymers, albeit the difference between the three values is normally spread over a much smaller range [141, 142].

When looking at the results of the frequency sweep, given in Figure 7.5a, it can be seen that the Arrhenius equation and the WLF equation provide a reliable fit for the temperatures below and above T_g respectively, given in Figure 7.5b. The results of these fits give the Arrhenius activation energy of 219 kJ, and WLF parameters $C_1 = 37$ and $C_2 = 148$ K when a T_g of 244.8K is used, obtained from the storage modulus in the temperature sweep.

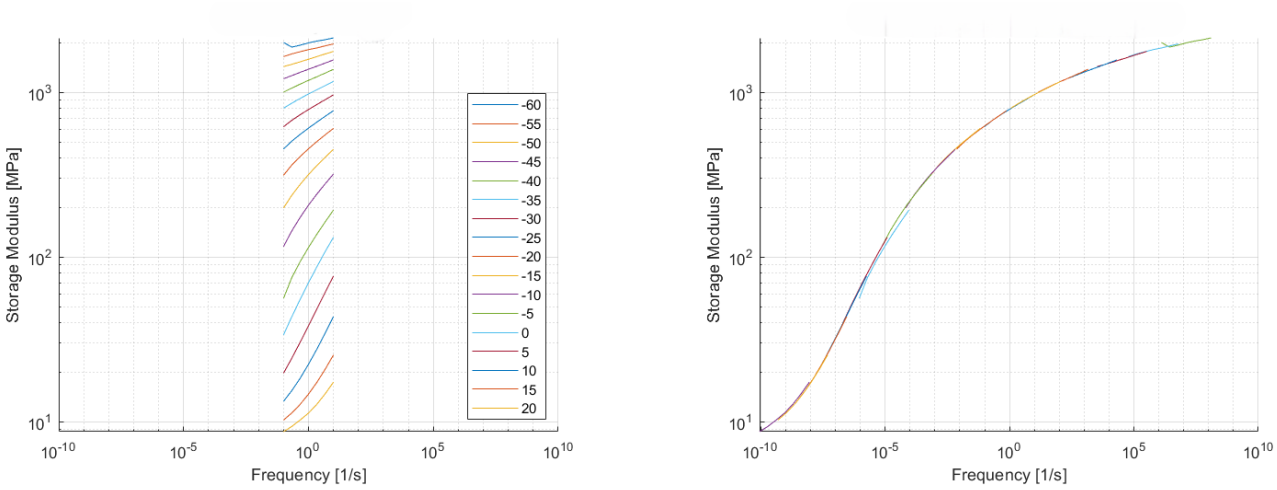

(a) (b)

Figure 7.5: Frequency sweep for TPE. a) Obtained data, b) Mastercurve using Arrhenius and WLF fits.

7.2.2 Tensile testing

Tensile testing results of the TPE material can be found in Figure 7.6a. Although there is a linear relation between the strain rate and the temperature at a given temperature, it can be seen that the strain rate dependence of the yield stress becomes less prevalent when the temperature is increased. This indicates that the chosen testing temperatures are above T_g, as the polymer chains have increasingly more chain mobility which leads to a less steep increase in the yield stress for higher temperatures. Something that is interesting to observe as well is the fact that the data points at the highest strain rate seem to be lower than the linear trend of the other data points at the same temperature.
Looking at the estimation of the yield stress beyond the used strain rates, the fit is obtained using the WLF parameters obtained from the DMA section. It can be seen that a proper fit can not be formed. Therefore, it was manually shown by trial-and-error that using the values of $C_1 = 18$ and $C_2 = 80$K provide the best fit if the yield stress of the TPE material needs to be estimated using the Ree-Eyring estimation provided by equation 2.9, using the T_g of 244.8K. This is given by the fit used in Figure 7.6b.

7.2.3 Fatigue testing

Using an extended version of the fit in Figure 7.6b at a reference temperature of 10 ^{o}C, together with the lowest temperature and the highest strain rate that were tested, it can be found that this TPE was tested equivalent to a maximum strain rate in the order of magnitude 10^4 s^{-1}, as can be seen in Figure 7.7 using the vertical red line. However, it can also be seen that an additional Ree-Eyring fit is plotted with a dashed red line, for a temperature of 20 ^oC. Although no tests were performed at this temperature, the Ree-Eyring fit allows for the estimation of the yield stress at this temperature. By including this temperature, a range of operation temperatures for wind turbines can be simulated without testing. The vertical red and green lines indicate an example of how the high strain rate characterization works. At a temperature of -30 ^{o}C and a strain rate of 0.66 s^{-1}, a horizontal line can be drawn until the fit of the reference temperature is reached. If one looks at the strain rate at this point, indicated by the vertical red and green line, the strain rate that is resembled by

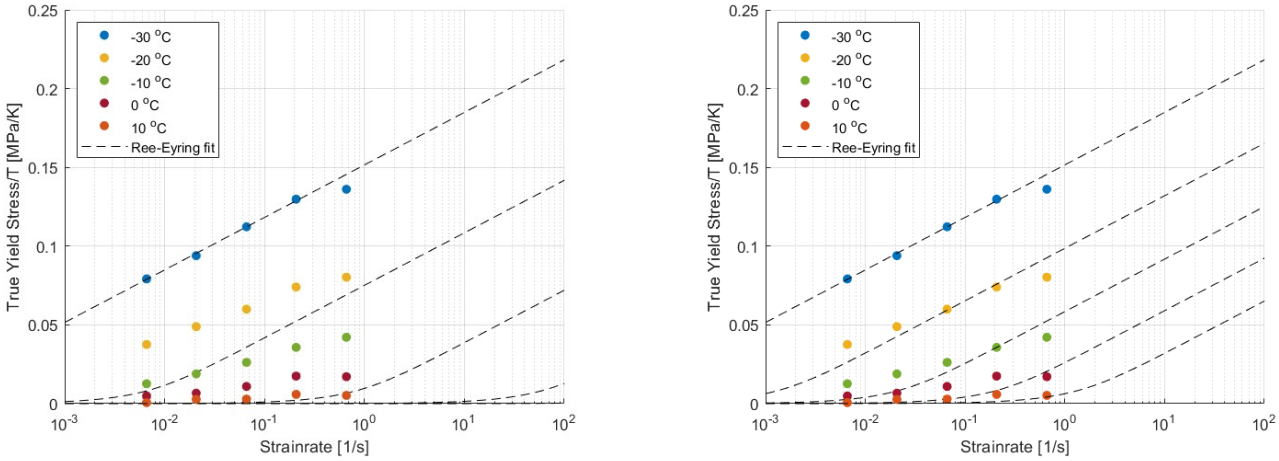

(a) (b)

Figure 7.6: True yield stress over temperature for TPE using Ree-Eyring fit, with a T_g of 244.8K. a) $C_1 = 37$, $C_2 = 148$ K. b) $C_1 = 13$, $C_2 = 80$ K.

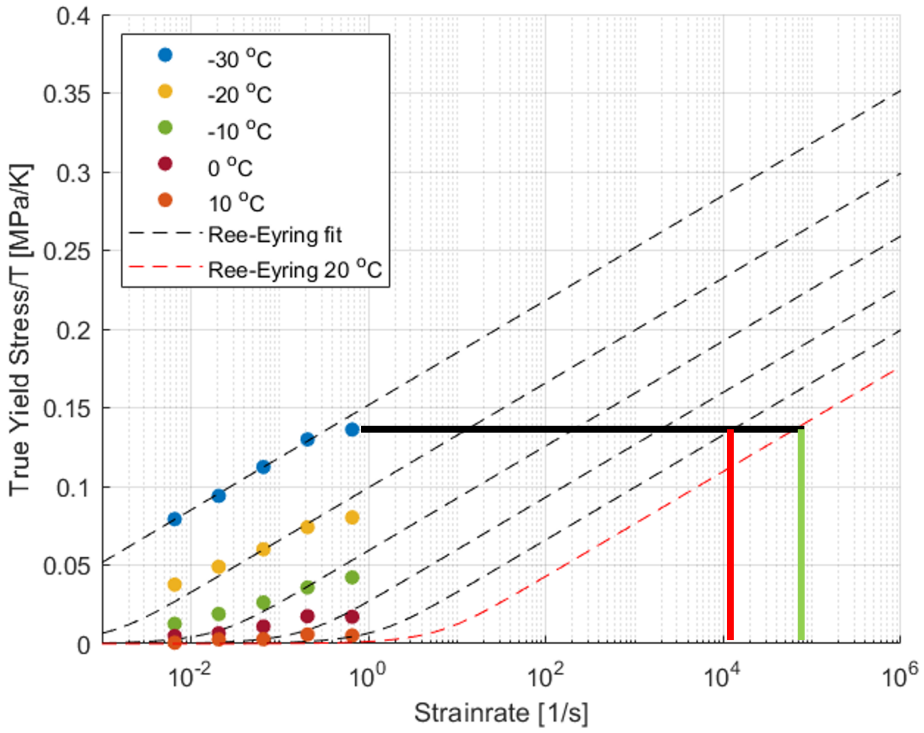

Figure 7.7: Characterization of high strain rate behaviour at a reference temperature of 10 ^{o}C using the Ree-Eyring estimation for the yield stress.

this data point can be estimated. Therefore, it can be stated that tests performed at -30 ^{o}C and 0.66 s^{-1} are equivalent to a strain rate of around 10^4 s^{-1} at 10 ^{o}C, and to around 10^5 s^{-1} at 20 ^{o}C. Looking at temperatures of -20 ^{o}C and -10 ^{o}C in combination with the highest strain rate yields a characterization of the material at a strain rate of 10^2 and $10s^{-1}$ respectively.

Firstly, a look is taken at the results when rectangular samples were used for fatigue testing. This can be seen in Figure 7.8a. Taking 1 cycle for the tensile tests that were performed up to failure, it can be seen that the material yields a linear relation between the applied stress and the lifetime of the TPE, for every temperature. This is also fitted using the Basquin fit, given by equation 4.2. The relevant parameters of the Basquin fit can be found in Table 7.2.

The spread of multiple data points for the same applied stress is acceptable. Changing the magnitude of the applied stress from above to below yield does not change the slope of the linear relation. Furthermore, the entire spectrum of the number of cycles until failure can be described by a linear relation with a single slope.

Temperature	m	B
-30 ^{o}C	-4.46	10^{34}
-20 ^{o}C	-4.31	10^{30}
-10 ^{o}C	-4.03	10^{26}

Table 7.2: Relevant Basquin parameters corresponding to Figure 7.8a.

This indicates that there is no change in the dominant failure mode, but that the material fails due to a single dominant failure mode. Furthermore, it can be seen that the slope of the number of cycles does not appear to change for varying temperatures. Lastly, the data points seem to shift linearly towards a lower number of cycles for higher temperatures, which indicates the temperature dependence on the fatigue lifetime.

However, it should be noted that the rectangular specimens gave rise to the problem that failure occurred in the clamp of the tensile tester, as there was a stress concentration at this point. Therefore, the same experiments were performed using dogbone samples. This can be found in Figure 7.8b. Although for these samples, the exact strain rate is not known due to their varying geometry, it gives a better indication of the lifetime of the material. Comparing the results of the dogbone samples, it can be seen that again there is a linear relation between the applied stress and the number of cycles until failure albeit that higher stresses are obtained as the dogbone samples allow for better spread of the stress. However, the data points show more spread at a given stress compared to the rectangular samples. Furthermore, it can be seen that the temperature dependence on the lifetime is prevalent for the temperature of -30 ^{o}C, but diminishes as the temperature increases. Data points of -20 ^{o}C, -10 ^{o}C and 0 ^{o}C show that within the logarithmic error range, values are quite similar in contrast to the rectangular samples where a clear shift can be observed. This means that the rate at which the failure mechanism occurs is dependent on the temperature for lower temperatures, but the temperature sensitivity is less prevalent for higher temperatures. Although the slope of all temperature data points is not unambiguous to identify, no visible shift in slope can be identified. That is, within one temperature the slope does not seem to change significantly, and the slopes of different temperatures compared to each other do not seem to differ significantly. This indicates that for dogbone samples, there is one active failure mechanism. Temperature does not change the failure mechanism that is present, but it does change the rate at which it propagates.

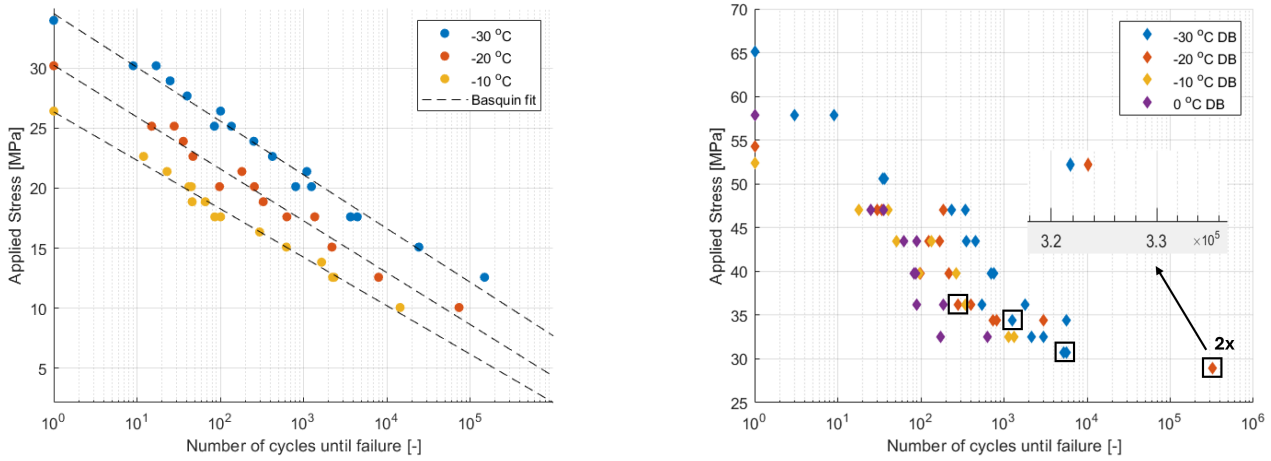

(a) (b)

Figure 7.8: Fatigue testing at a strain rate of 0.66 s^{-1} using a) rectangular samples with Basquin fit b) dogbone samples. Black boxes indicate samples investigated using SEM microscopy.

7.2.4 SEM microscopy

Following the fatigue testing, some dogbone samples were studied using SEM microscopy. The choice was made for dogbone samples instead of rectangular samples, as the dogbone samples represent the failure behaviour better. This was done to study the active dominant failure mechanism throughout the fatigue testing. The results can be found in Figure 7.9. Appendix 10.1 provides zoomed-in figures that allow for discussion of the results in higher resolution. It can be clearly seen that, based on the way how the sample was put in the SEM, either the right-hand side or the left-hand side shows plasticity-controlled failure, whereas the opposite side does not show significant plastic deformation, which indicates crack-growth failure. More specifically, looking at the samples individually, Figure 7.9a shows that the sample tested at -30 ^{o}C and 95N (34.3 MPa) has plasticity-controlled failure on the left-hand side and more crack-growth failure on the right-hand side. The plasticity-controlled region is around 40%, ending at the right-hand side of the crater-like deformation on the top. The region on the right from this is dominated by cracks, which can be observed. It can be seen that most cracks are in a horizontal direction, having the greatest lengths. Some vertical cracks are identified, but these are in general shorter in length. It should be noted that the density of the cracks does not change significantly when moving more to the crack-growth-controlled region. Figure 7.9b shows the dogbone sample at -30 ^{o}C and 85N (30.7 MPa). Here, it can be seen that the right-hand side is controlled by plastic deformation, whereas the crack-growth controlled region is dominant on the left-hand side of the sample. Around 30% of the sample shows plasticity-controlled failure, after which mostly vertical cracks are observed when inspecting the samples more to the left-hand side of the sample. One thing that should be noted is that the crack density increases when evaluating the sample more on the left-hand side of the sample. It can be seen that entering the crack-controlled region, the distance between the cracks is significantly larger compared to the left-hand side of the sample. Figure 7.9c shows the sample tested at -30 ^{o}C and 80N (29.9 MPa). It can be seen that the picture is not completely clear, but less than 30% of the sample shows a plasticity-controlled region. The crack appearing on the break surface can not be investigated properly. Figure 7.9d shows the samples tested at -20 ^{o}C and 100N (36.2 MPa). In the sample, a plasticity-controlled region can be identified by looking at the right-hand side of the sample. It covers around 50% of the sample. Looking at the left-hand side of the sample, it can be seen that more crack growth failure occurs. However, there are some vertical cracks present in the plasticity-controlled region as well. Going from the centre of the sample to the left-hand side, the crack density increases significantly. That is, the crack length decreases and the distance between the individual cracks decreases as well, allowing for more cracks per unit area. Furthermore, it can be seen that the cracks are mostly vertically oriented. The last thing that should be noted is the bright white curve that starts at the middle of the left-hand side of the sample and progresses towards the middle of the sample. The last sample to be discussed was tested at -20 ^{o}C and 80N (29.9 MPa), as shown in Figure 7.9e. It can be seen that around 25% of the region on the right-hand side is dominated by plastic deformation. From there on, cracks start to initiate with considerable length compared to the other sample at -20 ^{o}C, in a diagonal direction. Progressively moving towards the left-hand side of the sample, it can be seen that these cracks are subdivided into horizontal and vertical cracks, causing a rectangular pattern. As the cracks decrease in size moving to the left of the sample, the crack density increases.
It can be seen that all samples show cracks on the break surface. To be able to assess the cracks unambiguously, the middle 0.5 mm of the samples were taken as a reference. These regions can be found in Figure 7.10a-e. In this frame, the number of cracks is counted. By doing this, a 'crack density' can be distinguished. The number of counted cracks in this region can be found in Table 7.3. The samples -30 95N, -30 85N and -20 80N show the amount of cracks relatively well and the number of cracks can be counted relatively precisely. For samples -30 80N and -20 100N, the counting of the cracks is more difficult as the cracks are present less pronounced. For the -30 80N sample, this is caused by the fact that the SEM picture is of low quality. For the -20 100N sample, this is caused by the fact that there is still plastic deformation in this region, which makes the identification of cracks more difficult. Therefore, the results of the -30 80N sample are not taken into account, while the number of cracks for the -20 80N sample is estimated.

Sample	Number of cracks	Orientation
-30 95N	15	Vertical & Horizontal
-30 85N	25	Vertical
-30 80N	-	-
-20 100N	12	Vertical
-20 80N	23	Diagonal

Table 7.3: Number of cracks in the middle 0.5 mm of the samples tested for fatigue, including orientation of the counted cracks.

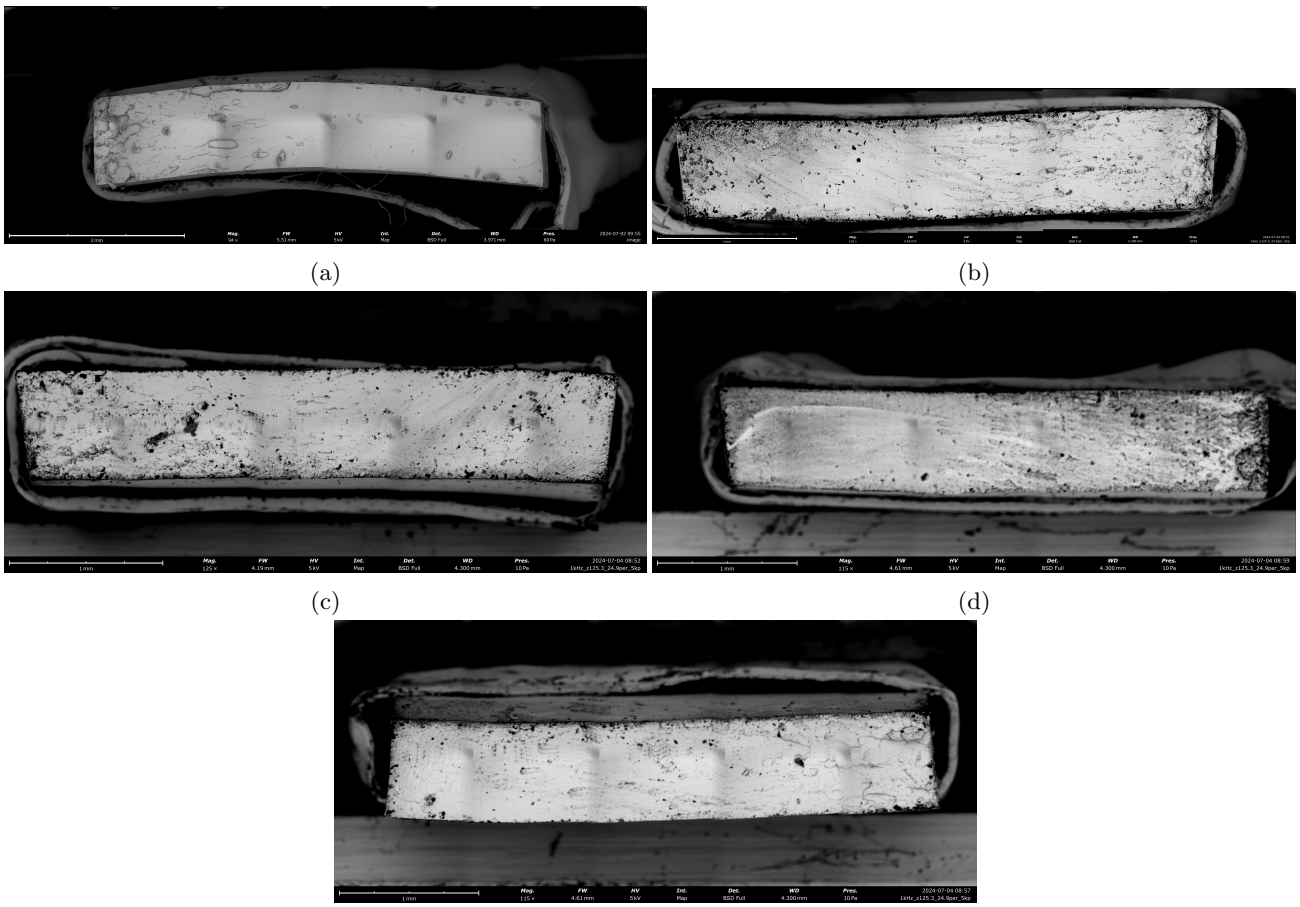

(a) (b)

(c) (d)

(e)

Figure 7.9: SEM results of dogbone samples tested at a) -30 ^{o}C and 95N. b) -30 ^{o}C and 85N. c) -30 ^{o}C and 80N. d) -20 ^{o}C and 100N. e) -20 ^{o}C and 80N.

7.2.5 Discussion

Firstly, looking at the results of the temperature sweep, the main discussion point is the rather large glass transition that is present, and the fact that the T_g based on the loss modulus is lower than the one obtained from the storage modulus. The large region for the glass transition originates from the complex behaviour of the TPE, where the constant interaction of the hydrogen bonds complicates the determination of T_g. The effect of temperature on hydrogen bonding has been studied for elevated temperatures [143], but the low-temperature behaviour of the hydrogen bond and the subsequent behaviour of the TPE as a whole is unknown. Therefore, comparing this to the given behaviour of a TPE under loading, as explained in Section 6.1.3, gives uncertainty about the temperature influence on the strength of the material. Furthermore, the exact composition of the material is unknown, such that no factual information is known about the number of hydrogen bonds that are present within the material. However, it is believed that the hydrogen bonds breaking and forming new bonds lead to rather complex material behaviour and might explain the large region over which the T_g is defined. The reason why the T_g obtained from the loss modulus is relatively low can be explained by the fact that the peak is occurring over a broad range. This can be attributed to the fact that fillers are added to the TPE, for example, silica. Furthermore, the fact that the T_g from the storage modulus and the T_g from the tan δ are separated significantly, makes the transition from a glassy to a rubbery state happen over a large temperature region. As the loss modulus resembles the viscous behaviour of the material that changes significantly during this transition region, the broad loss modulus peak can be attributed to this rather large region as well. Although the choice was made to use the T_g of -28 ^{o}C obtained from the storage modulus, consideration should be taken that the T_g determined by the loss modulus and tan δ can provide valuable information as well.
Regarding the frequency sweep, it can be seen that the Arrhenius and WLF equations give a proper fit to the obtained test data. Although the activation energy of the Arrhenius equation, being 219 kJ, is within a commonly reported value for polymers, there is no literature on TPEs tested within this temperature range. However, the WLF parameters are of greater interest as they help to estimate the yield stress at higher strain rates. Therefore, careful consideration should be taken when looking at the results. Although the WLF parameters $C_1 = 37$ and $C_2 = 148$ K yield a proper mastercurve for the frequency sweep, the values are

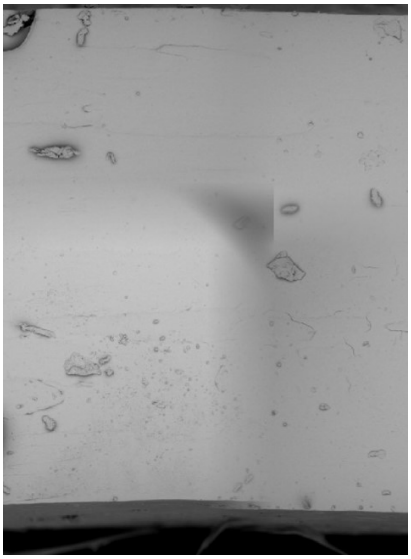

(a)

(b)

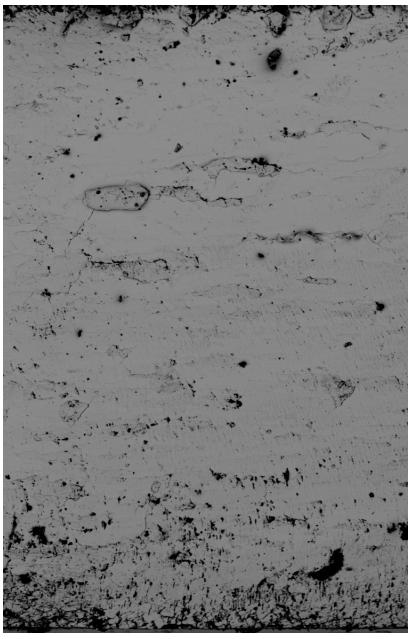

(c)

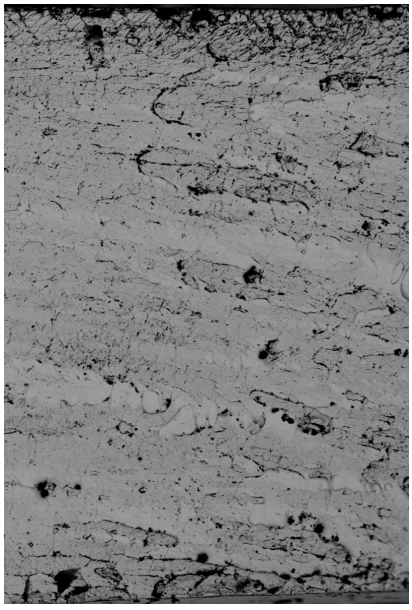

(d)

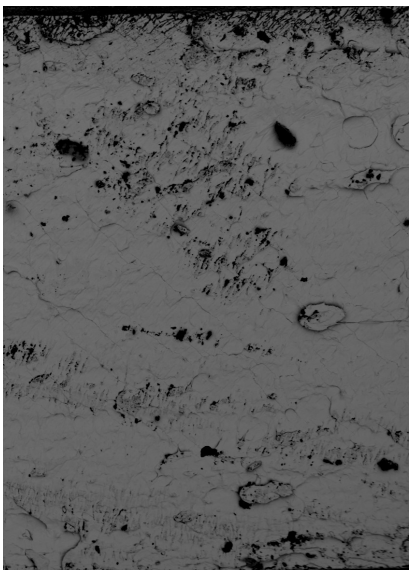

(e)

Figure 7.10: Portion of samples, 0.5 mm width in the centre for crack identification. a) -30 ^{o}C and 95N. b) -30 ^{o}C and 85N. c) -30 ^{o}C and 80N. d) -20 ^{o}C and 100N. e) -20 ^{o}C and 80N.

significantly higher than polymers in literature. As the effect of temperature on hydrogen bonding is not known, it is not possible to give an exact explanation for these high values, but it can be stated that this is related to the complex behaviour of the material in terms of hydrogen bond behaviour. As stated, the T_g is not unambiguous and occurs over a region. When looking at the influence of T_g on the WLF parameters, it was found that using the T_g from the loss modulus of -39 ^{o}C, C_1 = 49 and C_2 = 200 K were obtained. Increasing the T_g more towards the higher end of the transition region, at -10 ^{o}C, values of C_1 = 28 and C_2 = 140 K were obtained. So, it can be stated that increasing the T_g will decrease the WLF parameters.
Looking at the results of the tensile testing, the change in the strain rate sensitivity needs to be discussed. As stated, this behaviour is related to the chain mobility of the polymers and therefore, it is behaviour that can be expected. Furthermore, this behaviour is observed in epoxy resins [144], PC and PMMA as well [47], where the strain rate sensitivity decreased for increasing temperature. Furthermore, it can be seen that the data points representing the highest strain rates are below the linear trend of the other data points. One reason for this could be specimen heating. When the sample is deformed at the highest strain rate, the sample might heat up due to internal work. This leads to a local temperature increase, leading to less stiff behaviour and therefore, a subsequent drop in yield stress.
Looking at the results of the fits, it can be seen that the fit using the WLF parameters obtained from DMA using the T_g from the storage modulus does not give a proper fit, as presented in Figure 7.6a. The fact that it was found that increasing T_g leads to lower WLF parameters, and the fact that the values of C_1 = 37 and C_2 = 148 K are significantly too high, it was tried to relate the large T_g region with both the DMA testing and the Ree-Eyring equation by increasing the T_g to -10 ^{o}C. This was the highest T_g that could be considered in the frequency sweep without losing the accuracy of the WLF fit. New Ree-Eyring fits were obtained using the values of C_1 = 28 and C_2 = 140 K for a T_g of -10 ^{o}. The result of this fit can be found in Figure 7.11.

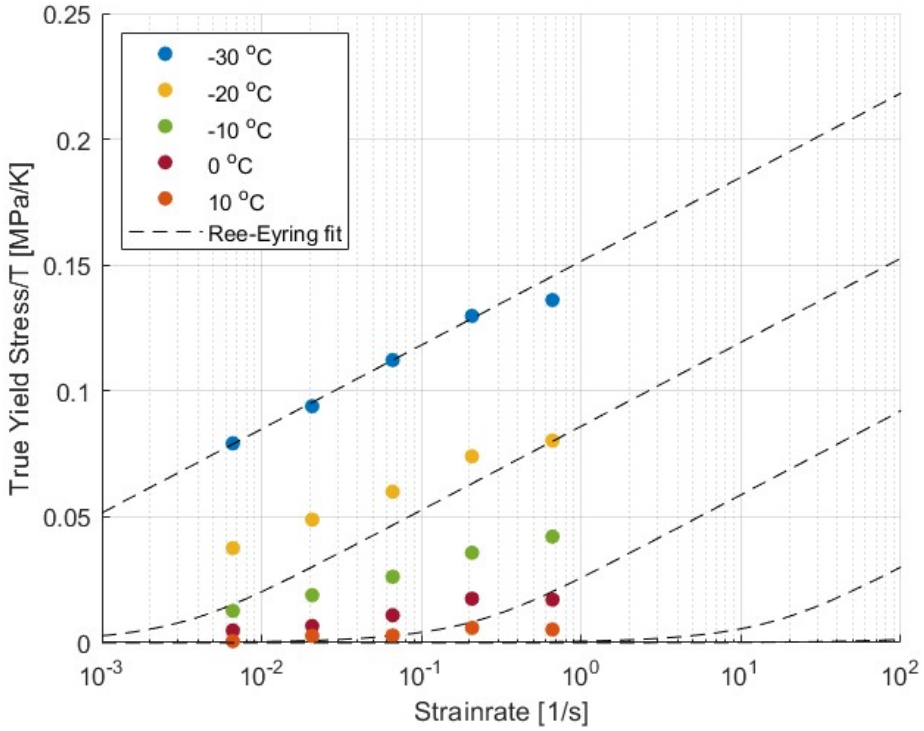

Figure 7.11: True yield stress over temperature for TPE using Ree-Eyring fit for T_g = -10 ^{o}C, C_1 = 28, C_2 = 140 K.

Again, it can be seen that the WLF parameters obtained from DMA do not yield a proper fit when being used in the Ree-Eyring equation, as could have been expected while the WLF parameters are still significantly higher than the best fit of C_1 = 13, C_2 = 80 K. It has been shown previously that the fit has less accuracy when the material enters the region above T_g [144]. However, the fit deviates too much from the actual data points to be caused by less accurate modelling alone. A reason for this can be the fact that the T_g is dependent on the strain rate as it is influenced by visco-elastic properties, as stated in Section 2.3.1. This visco-elastic dependency of the T_g is not taken into account in the Ree-Eyring fit. Also, the Ree-Eyring equation is limited by the fact that it considers a single T_g value whereas this material exhibits a rather large transition region. As the values of C_1 = 18 and C_2 = 80 K give the best fit, this would imply that the T_g of the TPE should be increased even further. Within the data obtained in this research, this can not be done as the amount of data points would

not suffice to get a reliable WLF fit.
So although it might be possible to come up with a T_g that gives similar WLF parameters compared to the best Ree-Eyring fit obtainable, the fact that a combination of a given T_g and its corresponding WLF values is not able to capture both DMA and tensile tests data is a reoccurring problem. As stated previously, the slopes of the yield stress plotted against the strain rate decrease for higher temperatures, which indicates that a maximum of one testing temperature can be below the T_g. This is because if for example, 3 testing temperatures were below T_g, it is expected that compared to each other, the three testing temperatures have similar slopes in their data points, similar to the Ree-Eyring equation where one relaxation process is present. So, this indicates that the actual T_g is at the lower end of the glass transition region. Therefore, it can be stated that the WLF parameters obtained from DMA and the WLF parameters needed for a proper yield estimation for this material do not match. This can be attributed to rather complex material behaviour, being the continuously newly formed hydrogen bonds upon loading. For the remainder of this study, the values of $C_1 = 13$ and $C_2 = 80$ K are used, as these give the best fit.

Regarding the discussion of the fatigue testing, the results of the rectangular specimen are considered first. It was already stated that the slope of the yield stress plotted against the number of cycles is similar, irrespective of the temperature. This can also be seen from the Basquin constant m, where there is only a small decrease in slope for increasing temperatures. Furthermore, the spread of the number of cycles for a particular stress is acceptable. This can be attributed to the fact that the strain rate is constant throughout the sample. Also, the clamps induce microcracks that initiate the crack growth, which causes the failure to be in the clamp. The fact that the slope of the data set does not change when applying stress above or below yield, and the fact that the entire data set of a single temperature can be captured by a single slope indicates that the failure is not dominated by yield behaviour and that there is only one dominant failure mode for all tests. The fact that the slope does not change for varying temperatures indicates that the failure mode that is dominant is not affected by temperature, but the amount of cycles the sample can endure is dependent on the temperature, as the datasets shift to lower lifetimes. This shift is linear as well, as the Basquin constant B decreases linearly with the logarithm of the variable. This implies that there is a relation between the temperature and the rate at which damage accumulates. It could be attributed to the fact that at lower temperatures, the TPE reacts more compliant and fewer cycles can be applied before failure. All these results, however, have the limitations that the failure happened in the clamp. Although this gave rise to failure being predictable, due to the constant strain rate and induced microcracks, it is not representative for the actual behaviour of the material. This is because the stress concentration and crack initiation at the clamp do not represent the actual behaviour of the samples if they were loaded more constantly, which is usually the case in tensile testing.
Therefore, the results of the dogbone samples should be considered. This leads to the fact that the exact strain rate in the sample is not known due to varying geometry, but the indication of the actual lifetime is more precise. More specifically, the rate at which this material is characterized is unknown, but the behaviour of the material is more precise in the given circumstances. The fact that the clamps do not induce microcracks in comparison to the rectangular samples indicates that these samples are driven by failure initiation rather than by crack growth failure. This means that the rectangular samples have a defect in the form of a microcrack present that grows upon fatigue loading, whereas the dogbone samples first have to 'create' a defect after which the sample can undergo crack growth. Apparently, this failure initiation gives rise to a more random distribution of the lifetime compared to crack-growth-dominated failure by a pre-introduced defect.
The first discussion point is the fact that higher stresses are obtained in these tests compared to rectangular specimens, which can be attributed to the fact that there is more spreading of the stress, allowing for higher load-bearing capacity. Furthermore, the linear relation between applied stress and lifetime is recurring, albeit there is more spread of the data points. The spread can be attributed to the fact that the dogbone samples failed at different locations along the sample and that strain rates vary. On a logarithmic scale, this spread can become quite significant. The fact that the temperature dependence on the lifetime, seen by the horizontal shift, is less prevalent compared to the rectangular samples. The fact that no visible shift in slope can be identified within one temperature, and respective of each other, indicates that there is one active failure mechanism. However, the fact that there is a distinct increase in lifetime for -30 ^{o}C that diminishes for higher temperatures indicates that the failure mode is sensitive to low temperatures and that the actual failure is not influenced by higher temperatures. More specifically, it could be that the failure mechanism, albeit the same mechanism throughout the test, is dependent on material behaviour above and below T_g, as -30 ^{o}C is considered to be below T_g, whereas the other testing temperatures are considered above. However, the failure mechanism should be studied more in-depth. Therefore, it should be investigated what the actual failure-driven mode is in order to look at the damage accumulation at the failure surface, for which SEM results will be discussed.
Looking at the results of all samples that were investigated using SEM-microscopy, it can be seen that all samples exhibit both crack-growth-controlled failure and plasticity-controlled failure, and all samples show a gradual transition from one failure mode to another, albeit at different regions in the specimen. This can be attributed to the fact that first, plastic deformation causes the material to reach a particular critical crack length.

This is the failure initiation that was discussed in the results section. After this critical length is reached, the material fails under crack propagation. In the region where failure is more brittle and therefore crack-growth controlled, cracks can be found that are progressing in the samples. This is most likely caused by crystal slip, as the crystal part of this material - the oriented hard segments of the TPE - allows displacement of the hard segments relatively well, as this movement is only restricted by relatively weak hydrogen bonds. However, this can not be stated with certainty. All samples show that the dominant failure mode is the crack-growth failure, which explains the fact that the fatigue testing of the dogbones did not show a significant change in slope within one testing temperature. So, it can be stated that there is indeed one dominant failure mechanism, irrespective of the temperature, being crack-growth failure. Therefore, it is important to discuss the different crack appearances, as there are some distinct differences between them. All samples showed cracks differing in length, density and direction between them. In the results, the number of cracks in the middle 0.5 mm of the sample was shown. These results indicate an increase in the number of cracks for an increasing number of cycles as well. However, the results should be interpreted with caution. Firstly, the counting of the individual samples could not be done unambiguously, as there was a variety of picture qualities obtained from the SEM. New pictures could not be taken as the material has a self-healing effect, causing the observed number of cracks to change over time. Secondly, there are not enough data points to establish the relation between the number of cracks and the number of cycles. Thirdly, the spread of the data points of the number of cycles for an applied stress is prevalent and the effect of this on the number of cracks is not known.
With these limitations in mind, a possible explanation for the increasing amount of cracks for longer lifetimes is given, based on the crack formation due to crystal slip, as was mentioned previously. Although this theory can not be proven with the current results, it is good practice to give thought to a possible reason for this crack behaviour. So, the theory of crystal slip is not something that happens undoubtedly, but it is a possible explanation for the phenomenon of cracks appearing on the break surface. This theory states that more energy is provided to the sample as the number of cycles increases, and this energy is partly absorbed by the crystal slip. So, the more cracks are present in the middle region of the sample, the more energy from the fatigue testing is dissipated into the sample by crystal slip. This dissipated energy can not contribute to the failure of the break surface anymore, which indicates that a larger number of cracks on the break surface contributes to a longer lifetime of the sample. It can be imagined that the density of the cracks in this region is a good indication of the lifetime of the sample. More specifically, if the density of the cracks increases, more energy is dissipated into the sample, rather than dissipated along the crack path of the break surface. This decrease in the amount of energy put into the failure of the sample leads to higher fatigue lifetimes. A schematic front view of this crack behaviour can be found in Figure 7.12. Referring to this schematic and the abovementioned phenomenon, the lifetime would increase if there is a larger number of green cracks in the designated area with a width of 0.5 mm.

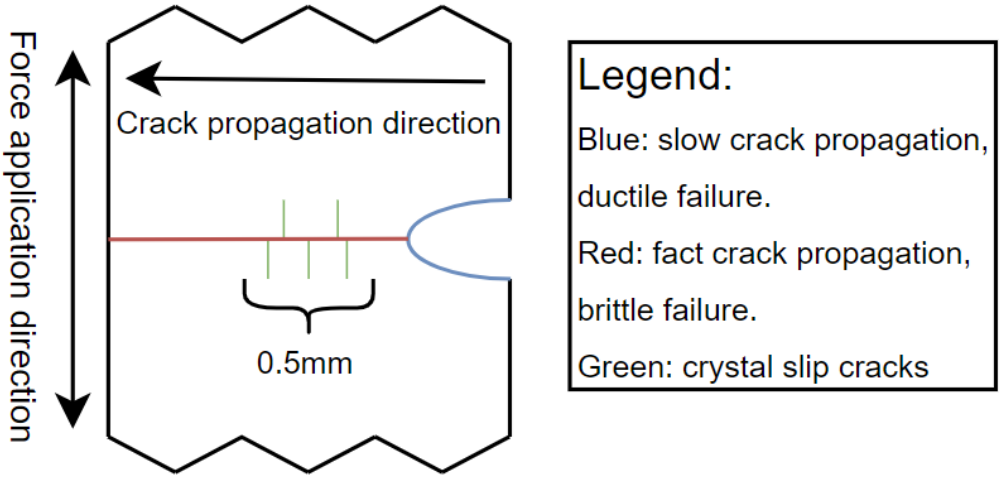

Figure 7.12: Front view schematic representation of the damage mechanisms in the samples.

CHAPTER 8

Conclusions & Recommendations

8.1 Conclusions

Based on the results of this study and the fact that it aims to develop a testing framework to characterize the mechanical properties of polymeric materials at high strain rates using low-temperature testing, the following conclusions can be drawn in general.

- The need to perform a temperature sweep on the material depends on the material characteristics that are known beforehand. If literature gives a clear reason to believe that the T_g of the tested material is significantly above the used testing temperatures, there is no need to perform a temperature sweep. If either there is not sufficient literature available on the material, e.g. for complex materials, or the T_g of the tested material is close to or within the range of testing temperatures, a temperature sweep can be carried out to determine the T_g.
- The need to perform a frequency sweep depends on the T_g of the material. If the tested material has a T_g close to or within the range of testing temperatures, it is useful to perform a frequency sweep that captures the range of testing temperatures broadly. In this way, WLF parameters and Arrhenius constants can be obtained to describe the materials' elastic behaviour over a range of temperatures. If the T_g is not close to the testing temperature range, a frequency sweep is not necessary as the Ree-Eyring equation below T_g will suffice for high strain rate characterization, albeit with one or more relaxation processes.
- The relation between WLF parameters obtained from a frequency sweep does not necessarily give accurate data to predict the yield stress at a certain temperature and strain rate. It has been proven that complex material behaviour negatively impacts the accuracy of this prediction using the Ree-Eyring equation above T_g in combination with WLF parameters.
- When a Ree-Eyring fit can be made accurately, one can predict the equivalent strain rate at a chosen reference temperature when testing at a predefined temperature and strain rate. This is valid for testing temperatures below or above T_g.
- One can predict the fatigue lifetime at this equivalent strain rate. However, when tests are conducted using the specific test equipment described, a tradeoff needs to be made between the used sample geometry. Either inaccurate lifetimes but accurate strain rates in combination with crack growth-dominated failure using rectangular samples, or accurate lifetimes with inaccurate strain rates in combination with failure initiation using dogbone samples can be chosen. If other test equipment is used, this problem might not arise.
- Looking at the break surface after performing tensile fatigue testing, the TPE material shows one prevalent failure mechanism, a crack-growth failure. First, slow crack propagation leads to ductile failure after which a brittle failure region can be identified. In this brittle failure, cracks parallel to the loading direction are found, which are likely to occur due to crystal slip.
- Although there is a lack of data points, there seems to be a relation between the number of cracks in the brittle region and the number of cycles. Crystal slip might cause additional energy dissipation in the sample, leading to a longer fatigue lifetime. Additional research is needed to prove this theory.

8.2 Test Framework

As was stated in the research question of this study, the goal of this study was the following:

The development of a reliable and less complex test procedure to characterize material properties at high strain rates using low-temperature testing, including fatigue behaviour to model rain erosion of wind turbine blades.

Based on the conclusions that can be drawn from this study, the following framework for accelerated rain erosion testing can be set up:

1. **Test Preparations**

   (a) **Temperature Sweep**
   Perform a literature study on the material that needs to be tested. If literature gives an unambiguous result on the value of T_g, and its value is significantly outside the range of testing temperatures, a temperature sweep does not need to be performed. If one or both of these criteria are not met, a temperature sweep can be carried out to determine the T_g of the material.

   (b) **Frequency Sweep**
   The need to perform a frequency sweep is based on the found value of T_g. If the tested material has a T_g that is close or within the range of testing temperatures, a frequency sweep should be carried out.

   (c) **Sample preparation**
   Choose to use dogbone or rectangular samples. If dogbone samples are used, ensure that samples meet NEN-ISO 37-S2 tolerances for consistent results. For rectangular samples, a width of 6 mm or less can be used. If the T_g of the material was found to be above room temperature, make sure to rejuvenate the samples by bringing them to a temperature above T_g for a sufficient amount of time.

2. **Testing Procedures** Every test is carried out to gather specific information. Therefore, the last line of every test procedure and analyzing method described will show the desired outcome of the test.

   (a) **Temperature Sweep** (if necessary)
   Use DMA testing equipment to carry out tensile tests. Make sure that the temperature range of the temperature sweep captures the testing temperatures of the tensile testing by at least 10 ^{o}C at the lower and higher end. Use a temperature increment of 2 ^{o}C. Use a frequency of 10Hz or lower.
   Outcome: T_g.

   (b) **Frequency Sweep** (if necessary)
   Use DMA testing equipment to carry out tensile tests. For this, set the temperature range of the frequency sweep such that the temperature range of the tensile testing is captured broadly, by at least 30 ^{o}C on the lower end of the lower end and 10 ^{o}C on the higher end. Use a temperature increment of 5 ^{o}C. Use frequencies of 10Hz and lower with a minimum of 3 decades.
   Outcome: WLF and Arrhenius parameters.

   (c) **Tensile Testing**
   Determine the desired testing temperature, such that the T_g of the material is effectively captured. Determine the desired testing speed that can be set for the machine. Firstly, for all materials, carry out tensile tests with all combinations of chosen temperatures and strain rates until failure, without a clip-on extensometer, to determine the yield point and force at break. These results can be used for high-displacement materials. Then, for low-displacement materials, ensure that the clip-on extensometer is mounted to the sample. Carry out the same set of tests while stopping the test just after yield.
   Outcome: Strain rate, yield point, force at break.

   (d) **Fatigue Testing**
   Set the testing speed to the maximum value and choose a testing temperature to ensure testing at the equivalent strain rate one is interested in. From the tensile test results, one can determine desired testing forces, e.g. at 80% and 60% of the force at break and at 100%, 80% and 60 % of the yield force. Apply a cyclic load to the material with the desired testing force as the maximum force and a value of 10% of the maximum force as the minimum force. Perform this test until the samples break.
   Outcome: Number of cycles up to failure.

3. **Analyzing results**

   (a) **Temperature Sweep**
   To analyze the data from the temperature sweep, the inflection method can be used by considering the storage modulus data. This is the most relevant method to determine the T_g of the tested material. However, the determination of T_g based on the loss modulus and tan δ can give valuable information on the complexity of the material and ambiguity of the found value of T_g.
   Outcome: T_g.

   (b) **Frequency Sweep**
   The data from the frequency sweep can be used to construct a mastercurve over a larger range of frequencies. For temperatures above T_g, this can be done using the WLF equation. For temperatures below T_g, this can be done using the Arrhenius equation.
   Outcome: WLF and Arrhenius parameters.

   (c) **Tensile Testing**
   Firstly, the precise strain rate can be determined from the extensometer, if this was used. If no extensometer is used, one can estimate it using the machine displacement rate that was set. Then, the yield point of the material for a combination of a certain temperature and strain rate needs to be determined. If no clear yield point can be observed, it can be estimated using the inflection method. Plot the found yield point against the strain rate on a logarithmic axis.
   Using Ree-Eyring equations, fit the found data. These fits can be extended to strain rates that one is interested in and that can not be experimentally obtained.
   Outcome: Equivalent strain rate for operating temperature.

   (d) **Fatigue Testing**
   Plot the applied maximum stress against the number of cycles up to failure on a logarithmic axis. Basquin fits can be used to fit the found data of the fatigue testing. It gives information on the linearity of the data: if one or more damage mechanisms are present, and what the influence of equivalent strain rate is on the lifetime of the material.
   To give a more precise indication of the damage mechanism present, SEM microscopy can be used to investigate the break surface. By coating the broken samples' surface in a gold layer, SEM microscopy gives a good presentation of the break surface and with these images, one can see the dominant failure mechanisms, which can be crucial for drawing conclusions on the behaviour of the tested material.
   Outcome: Number of cycles up to failure, Basquin parameters, dominant damage mechanisms.

8.3 Recommendations

Based on the conclusions drawn from the results and discussion in this study, some recommendations for further research can be given.

- The use of a non-contact extensometer, such as a laser or optical extensometer, would allow the measurement of displacement and the calculation of strains for a larger amount of materials, as there is no limitation to the amount of displacement compared to clip-on extensometers.
- The use of a climate chamber able to go to lower temperatures would enable the analysis of the material well below T_g, even with the uncertainties thereof. This can give a better indication of the material behaviour.
- More in-depth material analysis can be done to explain the complex behaviour of a TPE further. For example, DSC measurements can be carried out to verify the glass transition temperature, and DMA testing can be done at multiple frequencies to examine the effect of strain rates on the dynamic behaviour of the material.
- Notched fatigue testing can be carried out. By introducing a predetermined defect in a rectangular sample, the problem regarding inaccurate lifetimes can be minimized as the clamp failure is most likely not dominant in this type of testing.
- More SEM microscopy can be carried out to examine fracture behaviour of a material at different equivalent strain rates, and at stresses below and above yield. This should clarify the theory that more energy dissipation in the form of crystal slip leads to higher fatigue life.

All in all, looking at the broader perspective of this study, it can be finally concluded that accelerated rain erosion testing can be modelled to predict erosion damage in LEP systems used in wind turbine coating, with the limitation of either inaccurate strain rates or fatigue lifetimes. As a consequence, the results of this study use a prediction of the equivalent strain rate around 10^4-10^5 s^{-1} rather than an accurate number. Subsequently, this leads to a prediction of rain erosion lifetime rather than an actual depiction of the rain erosion damage accumulation. Being able to determine T_g more accurately, and testing substantially below this temperature in combination with eliminating the fatigue testing problems regarding inaccurate strain rates or lifetimes would lead to the ability of this test framework to more accurately predict accelerated rain erosion in future testing of LEP materials.

CHAPTER 9

Bibliography

[1] H. Ritchie, M. Roser, and P. Rosado, "Energy. published online at ourworldindata. org," 2020.

[2] L. Mishnaevsky Jr, C. B. Hasager, C. Bak, A.-M. Tilg, J. I. Bech, S. D. Rad, and S. Fæster, "Leading edge erosion of wind turbine blades: Understanding, prevention and protection," *Renewable Energy*, vol. 169, pp. 953–969, 2021.

[3] D. A. Katsaprakakis, N. Papadakis, and I. Ntintakis, "A comprehensive analysis of wind turbine blade damage," *Energies*, vol. 14, no. 18, p. 5974, 2021.

[4] F. Papi, L. Cappugi, S. Perez-Becker, and A. Bianchini, "Numerical modeling of the effects of leading-edge erosion and trailing-edge damage on wind turbine loads and performance," *Journal of Engineering for Gas Turbines and Power*, vol. 142, no. 11, p. 111005, 2020.

[5] A. Castorrini, A. Corsini, F. Rispoli, P. Venturini, K. Takizawa, and T. E. Tezduyar, "Computational analysis of performance deterioration of a wind turbine blade strip subjected to environmental erosion," *Computational Mechanics*, vol. 64, pp. 1133–1153, 2019.

[6] L. Mishnaevsky Jr, "Repair of wind turbine blades: Review of methods and related computational mechanics problems," *Renewable energy*, vol. 140, pp. 828–839, 2019.

[7] H. Slot, R. IJzerman, M. Le Feber, K. Nord-Varhaug, and E. van der Heide, "Rain erosion resistance of injection moulded and compression moulded polybutylene terephthalate pbt," *Wear*, vol. 414, pp. 234–242, 2018.

[8] A. Dashtkar, H. Hadavinia, M. N. Sahinkaya, N. A. Williams, S. Vahid, F. Ismail, and M. Turner, "Rain erosion-resistant coatings for wind turbine blades: A review," *Polymers and Polymer Composites*, vol. 27, no. 8, pp. 443–475, 2019.

[9] D. Major, J. Palacios, M. Maughmer, and S. Schmitz, "Aerodynamics of leading-edge protection tapes for wind turbine blades," *Wind Engineering*, vol. 45, no. 5, pp. 1296–1316, 2021.

[10] H. Busch, G. Hoff, G. Langbein, G. Taylor, D. Jenkins, M. Taunton, A. Fyall, R. Jones, and T. Harper, "Rain erosion properties of materials," *Philosophical Transactions for the Royal Society of London. Series A, Mathematical and Physical Sciences*, pp. 168–181, 1966.

[11] W. F. Adler, "Liquid drop collisions on deformable media," *Journal of Materials Science*, vol. 12, pp. 1253–1271, 1977.

[12] G. F. Schmitt Jr, "Materials parameters that govern the rain erosion behavior of polymeric coatings and composites at subsonic velocities," *Air Force Materials Laboratory Wright-Patterson AFB: Greene County, OH, USA*, 1971.

[13] N. Hoksbergen, R. Akkerman, and I. Baran, "The springer model for lifetime prediction of wind turbine blade leading edge protection systems: A review and sensitivity study," *Materials*, vol. 15, no. 3, p. 1170, 2022.

[14] G. S. Springer and C. B. Baxi, "A model for rain erosion of homogeneous materials," *Erosion, Wear, and Interfaces with Corrosion*, pp. 106–124, 1974.

[15] A. D. Mulliken and M. C. Boyce, "Mechanics of the rate-dependent elastic–plastic deformation of glassy polymers from low to high strain rates," *International journal of solids and structures*, vol. 43, no. 5, pp. 1331–1356, 2006.

[16] E. M. Arruda, M. C. Boyce, and R. Jayachandran, "Effects of strain rate, temperature and thermomechanical coupling on the finite strain deformation of glassy polymers," *Mechanics of Materials*, vol. 19, no. 2-3, pp. 193–212, 1995.

[17] Z. Li and J. Lambros, "Strain rate effects on the thermomechanical behavior of polymers," *International Journal of solids and structures*, vol. 38, no. 20, pp. 3549–3562, 2001.

[18] R. Ullman, "Deformation kinetics, A. S. Krausz and H. Eyring, Wiley-Interscience, New York, 1975, 398 pp. $24.95," *Journal of Polymer Science: Polymer Letters Edition*, vol. 14, pp. 245–245, Apr. 1976.

[19] T. Technology, "Shrinkage in plastics," *Plastic Topics*, 2024.

[20] C. A. Angell, K. L. Ngai, G. B. McKenna, P. F. McMillan, and S. W. Martin, "Relaxation in glassforming liquids and amorphous solids," *Journal of applied physics*, vol. 88, no. 6, pp. 3113–3157, 2000.

[21] L. C. E. Struik *et al.*, *Physical aging in amorphous polymers and other materials*, vol. 106. Citeseer, 1978.

[22] L. E. Govaert, A. K. van der Vegt, and M. van Drongelen, *Polymers: from structure to properties*. Delft University Press, 2020.

[23] J. N. Hay, "The physical ageing of amorphous and crystalline polymers," *Pure and applied chemistry*, vol. 67, no. 11, pp. 1855–1858, 1995.

[24] L. Struik, "The mechanical and physical ageing of semicrystalline polymers: 1," *Polymer*, vol. 28, no. 9, pp. 1521–1533, 1987.

[25] L. Struik, "Mechanical behaviour and physical ageing of semi-crystalline polymers: 4," *Polymer*, vol. 30, no. 5, pp. 815–830, 1989.

[26] T. Chow, "Stress-strain behaviour of physically ageing polymers," *Polymer*, vol. 34, no. 3, pp. 541–545, 1993.

[27] C. C. Clarijs, M. J. Kanters, M. J. van Erp, T. A. Engels, and L. E. Govaert, "Predicting plasticity-controlled failure of glassy polymers: Influence of stress-accelerated progressive physical aging," *Journal of Polymer Science Part B: Polymer Physics*, vol. 57, no. 19, pp. 1300–1314, 2019.

[28] I. M. Hodge, "Physical aging in polymer glasses," *Science*, vol. 267, no. 5206, pp. 1945–1947, 1995.

[29] L. C. E. Struik, "Physical aging in plastics and other glassy materials," *Polymer Engineering & Science*, vol. 17, no. 3, pp. 165–173, 1977.

[30] A. International, *Standard test method for tensile properties of plastics*. ASTM international, 2014.

[31] W. D. Callister Jr, *Materials science and engineering an introduction*. 2007.

[32] J. F. Shackelford, "Materials science for engineers," *Upper Saddle River, New Jersey*, 2000.

[33] R. J. Rice, "The localization of plastic deformation," *Theoretical and Applied Mechanics*, vol. 1, pp. 207–220, 1976.

[34] W. D. Callister, "Fundamentals of materials science and engineering," 2007.

[35] E. Oleynik, "Plastic deformation and mobility in glassy polymers," in *Relaxation in Polymers*, pp. 140–150, Springer, 1989.

[36] A. Peterlin, "Plastic deformation of crystalline polymers," *Polymer Engineering & Science*, vol. 17, no. 3, pp. 183–193, 1977.

[37] G. McKenna, "Comprehensive polymer science," *Polymer properties*, vol. 2, pp. 311–362, 1989.

[38] T. A. Engels, S. H. Söntjens, T. H. Smit, and L. E. Govaert, "Time-dependent failure of amorphous polylactides in static loading conditions," *Journal of Materials Science: Materials in Medicine*, vol. 21, pp. 89–97, 2010.

[39] H.-N. Lee, K. Paeng, S. F. Swallen, and M. Ediger, "Direct measurement of molecular mobility in actively deformed polymer glasses," *Science*, vol. 323, no. 5911, pp. 231–234, 2009.

[40] L. S. Loo, R. E. Cohen, and K. K. Gleason, "Chain mobility in the amorphous region of nylon 6 observed under active uniaxial deformation," *Science*, vol. 288, no. 5463, pp. 116–119, 2000.

[41] K. Chen and K. S. Schweizer, "Theory of yielding, strain softening, and steady plastic flow in polymer glasses under constant strain rate deformation," *Macromolecules*, vol. 44, no. 10, pp. 3988–4000, 2011.

[42] C. R. Siviour and J. L. Jordan, "High strain rate mechanics of polymers: a review," *Journal of Dynamic Behavior of Materials*, vol. 2, pp. 15–32, 2016.

[43] C. Bauwens-Crowet, J. C. Bauwens, and G. Homes, "Tensile yield-stress behavior of glassy polymers," *Journal of Polymer Science Part A-2: Polymer Physics*, vol. 7, no. 4, pp. 735–742, 1969.

[44] O. D. Sherby and J. Dorn, "Anelastic creep of polymethyl methacrylate," *Journal of the Mechanics and Physics of Solids*, vol. 6, no. 2, pp. 145–162, 1958.

[45] F. Rietsch and B. Bouette, "The compression yield behaviour of polycarbonate over a wide range of strain rates and temperatures," *European Polymer Journal*, vol. 26, no. 10, pp. 1071–1075, 1990.

[46] J. C. Bauwens, "Relation between the compression yield stress and the mechanical loss peak of bisphenol-a-polycarbonate in the β transition range," *Journal of Materials Science*, vol. 7, pp. 577–584, 1972.

[47] J. Richeton, S. Ahzi, L. Daridon, and Y. Rémond, "A formulation of the cooperative model for the yield stress of amorphous polymers for a wide range of strain rates and temperatures," *Polymer*, vol. 46, no. 16, pp. 6035–6043, 2005.

[48] R. Haward, B. Murphy, and E. White, "Relationship between compressive yield and tensile behavior in glassy thermoplastics," *Journal of Polymer Science Part A-2: Polymer Physics*, vol. 9, no. 5, pp. 801–814, 1971.

[49] E. Hoff, "Some mechanical properties of a commercial polymethyl methacrylate," *Journal of Applied Chemistry*, vol. 2, no. 8, pp. 441–448, 1952.

[50] G. Gurevich and P. Kobeko, "A study of polymers. iii. technique of mechanical tests of vulcanizates of rubber and plastics," *Rubber Chemistry and Technology*, vol. 13, no. 4, pp. 904–917, 1940.

[51] S. M. Walley, J. E. Field, P. Pope, and N. Safford, "A study of the rapid deformation behaviour of a range of polymers," *Philosophical Transactions of the Royal Society of London. Series A, Mathematical and Physical Sciences*, vol. 328, no. 1597, pp. 1–33, 1989.

[52] P. Rae and D. Dattelbaum, "The properties of poly (tetrafluoroethylene)(ptfe) in compression," *Polymer*, vol. 45, no. 22, pp. 7615–7625, 2004.

[53] E. N. Brown, P. J. Rae, E. B. Orler, G. T. Gray III, and D. M. Dattelbaum, "The effect of crystallinity on the fracture of polytetrafluoroethylene (ptfe)," *Materials Science and Engineering: C*, vol. 26, no. 8, pp. 1338–1343, 2006.

[54] H. Eyring, "Viscosity, plasticity, and diffusion as examples of absolute reaction rates," *The Journal of chemical physics*, vol. 4, no. 4, pp. 283–291, 1936.

[55] A. S. Krausz and H. Eyring, "Deformation kinetics," *John Wiley & Sons*, 1975.

[56] S. Glasstone, "laidler, kj; and eyring, h, the theory of rate processes," 1941.

[57] J. White, "On internal stress and activation volume in polymers," *Journal of Materials Science*, vol. 16, no. 12, pp. 3249–3262, 1981.

[58] S. Arrhenius, "Über die dissociationswärme und den einfluss der temperatur auf den dissociationsgrad der elektrolyte," *Zeitschrift für physikalische Chemie*, vol. 4, no. 1, pp. 96–116, 1889.

[59] D. J. Senden, S. Krop, J. van Dommelen, and L. Govaert, "Rate-and temperature-dependent strain hardening of polycarbonate," *Journal of Polymer Science Part B: Polymer Physics*, vol. 50, no. 24, pp. 1680–1693, 2012.

[60] E. Klompen and L. E. Govaert, "Nonlinear viscoelastic behaviour of thermorheologically complex materials," *Mechanics of Time-Dependent Materials*, vol. 3, pp. 49–69, 1999.

[61] J. Roetling, "Yield stress behaviour of polymethylmethacrylate," *Polymer*, vol. 6, no. 6, pp. 311–317, 1965.

[62] T. Ree and H. Eyring, "Theory of non-newtonian flow. i. solid plastic system," *Journal of Applied Physics*, vol. 26, no. 7, pp. 793–800, 1955.

[63] C. Bauwens-Crowet, J. C. Bauwens, and G. Homes, "The temperature dependence of yield of polycarbonate in uniaxial compression and tensile tests," *Journal of Materials Science*, vol. 7, pp. 176–183, 1972.

[64] C. H. Huu and T. Vu-Khanh, "Effects of physical aging on yielding kinetics of polycarbonate," *Theoretical and applied fracture mechanics*, vol. 40, no. 1, pp. 75–83, 2003.

[65] F. Ree, T. Ree, and H. Eyring, "Relaxation theory of transport problems in condensed systems," *Industrial & Engineering Chemistry*, vol. 50, no. 7, pp. 1036–1040, 1958.

[66] E. N. Brown and D. M. Dattelbaum, "The role of crystalline phase on fracture and microstructure evolution of polytetrafluoroethylene (ptfe)," *Polymer*, vol. 46, no. 9, pp. 3056–3068, 2005.

[67] E. Brown, P. J. Rae, and G. T. Gray, "The influence of temperature and strain rate on the tensile and compressive constitutive response of four fluoropolymers," in *Journal de Physique IV (Proceedings)*, vol. 134, pp. 935–940, EDP sciences, 2006.

[68] C. Cady, W. Blumenthal, G. Gray III, and D. Idar, "Determining the constitutive response of polymeric materials as a function of temperature and strain rate," in *Journal de physique IV (proceedings)*, vol. 110, pp. 27–32, EDP sciences, 2003.

[69] F. Irgens, *Rheology and non-newtonian fluids*, vol. 1. Springer, 2014.

[70] F. A. Morrison *et al.*, *Understanding rheology*, vol. 1. Oxford university press New York, 2001.

[71] N. R. Sgreva, *Influence of the fluid structure and elasticity on motions in a yield-stress material-Implications for geological systems*. PhD thesis, Université Paris-Saclay, 2020.

[72] C. Villa, M. A. Chaplain, A. Gerisch, and T. Lorenzi, "Mechanical models of pattern and form in biological tissues: The role of stress–strain constitutive equations," *Bulletin of Mathematical Biology*, vol. 83, no. 7, p. 80, 2021.

[73] X. Zhou, D. Yu, and O. Barrera, "Mechanics constitutive models for viscoelastic solid materials: Development and a critical review," *Advances in Applied Mechanics*, vol. 56, pp. 189–321, 2023.

[74] B. McCrum, "Bucknell," *Principles of Polymer Engineering*, pp. 117–176, 2003.

[75] A. Franck and T. Germany, "Viscoelasticity and dynamic mechanical testing," *TA Instruments, New Castle, DE, USA AN004*, 1993.

[76] M. A. Meyers and K. K. Chawla, *Mechanical behavior of materials*. Cambridge university press, 2008.

[77] V. N. Pokrovskii, *The mesoscopic theory of polymer dynamics*. Springer, 2002.

[78] M. L. Williams, R. F. Landel, and J. D. Ferry, "The temperature dependence of relaxation mechanisms in amorphous polymers and other glass-forming liquids," *Journal of the American Chemical society*, vol. 77, no. 14, pp. 3701–3707, 1955.

[79] I. Ward, "Mechanical properties of polymers, 1983."

[80] T. P. Lodge and P. C. Hiemenz, *Polymer chemistry*. CRC press, 2020.

[81] A. Álvarez-Vázquez, A. Fernández-Canteli, E. Castillo Ron, P. Fernandez Fernandez, M. Muñiz-Calvente, and M. J. Lamela Rey, "A novel approach to describe the time–temperature conversion among relaxation curves of viscoelastic materials," *Materials*, vol. 13, no. 8, p. 1809, 2020.

[82] J. D. Ferry, *Viscoelastic properties of polymers*. John Wiley & Sons, 1980.

[83] W. Brostow, "Dynamic mechanical analysis: a practical introduction," *ed: CRC Press, USA*, 2007.

[84] T. M. Nair, M. Kumaran, G. Unnikrishnan, and V. Pillai, "Dynamic mechanical analysis of ethylene–propylene–diene monomer rubber and styrene–butadiene rubber blends," *Journal of Applied Polymer Science*, vol. 112, no. 1, pp. 72–81, 2009.

[85] M. Schneider, W. Rippard, M. Pufall, T. Cecil, T. Silva, and S. Russek, "Temperature dependence of spin-torque-driven self-oscillations," *Physical Review B*, vol. 80, no. 14, p. 144412, 2009.

[86] K. Whitcomb, "Measurement of glass transition temperatures by dynamic mechanical analysis and rheology," *TA Instruments https://www. tainstruments. com/pdf/literature/(accesed Nov 26, 2022).*, 2022.

[87] M. A. Bashir, "Use of dynamic mechanical analysis (dma) for characterizing interfacial interactions in filled polymers," *Solids*, vol. 2, no. 1, pp. 108–120, 2021.

[88] I. M. Barszczewska-Rybarek, A. Korytkowska-Wałach, M. Kurcok, G. Chladek, and J. Kasperski, "Dma analysis of the structure of crosslinked poly (methyl methacrylate) s," *Acta of bioengineering and biomechanics*, vol. 19, no. 1, 2017.

[89] I. Henriques, L. Borges, M. Costa, B. Soares, and D. Castello, "Comparisons of complex modulus provided by different dma," *Polymer Testing*, vol. 72, pp. 394–406, 2018.

[90] A. Paar, "Basics of rheology - frequency sweeps, 2024."

[91] U. Gedde, J. Viebke, H. Leijström, and M. Ifwarson, "Long-term properties of hot-water polyolefin pipes—a review," *Polymer Engineering & Science*, vol. 34, no. 24, pp. 1773–1787, 1994.

[92] L. V. Pastukhov, F. P. Mercx, T. Peijs, and L. E. Govaert, "Long-term performance and durability of polycarbonate/carbon nanotube nanocomposites," *Nanocomposites*, vol. 4, no. 4, pp. 223–237, 2018.

[93] J. E. Field, t. M. Walley, W. Proud, H. Goldrein, and C. Siviour, "Review of experimental techniques for high rate deformation and shock studies," *International journal of impact engineering*, vol. 30, no. 7, pp. 725–775, 2004.

[94] G. Gray III and W. R. Blumenthal, "Split-hopkinson pressure bar testing of soft materials," *ASM handbook*, vol. 8, pp. 488–496, 2000.

[95] G. T. Gray III, "Classic split-hopkinson pressure bar testing," *ASM Handbook, Mechanical testing and evaluation*, vol. 8, pp. 462–476, 2000.

[96] W. W. Chen and B. Song, *Split Hopkinson (Kolsky) bar: design, testing and applications*. Springer Science & Business Media, 2010.

[97] C. R. Siviour, "High strain rate characterization of polymers," in *AIP Conference Proceedings*, vol. 1793, AIP Publishing, 2017.

[98] J. Harding, E. Wood, and J. Campbell, "Tensile testing of materials at impact rates of strain," *Journal of Mechanical Engineering Science*, vol. 2, no. 2, pp. 88–96, 1960.

[99] S. Fu, Y. Wang, and Y. Wang, "Tension testing of polycarbonate at high strain rates," *Polymer Testing*, vol. 28, no. 7, pp. 724–729, 2009.

[100] B. Song, Y. Ge, W. Chen, and T. Weerasooriya, "Radial inertia effects in kolsky bar testing of extra-soft specimens," *Experimental Mechanics*, vol. 47, pp. 659–670, 2007.

[101] D. Gorham, "Specimen inertia in high strain-rate compression," *Journal of Physics D: Applied Physics*, vol. 22, no. 12, p. 1888, 1989.

[102] R. Gerlach, S. K. Sathianathan, C. Siviour, and N. Petrinic, "A novel method for pulse shaping of split hopkinson tensile bar signals," *International Journal of Impact Engineering*, vol. 38, no. 12, pp. 976–980, 2011.

[103] R. Gerlach, C. Kettenbeil, and N. Petrinic, "A new split hopkinson tensile bar design," *International Journal of Impact Engineering*, vol. 50, pp. 63–67, 2012.

[104] X. Nie, B. Song, Y. Ge, W. Chen, and T. Weerasooriya, "Dynamic tensile testing of soft materials," *Experimental mechanics*, vol. 49, pp. 451–458, 2009.

[105] B. Briscoe and I. Hutchings, "Impact yielding of high density polyethylene," *Polymer*, vol. 17, no. 12, pp. 1099–1102, 1976.

[106] D. Erlich, "Rod impact (taylor) test," *Metals handbook*, vol. 8, pp. 203–207, 1985.

[107] W. Carrington and M. L. Gayler, "The use of flat-ended projectiles for determining dynamic yield stress iii. changes in microstructure caused by deformation under impact at high-striking velocities," *Proceedings of the Royal Society of London. Series A. Mathematical and Physical Sciences*, vol. 194, no. 1038, pp. 323–331, 1948.

[108] W. N. Sharpe, *Springer handbook of experimental solid mechanics*. Springer Science & Business Media, 2008.

[109] J. Furmanski, C. P. Trujillo, D. T. Martinez, G. T. Gray III, and E. N. Brown, "Dynamic-tensile-extrusion for investigating large strain and high strain rate behavior of polymers," *Polymer testing*, vol. 31, no. 8, pp. 1031–1037, 2012.

[110] J. Furmanski, E. N. Brown, G. T. Gray, C. Trujillo, D. T. Martinez, S. Bilyk, and R. Becker, "Extreme tensile damage and failure in glassy polymers via dynamic-tensile-extrusion," in *Dynamic Behavior of Materials, Volume 1: Proceedings of the 2013 Annual Conference on Experimental and Applied Mechanics*, pp. 107–112, Springer, 2014.

[111] E. Brown, J. Furmanski, K. Ramos, D. Dattelbaum, B. Jensen, A. Iverson, C. Carlson, K. Fezzaa, G. Gray, B. Patterson, *et al.*, "High-density polyethylene damage at extreme tensile conditions," in *Journal of Physics: Conference Series*, vol. 500, p. 112011, IOP Publishing, 2014.

[112] C. Bauwens-Crowet, "The compression yield behaviour of polymethyl methacrylate over a wide range of temperatures and strain-rates," *Journal of Materials Science*, vol. 8, pp. 968–979, 1973.

[113] J. Rinde and K. Hoge, "Time and temperature dependence of the mechanical properties of polystyrene bead foam," *Journal of Applied Polymer Science*, vol. 15, no. 6, pp. 1377–1395, 1971.

[114] C. Siviour, S. Walley, W. Proud, and J. Field, "The high strain rate compressive behaviour of polycarbonate and polyvinylidene difluoride," *Polymer*, vol. 46, no. 26, pp. 12546–12555, 2005.

[115] M. J. Kendall and C. R. Siviour, "Rate dependence of poly (vinyl chloride), the effects of plasticizer and time–temperature superposition," *Proceedings of the Royal Society A: Mathematical, Physical and Engineering Sciences*, vol. 470, no. 2167, p. 20140012, 2014.

[116] M. Kanters, "Prediction of long-term performance of load-bearing thermoplastics," 2015.

[117] E. Brown, R. Willms, G. Gray, P. Rae, C. Cady, K. Vecchio, J. Flowers, and M. Martinez, "Influence of molecular conformation on the constitutive response of polyethylene: a comparison of hdpe, uhmwpe, and pex," *Experimental mechanics*, vol. 47, pp. 381–393, 2007.

[118] I. Katsivalis, A. Chanteli, W. Finnegan, and T. M. Young, "Mechanical and interfacial characterisation of leading-edge protection materials for wind turbine blade applications," *Wind Energy*, vol. 25, no. 10, pp. 1758–1774, 2022.

[119] M. Forrestal, T. Wright, and W. Chen, "The effect of radial inertia on brittle samples during the split hopkinson pressure bar test," *International Journal of Impact Engineering*, vol. 34, no. 3, pp. 405–411, 2007.

[120] S. Chou, K. Robertson, and J. Rainey, "The effect of strain rate and heat developed during deformation on the stress-strain curve of plastics: Temperature rise developed during deformation can have significant effects on the stress-strain relationship. four hard plastics are tested at various strain rates, and temperature changes are measured during deformation of the specimen," *Experimental mechanics*, vol. 13, no. 10, pp. 422–432, 1973.

[121] D. Rittel, "On the conversion of plastic work to heat during high strain rate deformation of glassy polymers," *Mechanics of Materials*, vol. 31, no. 2, pp. 131–139, 1999.

[122] M. J. Kendall and C. R. Siviour, "Experimentally simulating adiabatic conditions: approximating high rate polymer behavior using low rate experiments with temperature profiles," *Polymer*, vol. 54, no. 18, pp. 5058–5063, 2013.

[123] M. J. Kendall and C. R. Siviour, "Experimentally simulating high rate composite deformation in tension and compression: polymer bonded explosive simulant," *Journal of Dynamic Behavior of Materials*, vol. 1, pp. 114–123, 2015.

[124] J. Radon and L. Culver, "Effect of temperature and frequency in fatigue of polymers," *Polymer*, vol. 16, no. 7, pp. 539–544, 1975.

[125] G. Hartwig and S. Knaak, "Fatigue behaviour of polymers," *Cryogenics*, vol. 31, no. 4, pp. 231–233, 1991.

[126] A. Mura, A. Ricci, and G. Canavese, "Investigation of fatigue behavior of abs and pc-abs polymers at different temperatures," *Materials*, vol. 11, no. 10, p. 1818, 2018.

[127] J. Radon and L. Culver, "Fatigue crack growth in polymers. i. effect of frequency and temperature," *Polymer Engineering & Science*, vol. 15, no. 7, pp. 500–506, 1975.

[128] A. Al-Abduljabbar, B. Melve, N. Dodds, and A. Gibson, "Investigation of low temperature effects on fatigue behavior of pvdf," *Engineering Failure Analysis*, vol. 14, no. 8, pp. 1594–1604, 2007.

[129] H. Visser, T. C. Bor, M. Wolters, L. Warnet, and L. Govaert, "Influence of physical aging on impact embrittlement of upvc pipes," *Plastics, rubber and composites*, vol. 40, no. 5, pp. 201–212, 2011.

[130] I. NEN, "Iso 37:2017 - rubber, vulcanized or thermoplastic - determination of tensile stress-strain properties," May 2023.

[131] R. Kalia, S. Kumar, H. Bhatti, and J. Sharma, "Study of dielectric behavior of nanoporous polycarbonate membrane for future nano-electret applications," *Digest Journal of Nanomaterials and Biostructures*, vol. 3, no. 4, pp. 237–243, 2008.

[132] M. Dixit, V. Mathur, S. Gupta, M. Baboo, K. Sharma, and N. Saxena, "Morphology, miscibility and mechanical properties of pmma/pc blends," *Phase Transitions*, vol. 82, no. 12, pp. 866–878, 2009.

[133] M. Chanda and S. K. Roy, *Plastics technology handbook*. CRC press, 2006.

[134] Simona, "Technical data sheet simona® pvc-caw."

[135] E. H. Backes, S. V. Harb, L. A. Pinto, N. K. de Moura, G. F. de Melo Morgado, J. Marini, F. R. Passador, and L. A. Pessan, "Thermoplastic polyurethanes: synthesis, fabrication techniques, blends, composites, and applications," *Journal of Materials Science*, vol. 59, no. 4, pp. 1123–1152, 2024.

[136] J. O. Akindoyo, M. Beg, S. Ghazali, M. Islam, N. Jeyaratnam, and A. Yuvaraj, "Polyurethane types, synthesis and applications–a review," *Rsc Advances*, vol. 6, no. 115, pp. 114453–114482, 2016.

[137] F. Günther, E. F. Lima, K. M. Rossi de Aguiar, J. R. Bearzi, M. B. Simões, R. Schneider, R. A. Bini, S. J. Ribeiro, M. W. C. Man, K. Rischka, *et al.*, "Pdms-urethanesil hybrid multifunctional materials: combining co2 use and sol-gel processing," *Journal of Sol-Gel Science and Technology*, vol. 95, no. 3, pp. 693–709, 2020.

[138] P. H. Daniels and A. Cabrera, "Plasticizer compatibility testing: Dynamic mechanical analysis and glass transition temperatures," *Journal of Vinyl and Additive Technology*, vol. 21, no. 1, pp. 7–11, 2015.

[139] V. Mathur and P. K. Arya, "Dynamic mechanical analysis of pvc/tio 2 nanocomposites," *Advanced Composites and Hybrid Materials*, vol. 1, pp. 741–747, 2018.

[140] A. A. Al-Juaid and R. Othman, "Modeling of the strain rate dependency of polycarbonate's yield stress: evaluation of four constitutive equations," *Journal of Engineering*, vol. 2016, no. 1, p. 6315421, 2016.

[141] R. Hagen, L. Salmén, H. Lavebratt, and B. Stenberg, "Comparison of dynamic mechanical measurements and tg determinations with two different instruments," *Polymer testing*, vol. 13, no. 2, pp. 113–128, 1994.

[142] D. Dunson, "Characterization of polymers using dynamic mechanical analysis (dma)," *EAG Appl Note*, pp. 1–8, 2017.

[143] Q. Yuan, T. Zhou, L. Li, J. Zhang, X. Liu, X. Ke, and A. Zhang, "Hydrogen bond breaking of tpu upon heating: understanding from the viewpoints of molecular movements and enthalpy," *Rsc Advances*, vol. 5, no. 39, pp. 31153–31165, 2015.

[144] S. Tamrakar, R. Ganesh, S. Sockalingam, B. Z. Haque, and J. W. Gillespie Jr, "Strain rate-dependent large deformation inelastic behavior of an epoxy resin," *Journal of Composite Materials*, vol. 54, no. 1, pp. 71–87, 2020.

CHAPTER 10

Appendix

10.1 SEM results

This Appendix shows the results of the SEM microscopy. First, the full sample is shown, after which each sample is divided into 5 regions: Left-Hand Side (LHS), Left-Middle (LM), Middle (M), Right-Middle, and Right-Hand Side (RHS).

-30 ^{o}C, 95N

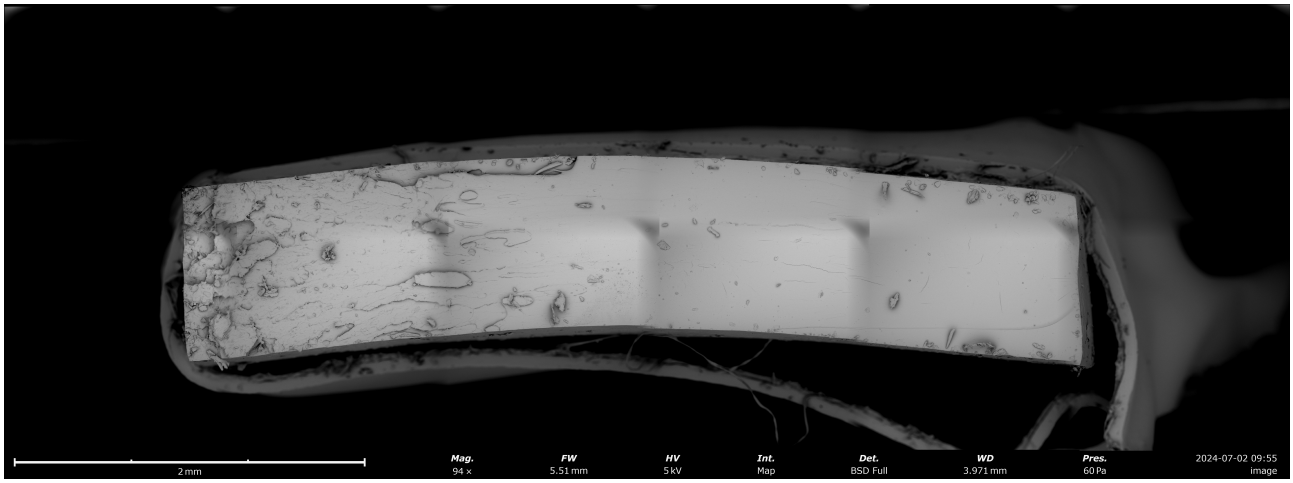

Figure 10.1: SEM image of sample tested at -30 ^{o}C and 95N - Full sample

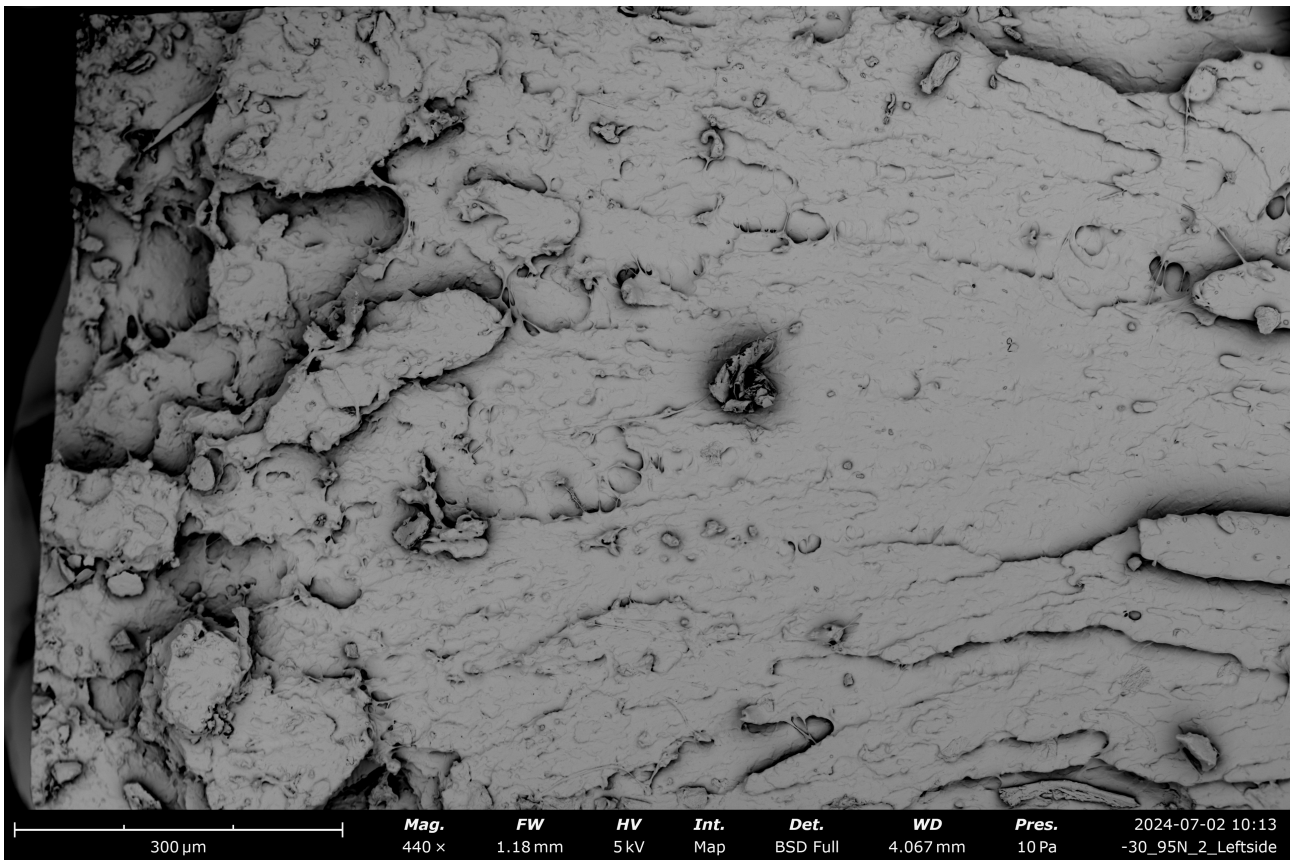

Figure 10.2: SEM image of sample tested at -30 ^{o}C and 95N - LHS

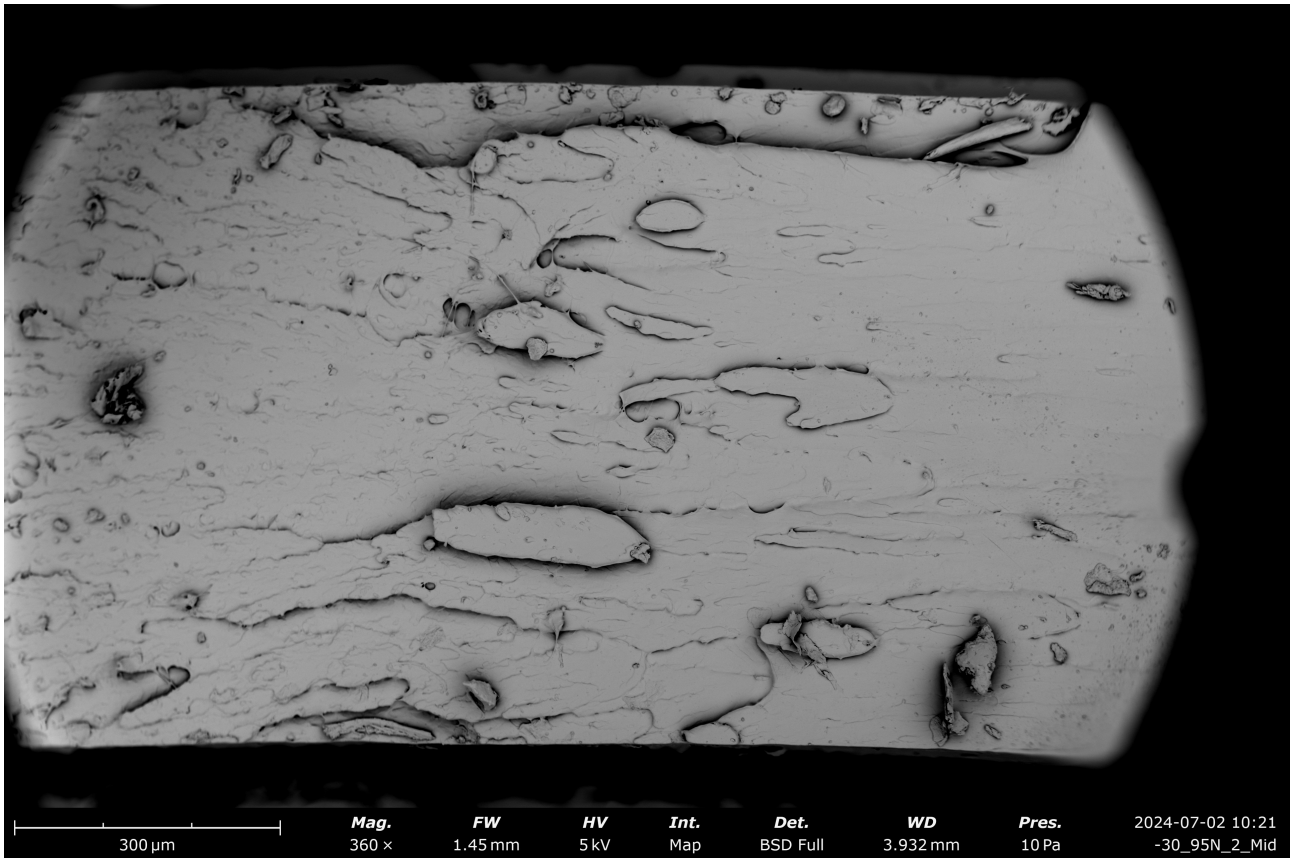

Figure 10.3: SEM image of sample tested at -30 ^{o}C and 95N - LM

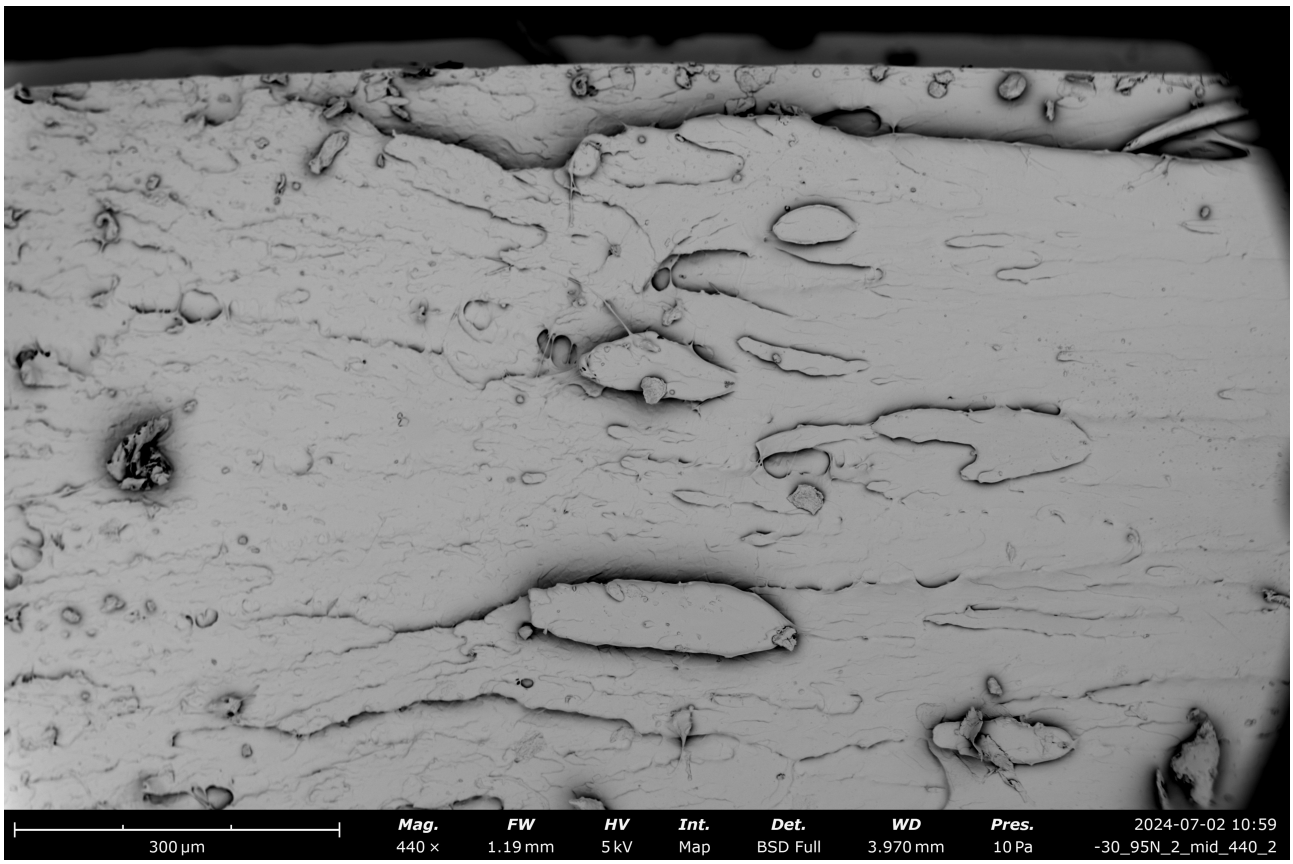

Figure 10.4: SEM image of sample tested at -30 ^{o}C and 95N - M

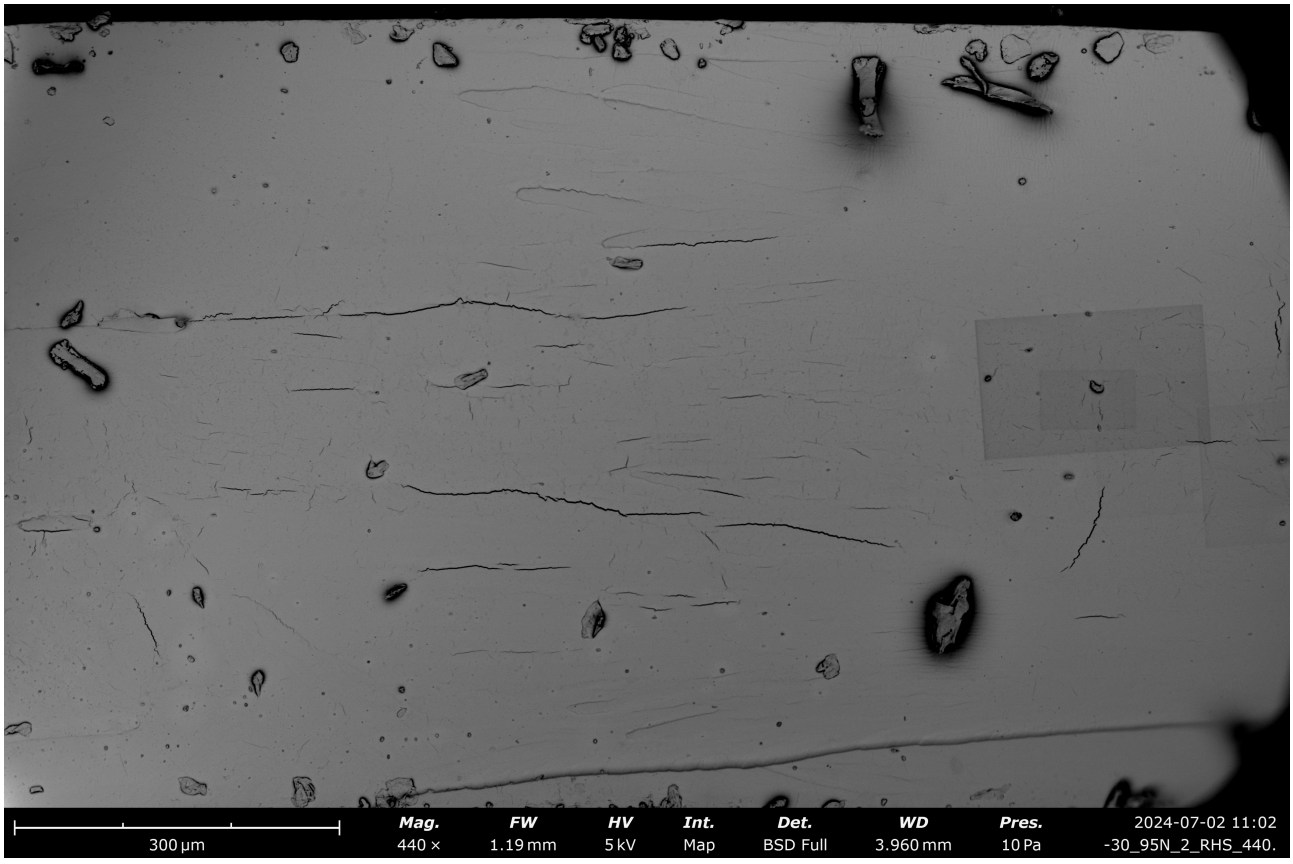

Figure 10.5: SEM image of sample tested at -30 ^{o}C and 95N - RM

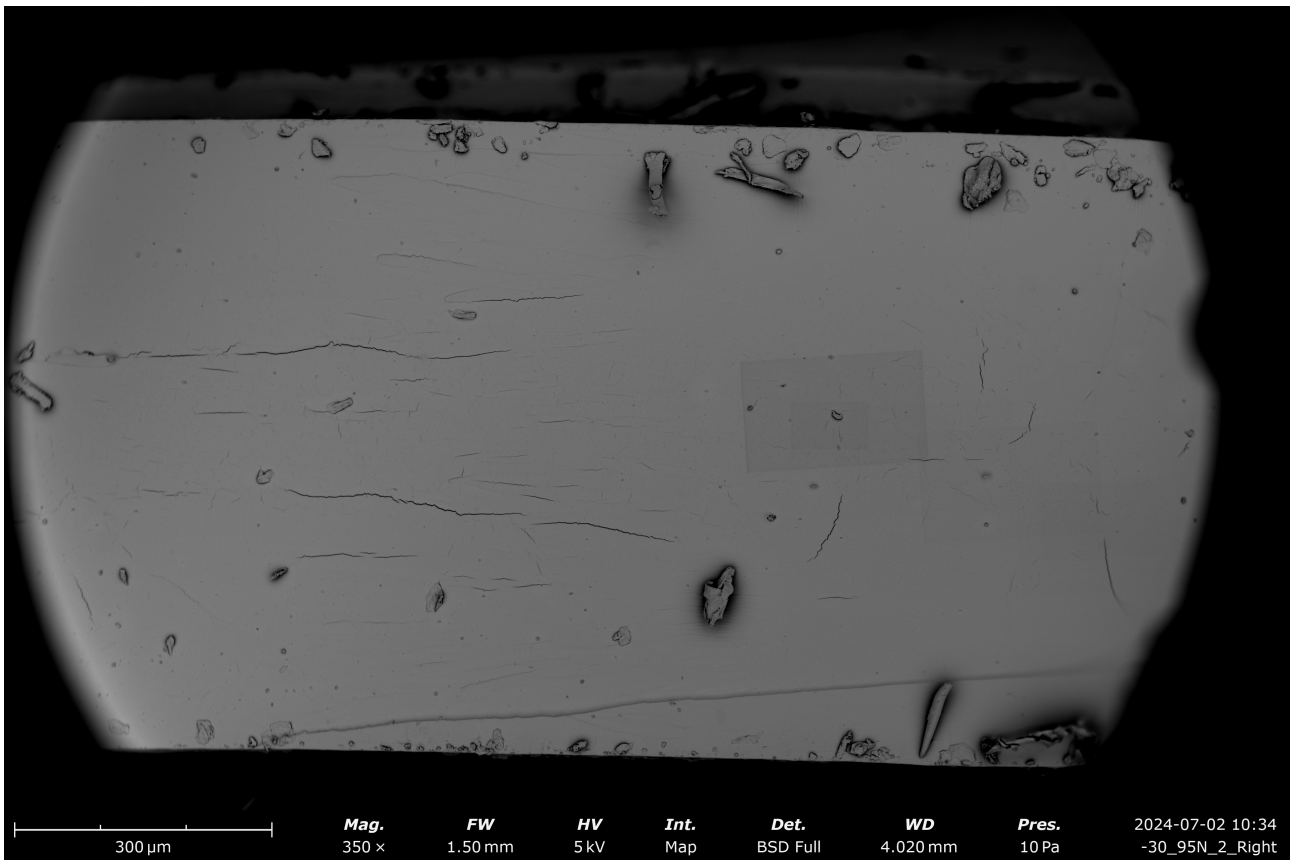

Figure 10.6: SEM image of sample tested at -30 ^{o}C and 95N - RHS

-30 ^{o}C, 85N

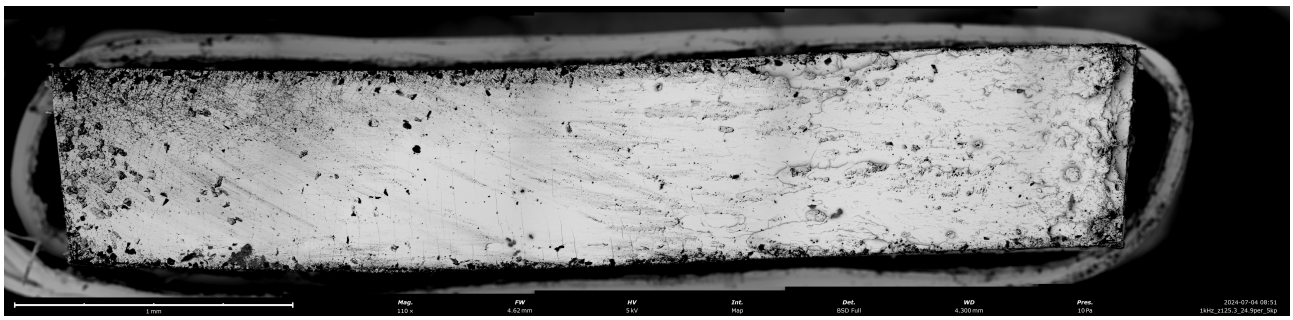

Figure 10.7: SEM image of sample tested at -30 ^{o}C and 85N - Full sample

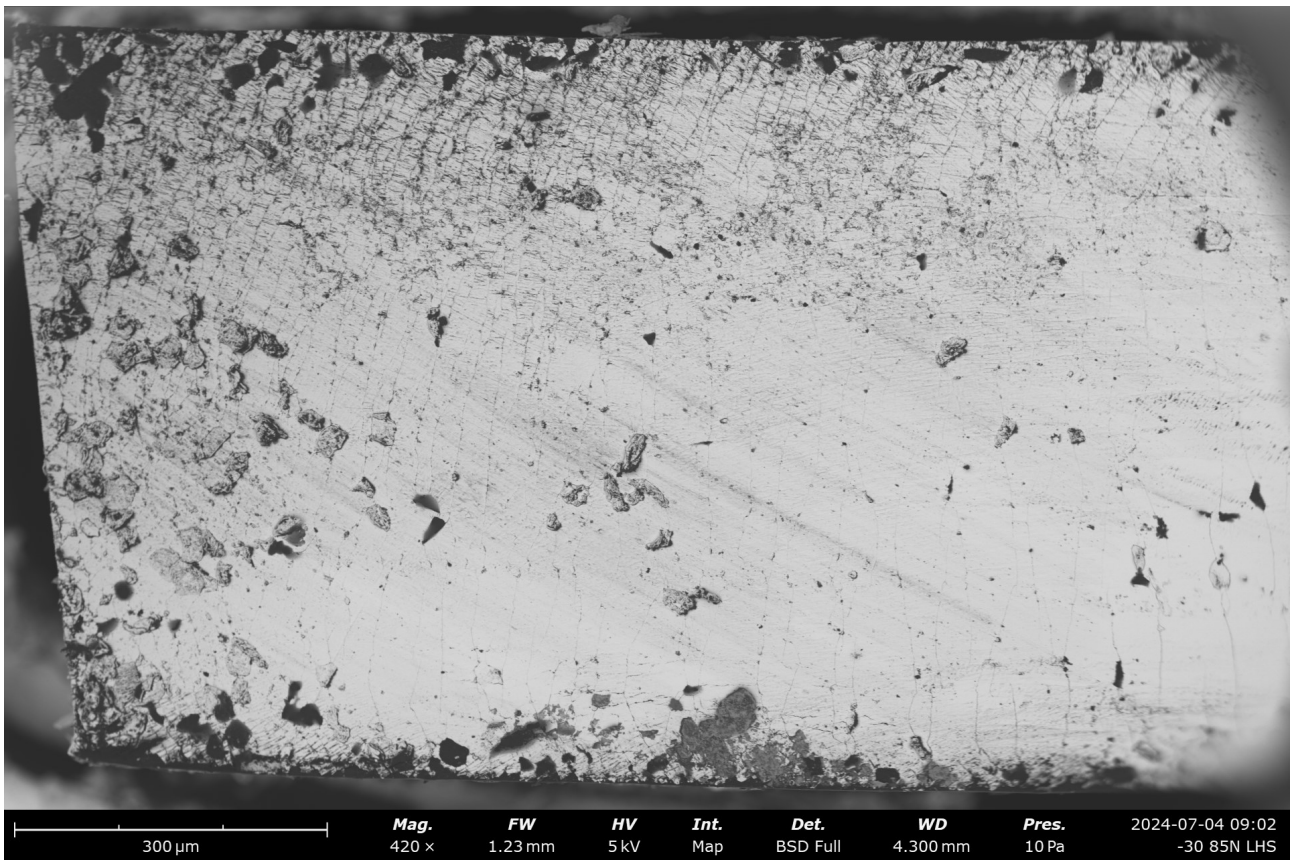

Figure 10.8: SEM image of sample tested at -30 ^{o}C and 85N - LHS

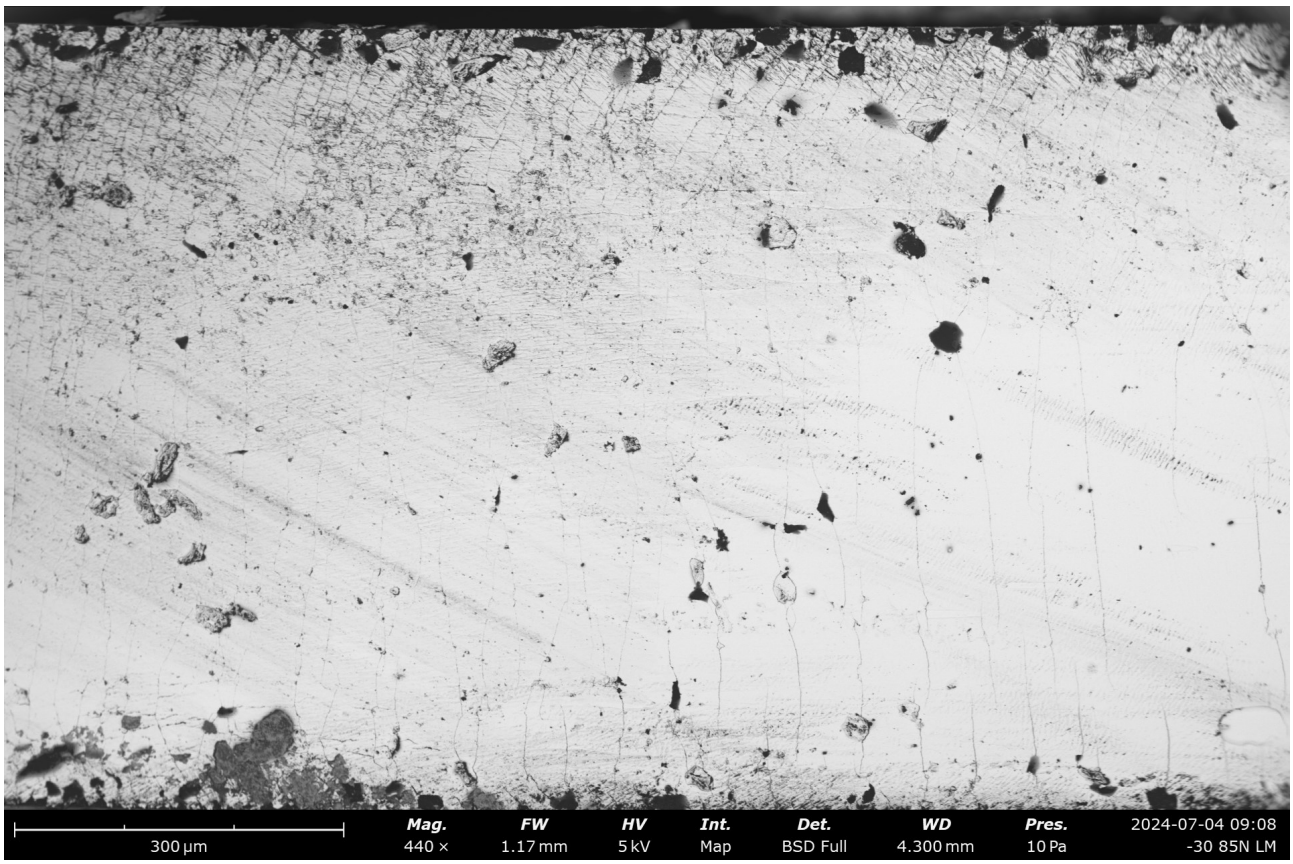

Figure 10.9: SEM image of sample tested at -30 ^{o}C and 85N - LM

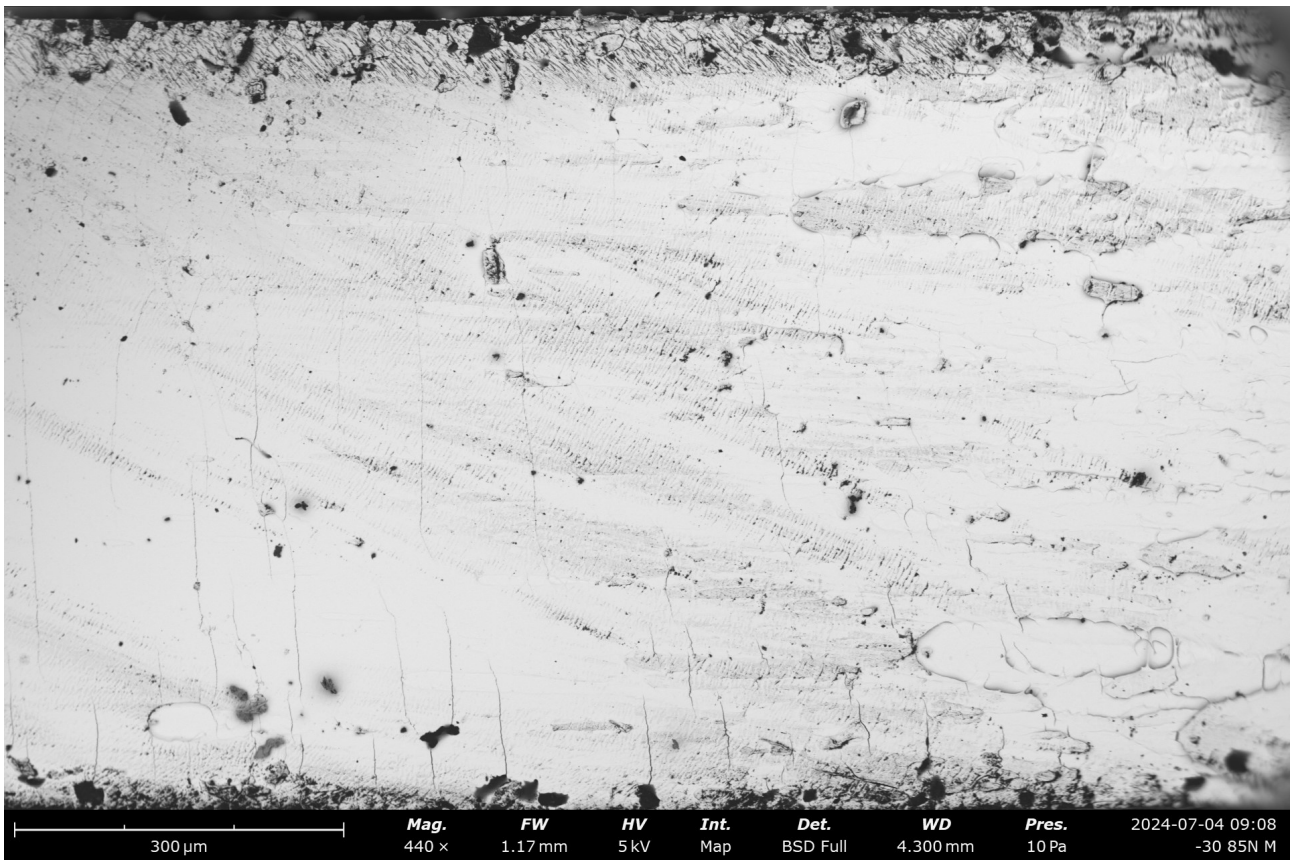

Figure 10.10: SEM image of sample tested at -30 ^{o}C and 85N - M

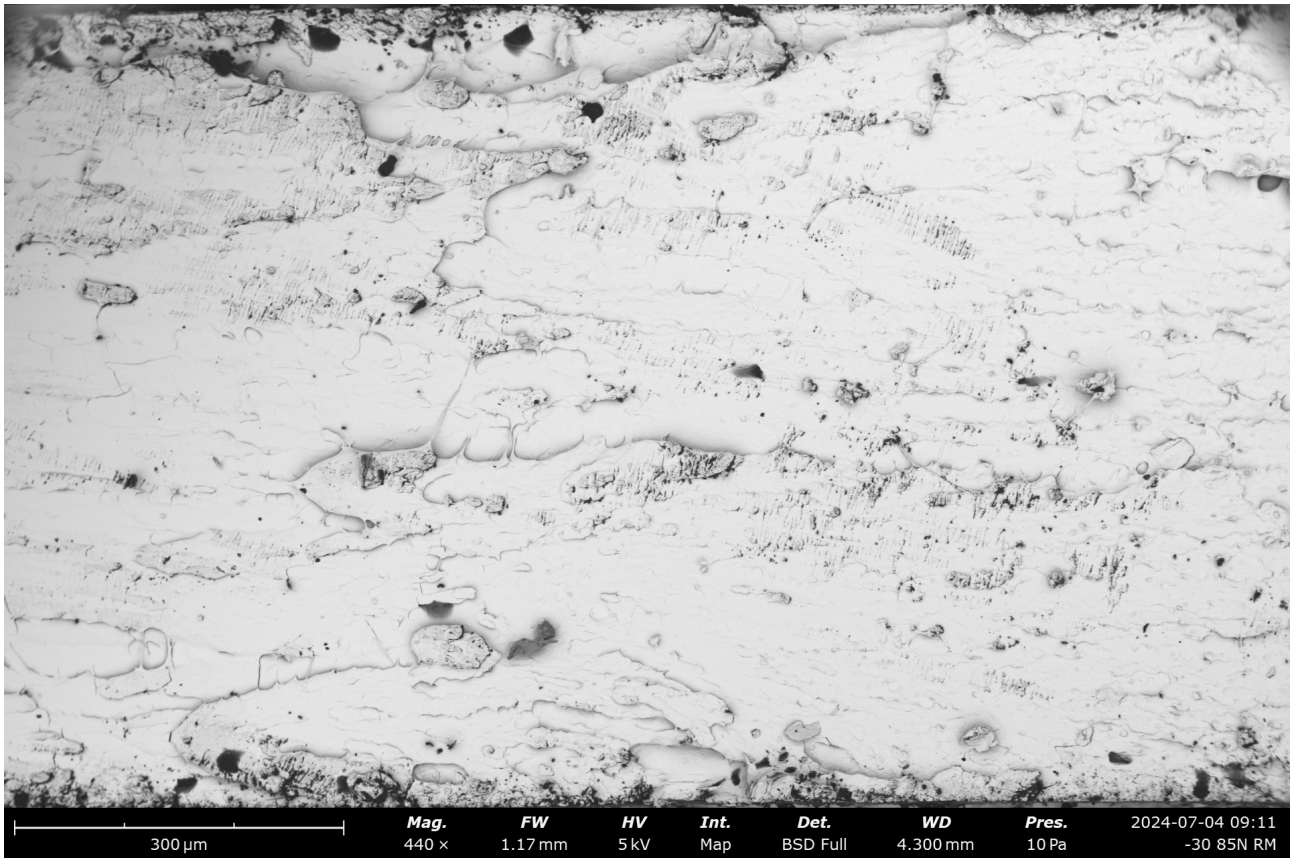

Figure 10.11: SEM image of sample tested at -30 ^{o}C and 85N - RM

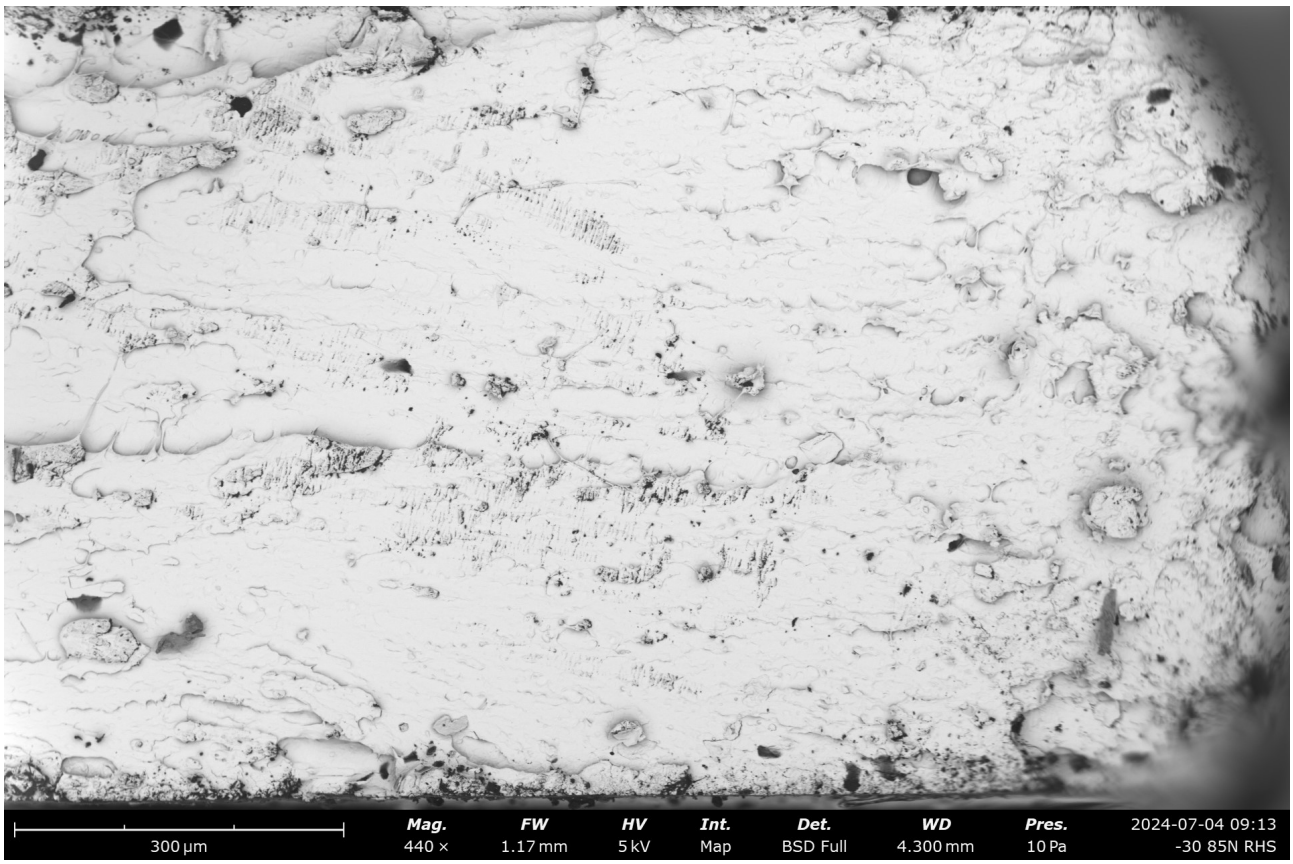

Figure 10.12: SEM image of sample tested at -30 ^{o}C and 85N - RHS

-30 ^{o}C, 80N

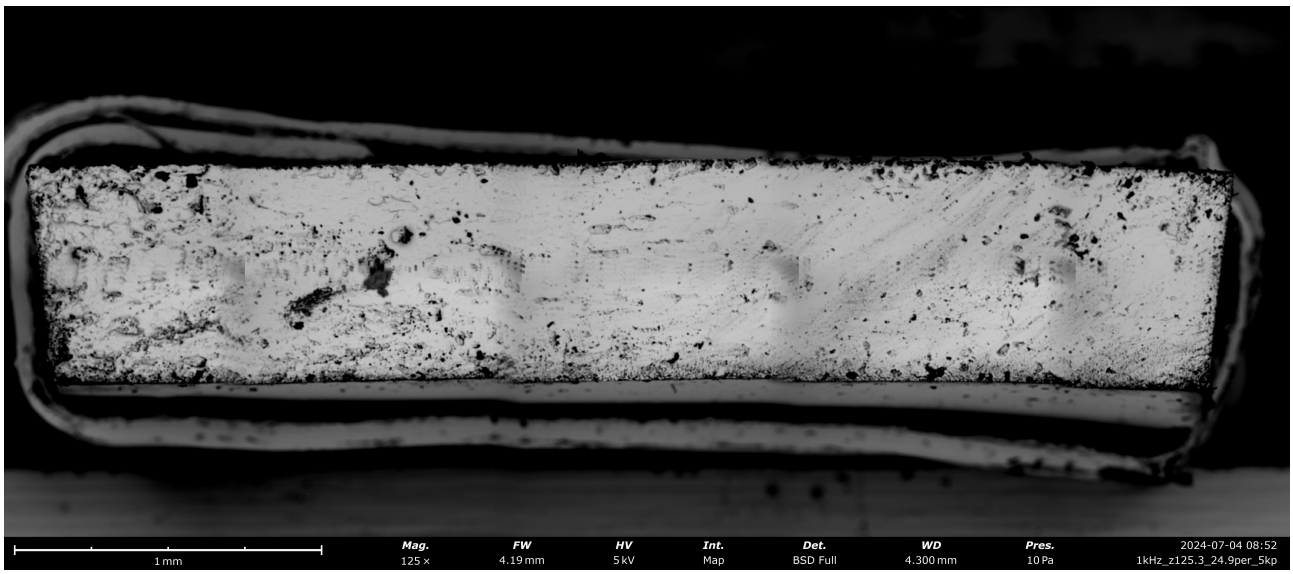

Figure 10.13: SEM image of sample tested at -30 ^{o}C and 80N - Full sample

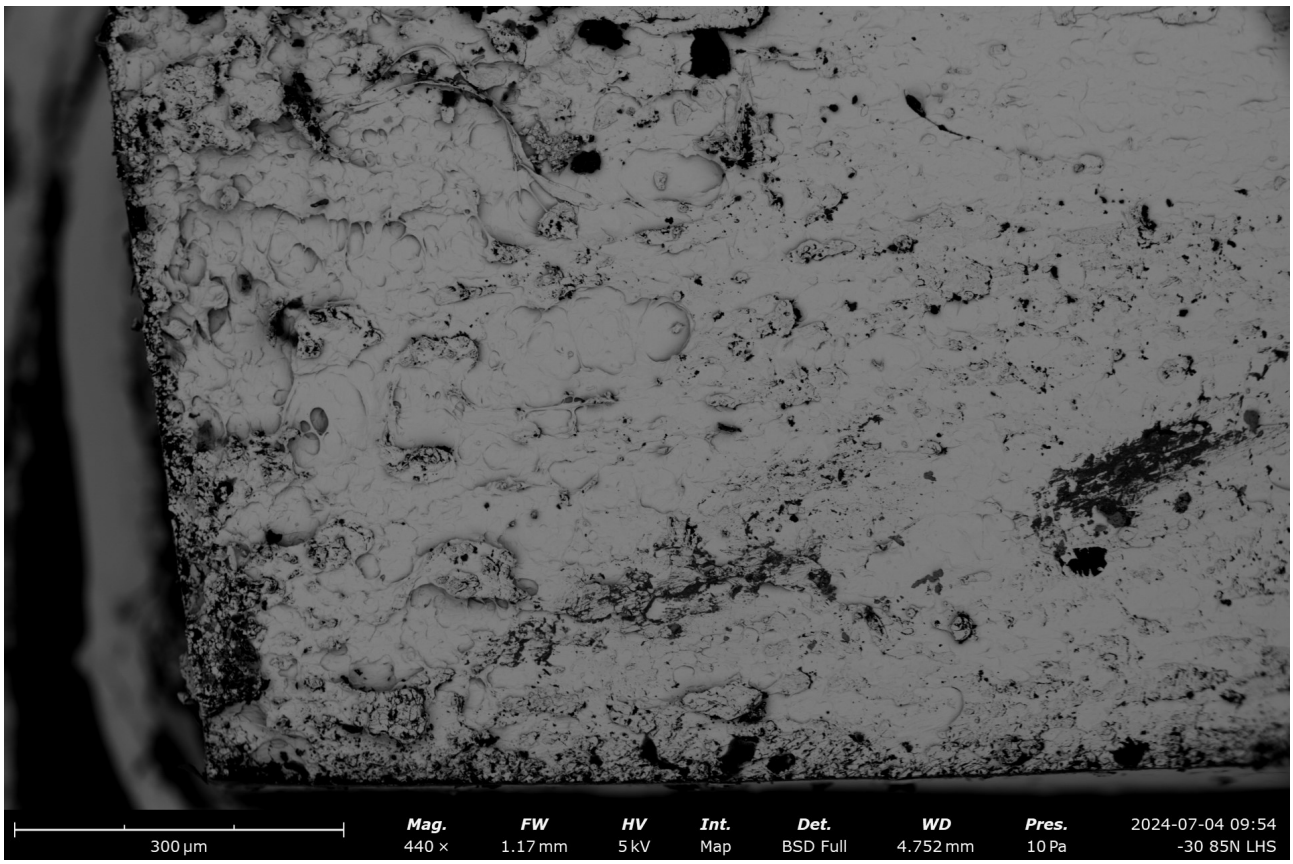

Figure 10.14: SEM image of sample tested at -30 ^{o}C and 80N - LHS

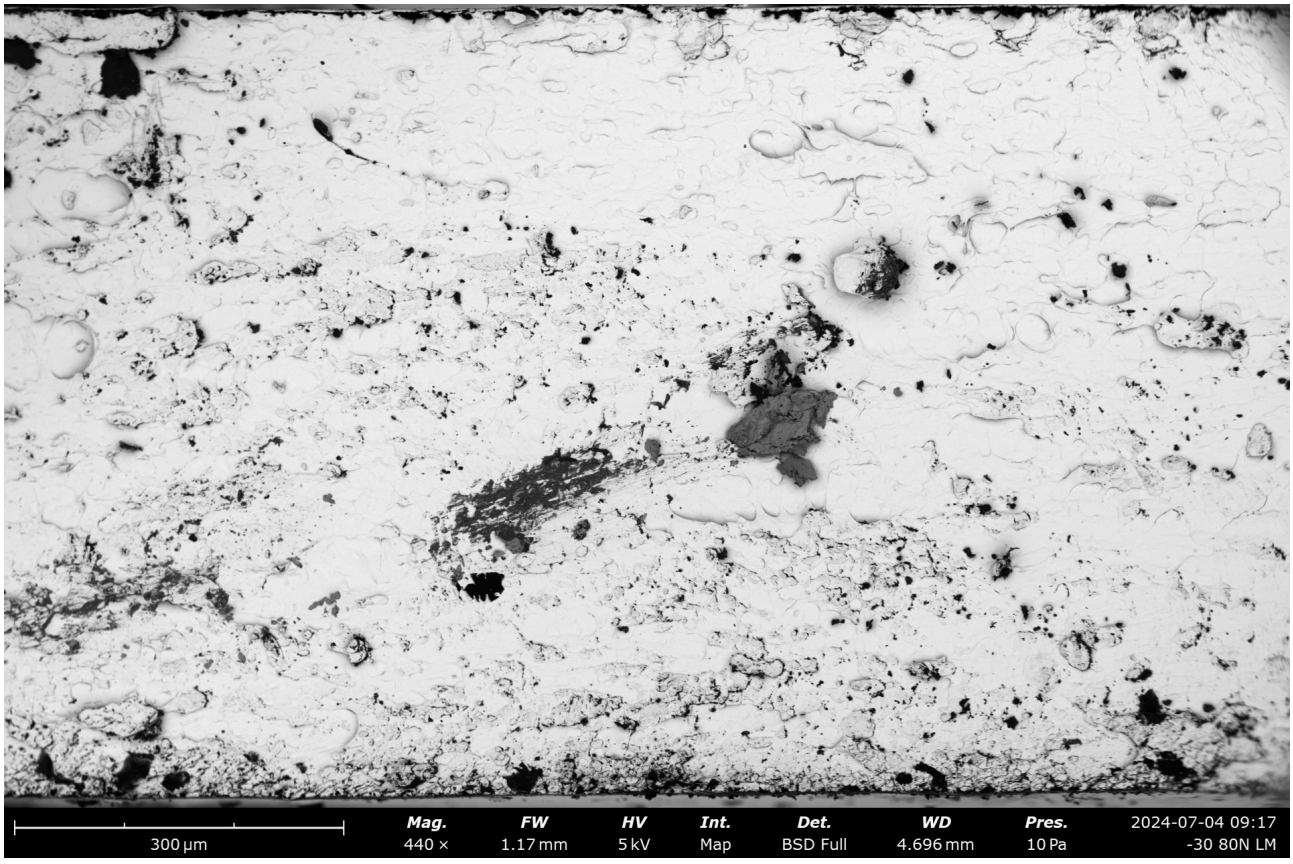

Figure 10.15: SEM image of sample tested at -30 ^{o}C and 80N - LM

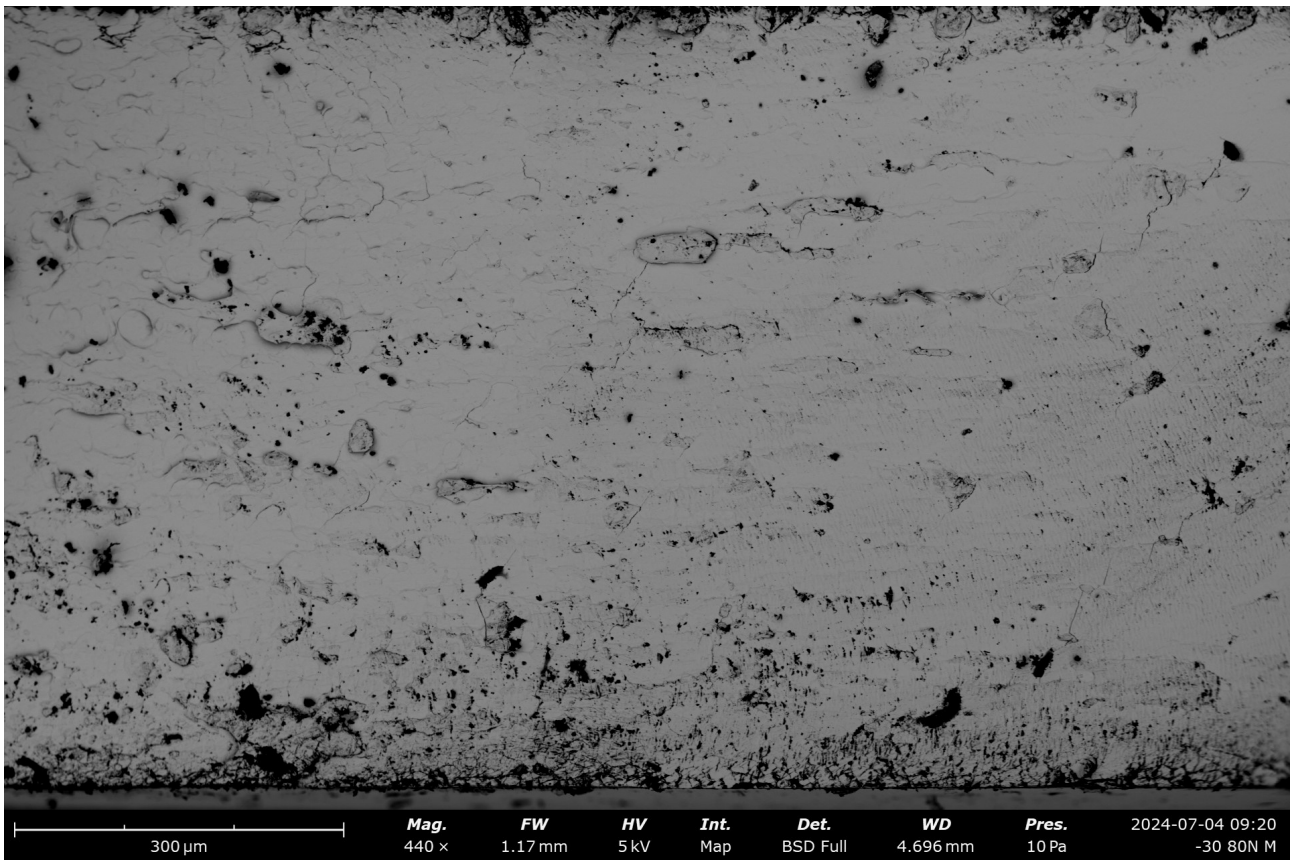

Figure 10.16: SEM image of sample tested at -30 ^{o}C and 80N - M

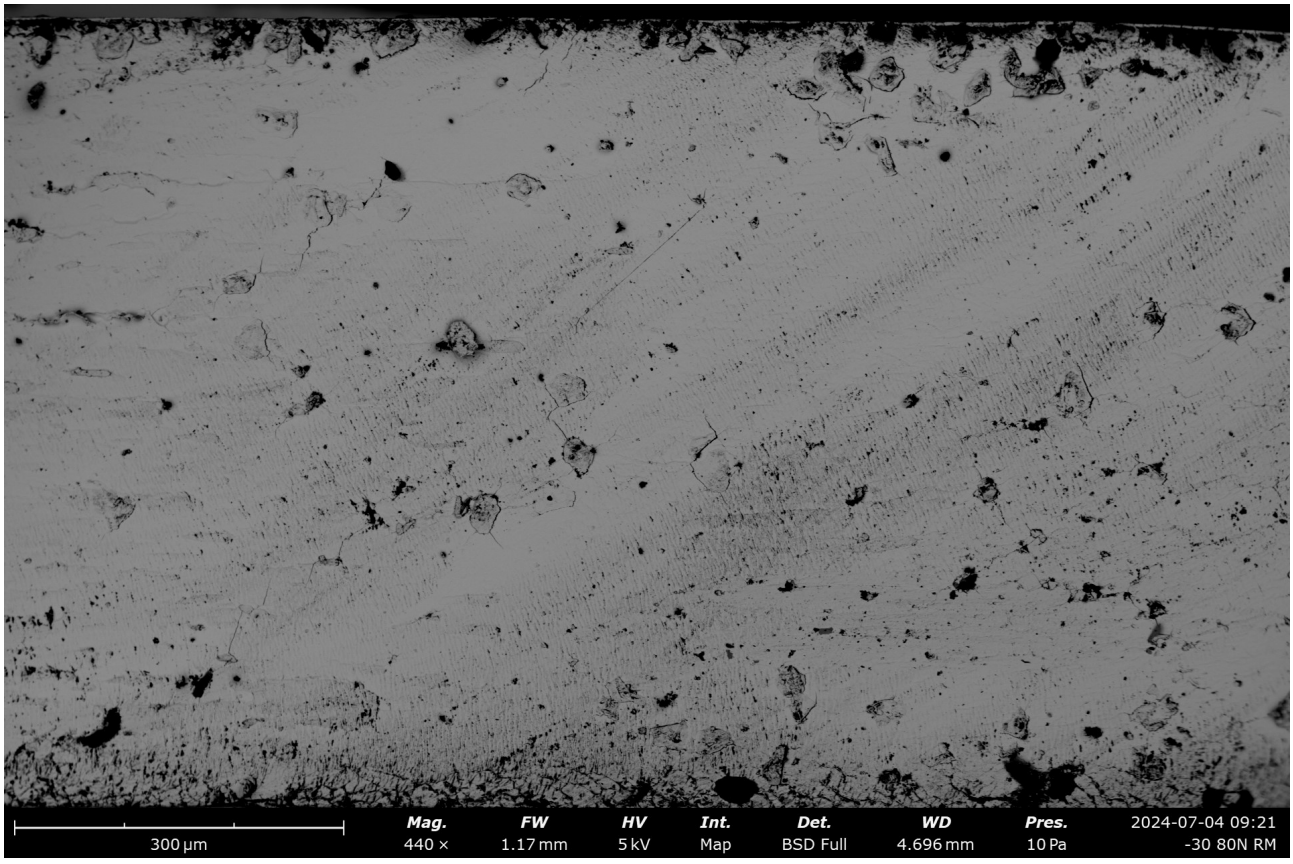

Figure 10.17: SEM image of sample tested at -30 ^{o}C and 80N - RM

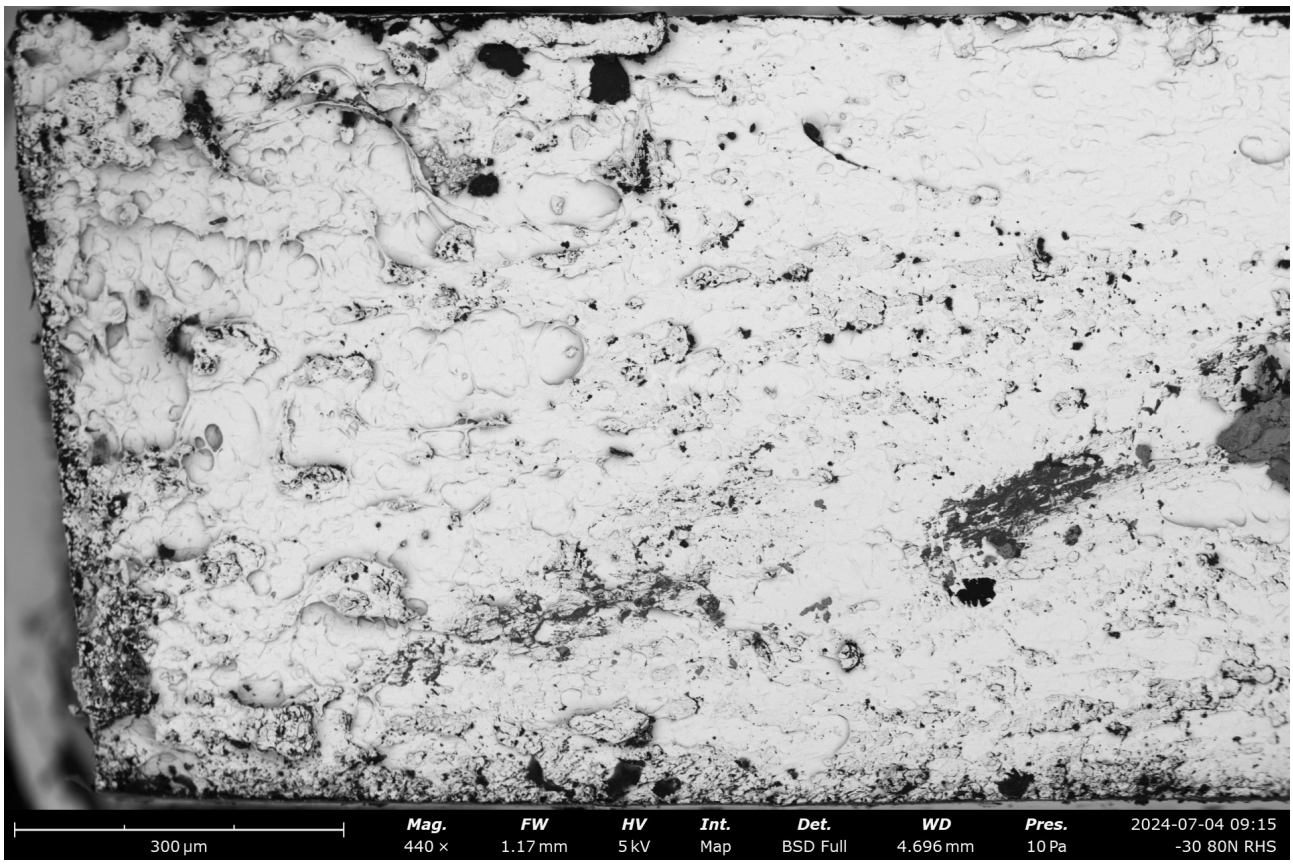

Figure 10.18: SEM image of sample tested at -30 ^{o}C and 80N - RHS

-20 ^{o}C, 100N

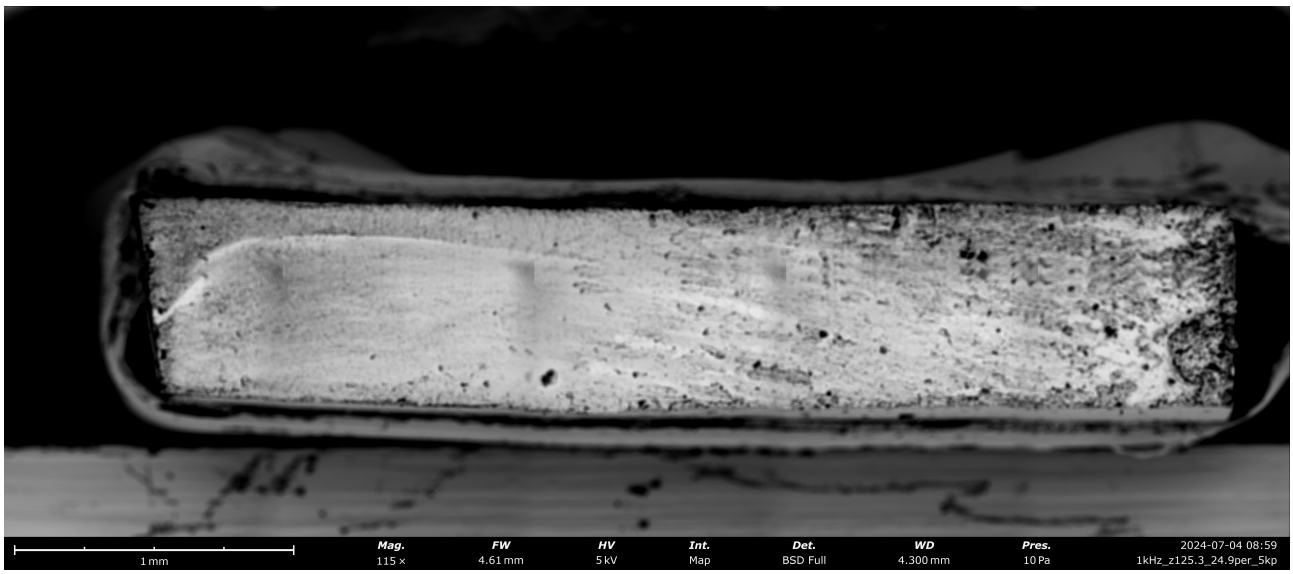

Figure 10.19: SEM image of sample tested at -20 ^{o}C and 100N - Full sample

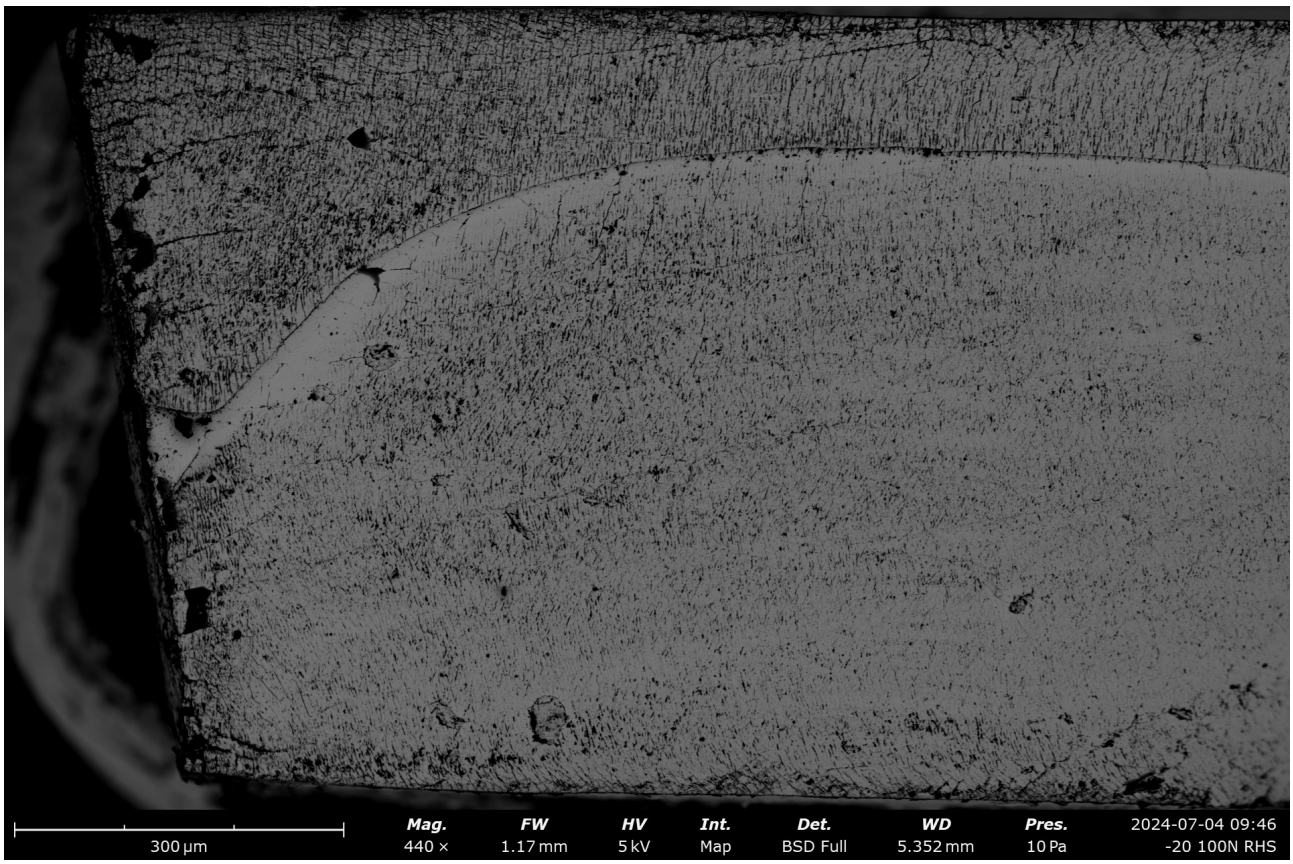

Figure 10.20: SEM image of sample tested at -20 ^{o}C and 100N - LHS

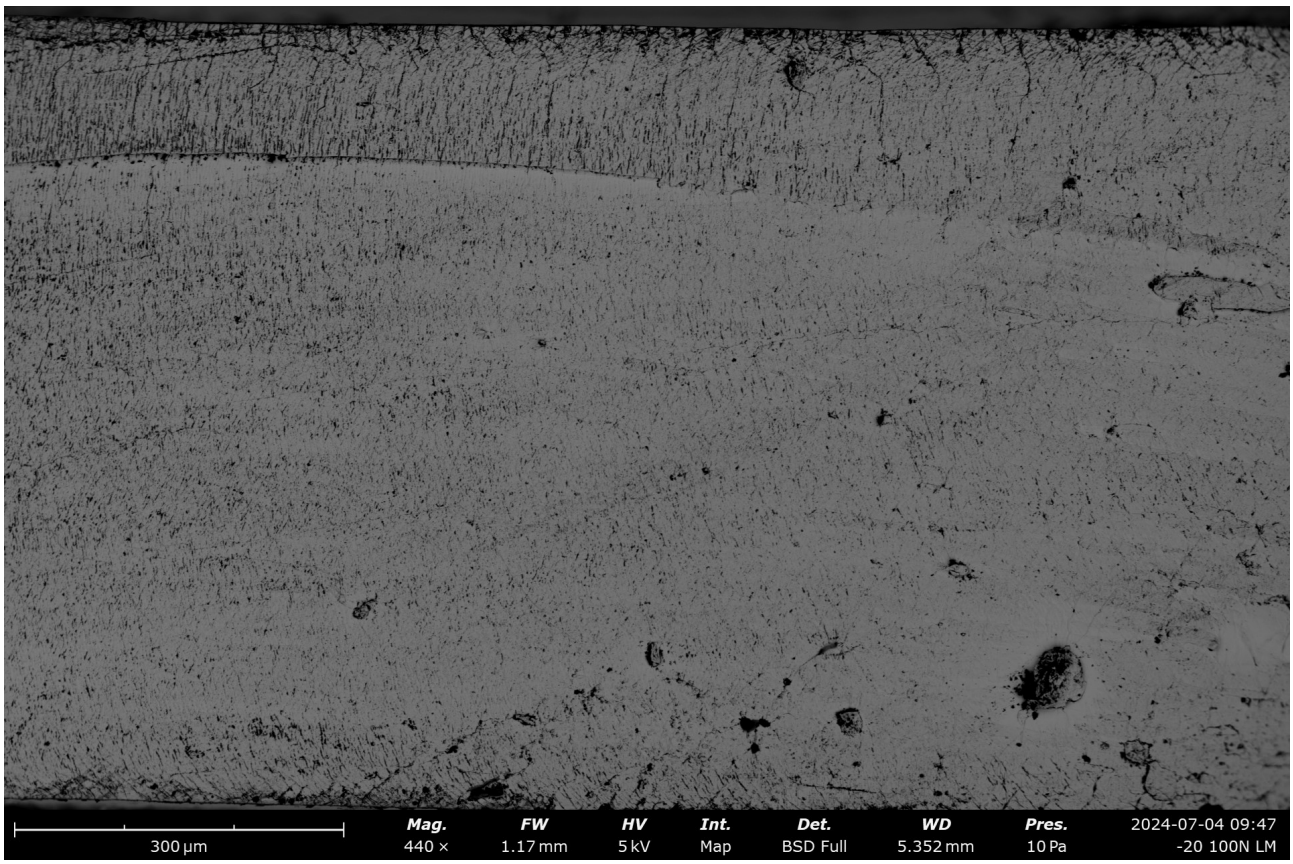

Figure 10.21: SEM image of sample tested at -20 ^{o}C and 100N - LM

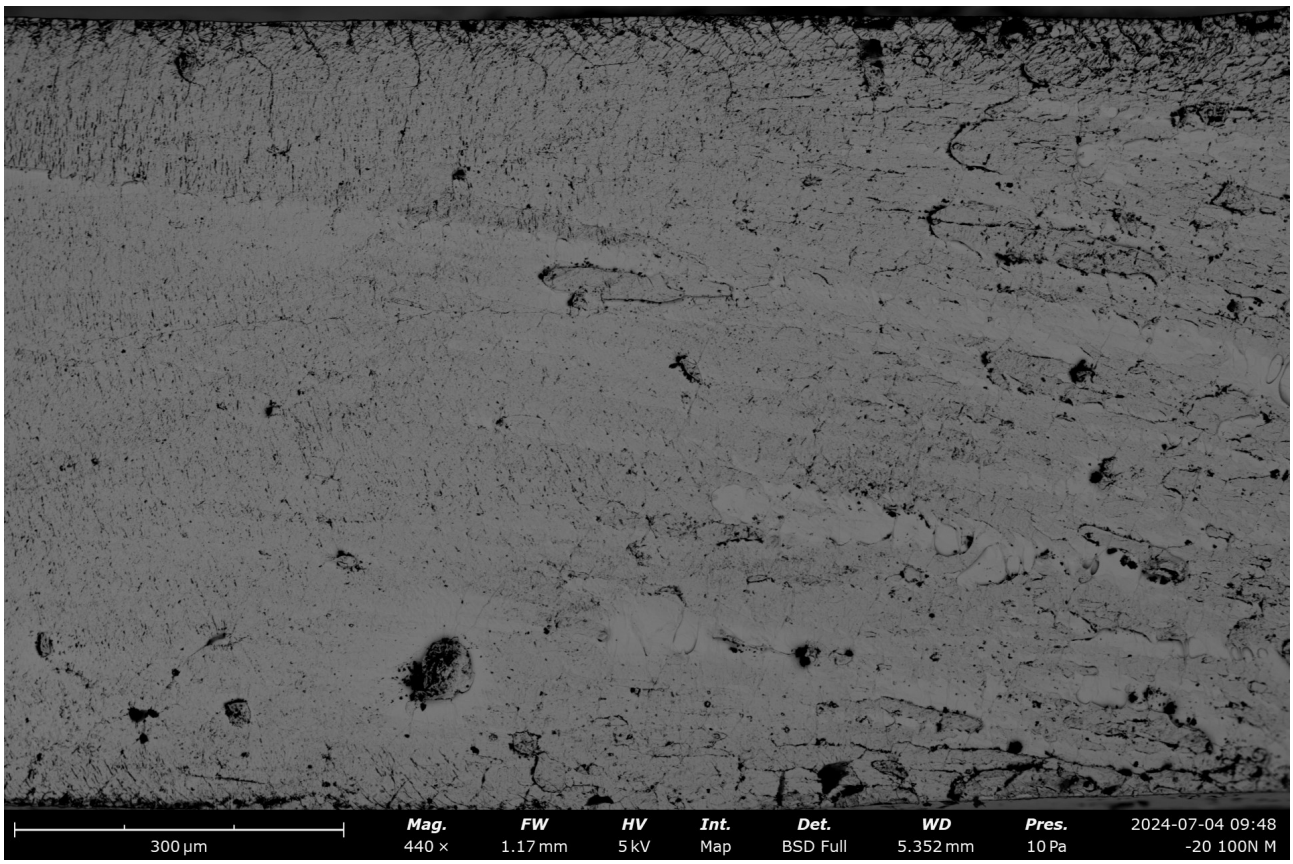

Figure 10.22: SEM image of sample tested at -20 ^{o}C and 100N - M

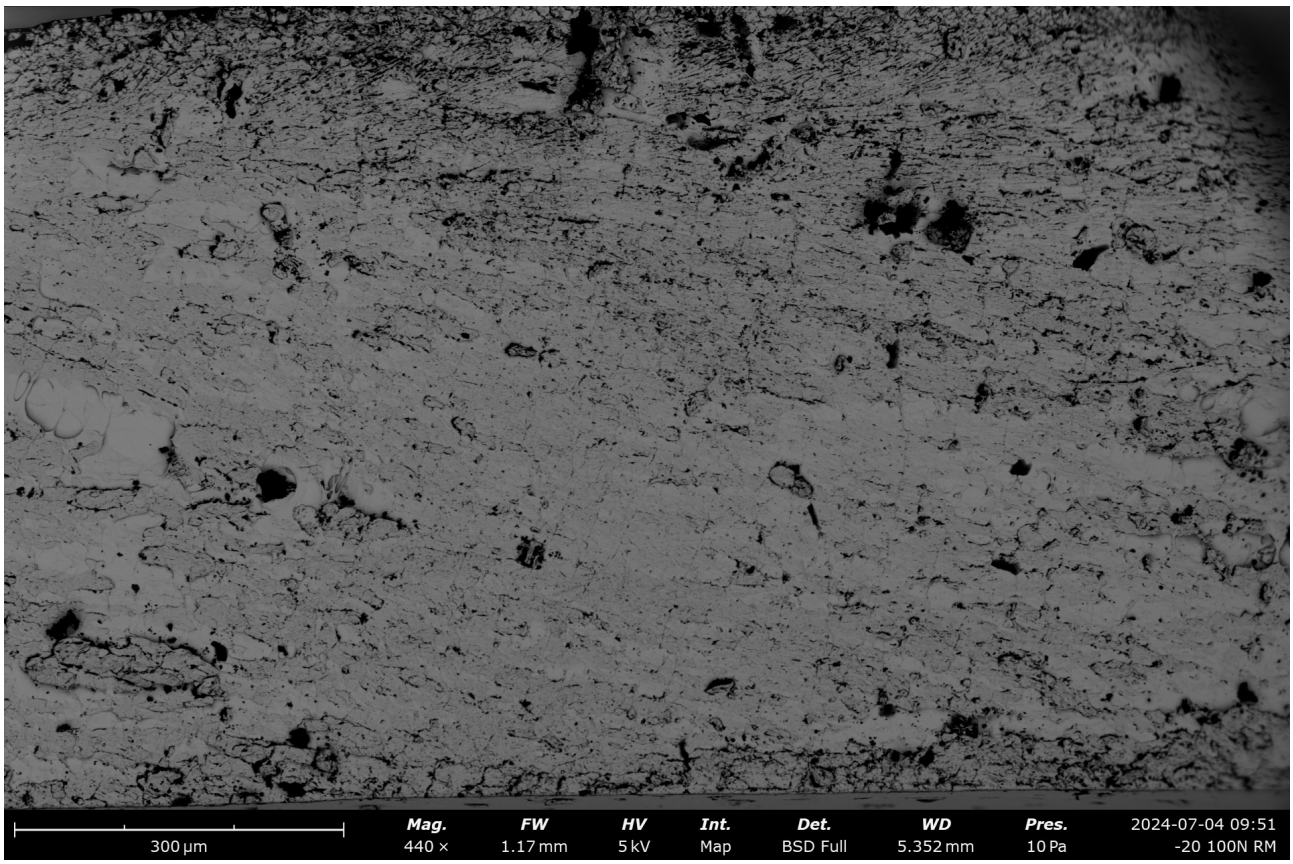

Figure 10.23: SEM image of sample tested at -20 ^{o}C and 100N - RM

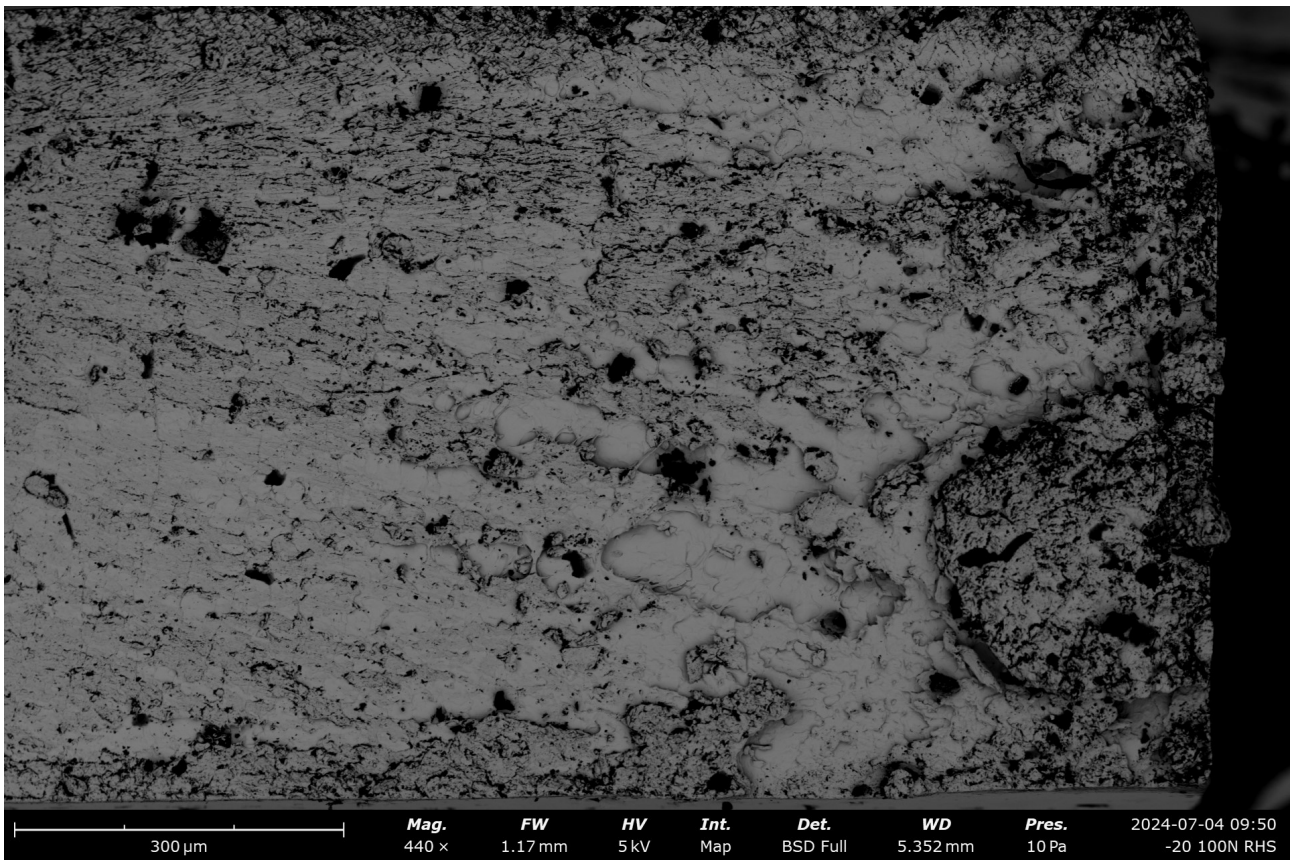

Figure 10.24: SEM image of sample tested at -20 ^{o}C and 100N - RHS

-20 ^{o}C, 80N

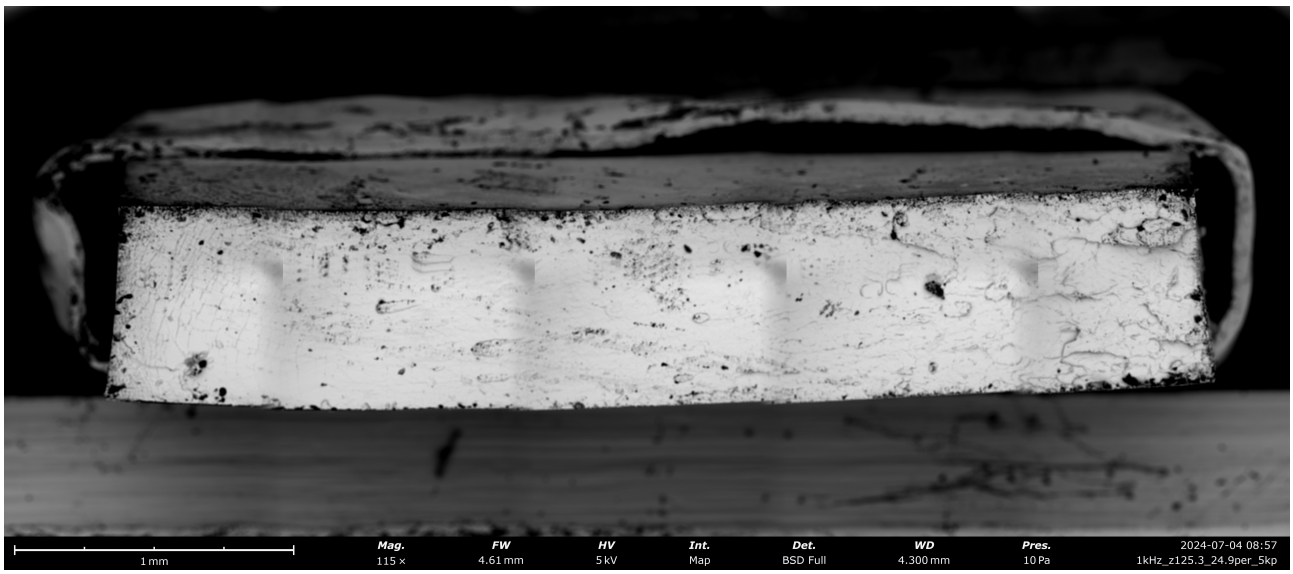

Figure 10.25: SEM image of sample tested at -20 ^{o}C and 80N - Full sample

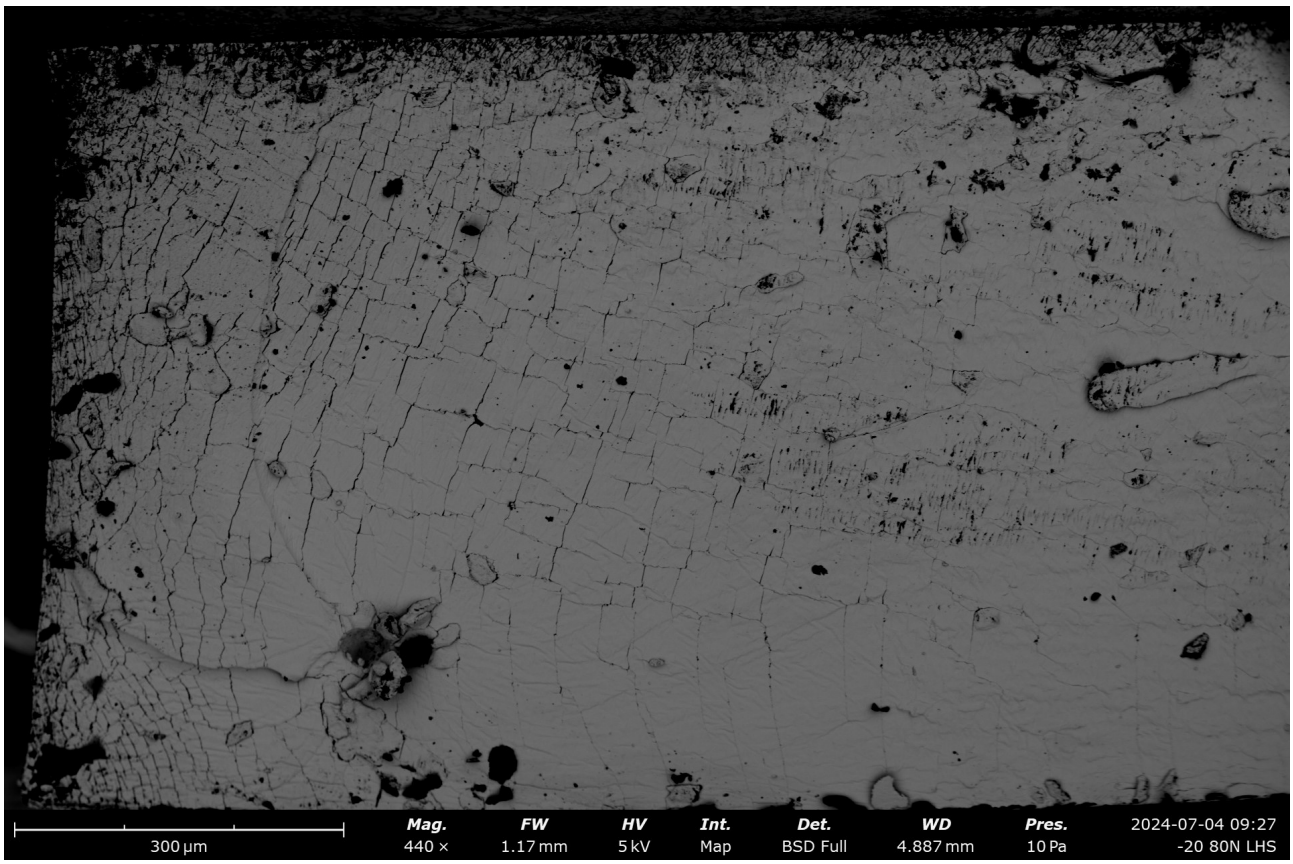

Figure 10.26: SEM image of sample tested at -20 ^{o}C and 80N - LHS

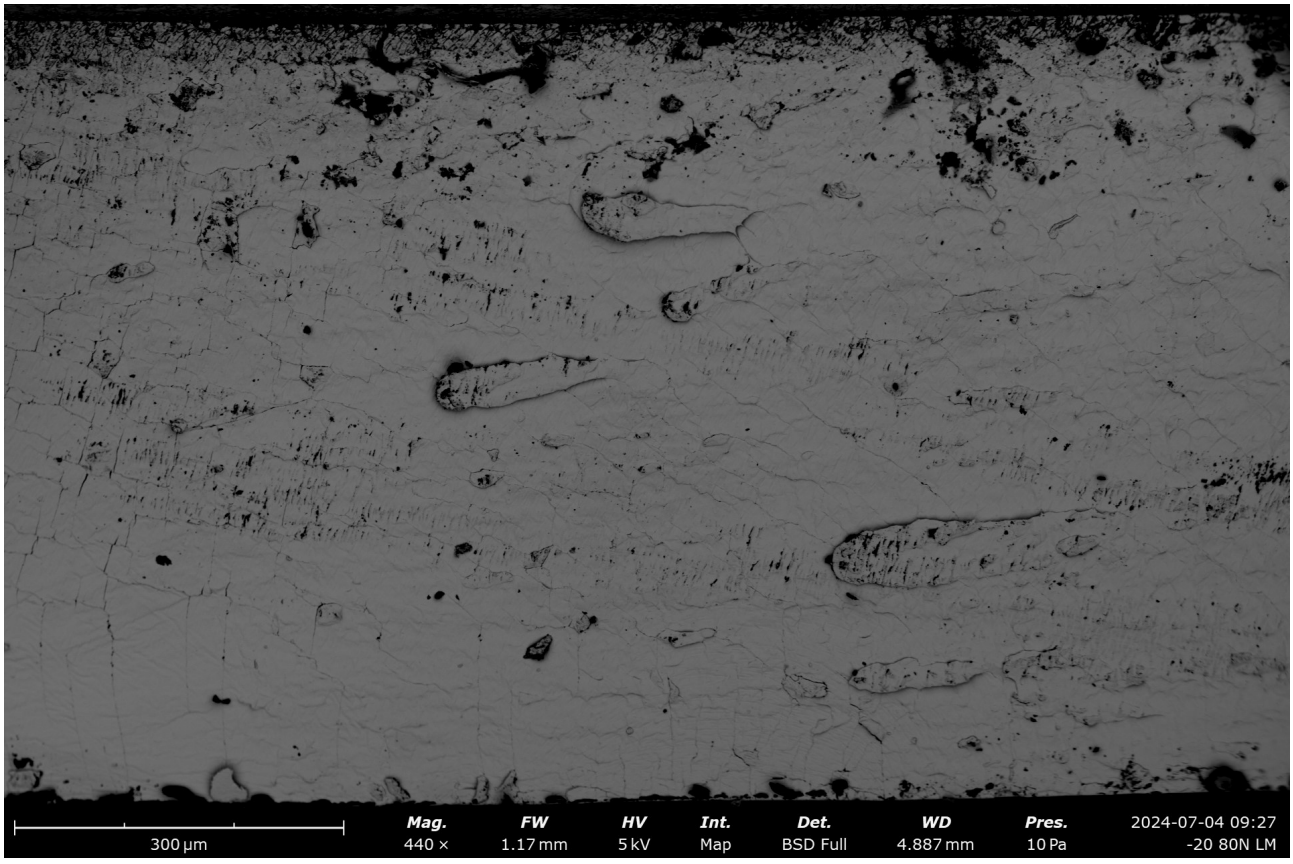

Figure 10.27: SEM image of sample tested at -20 ^{o}C and 80N - LM

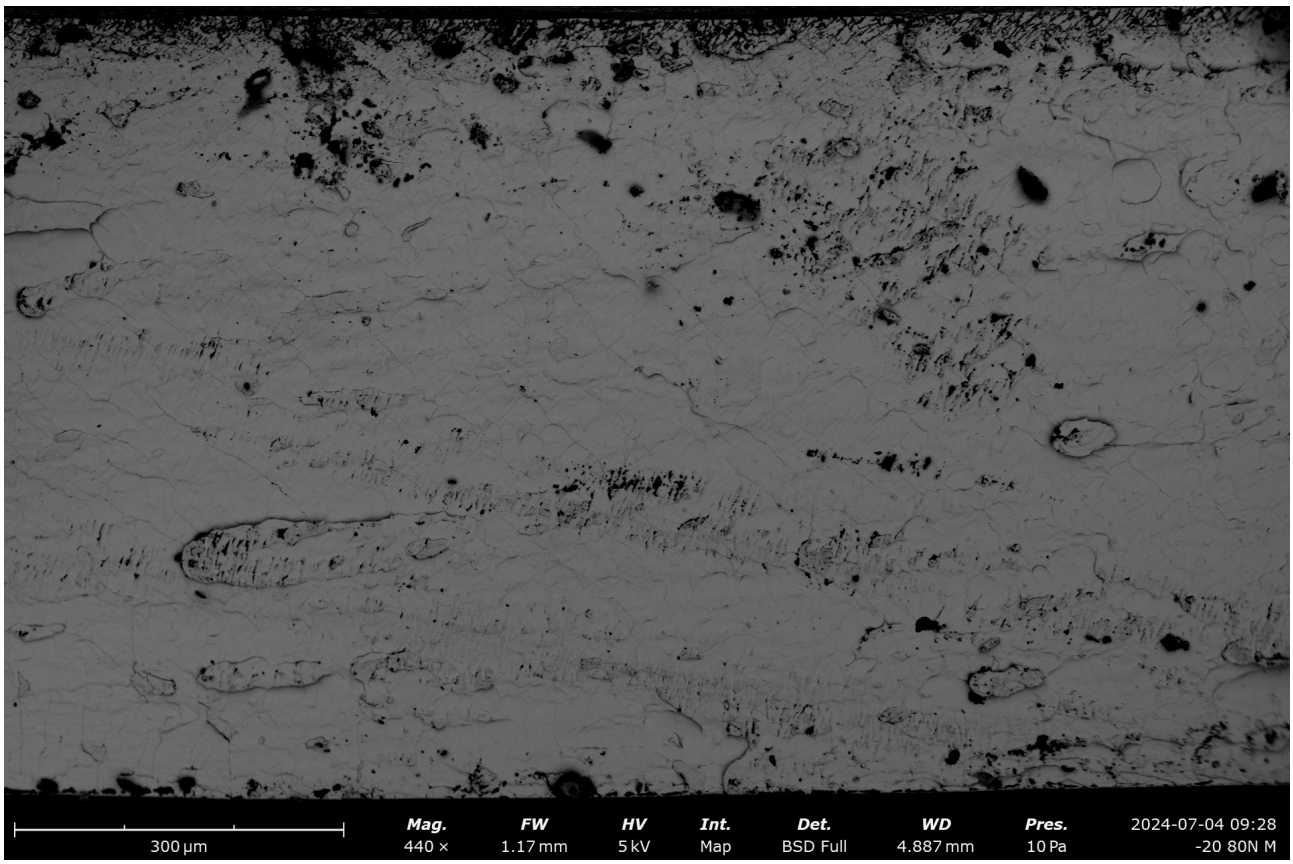

Figure 10.28: SEM image of sample tested at -20 ^{o}C and 80N - M

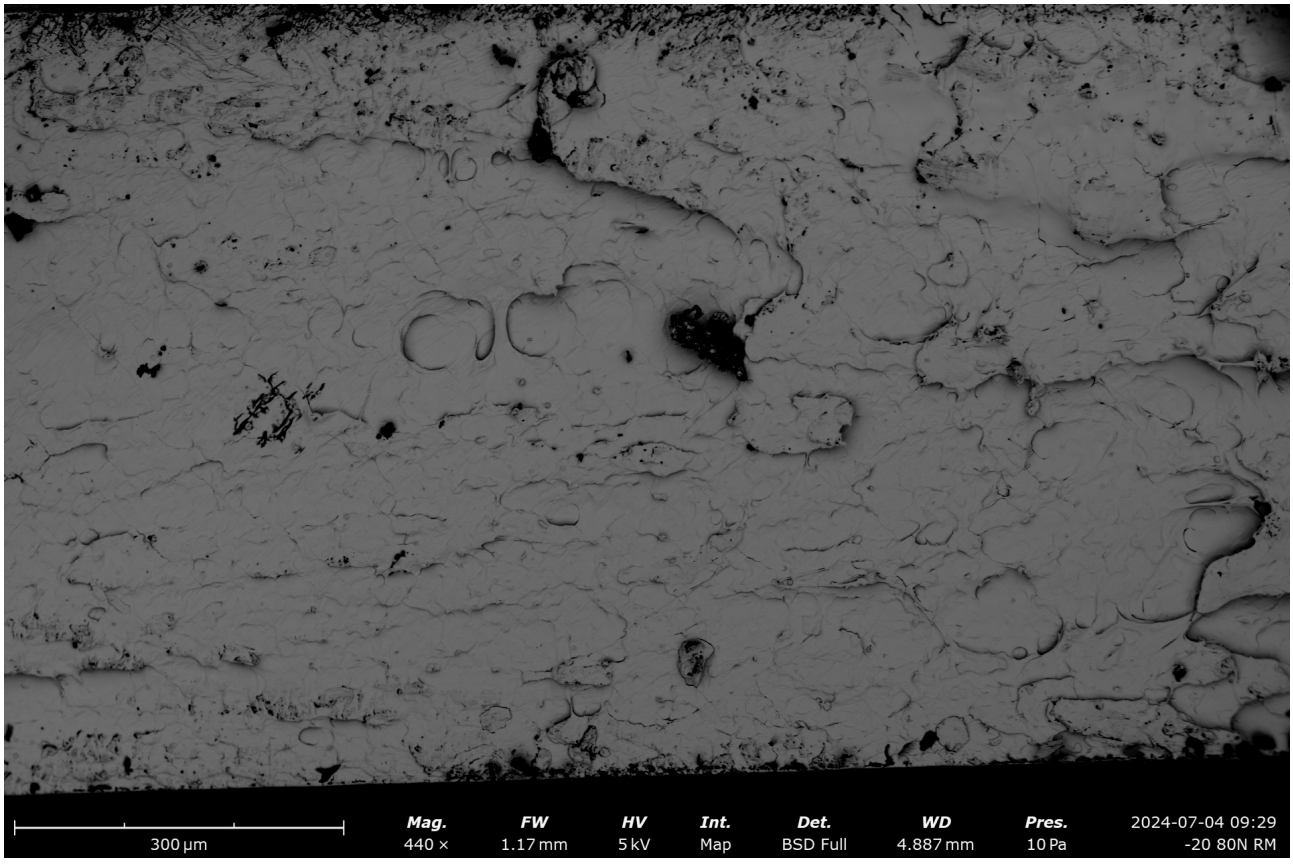

Figure 10.29: SEM image of sample tested at -20 ^{o}C and 80N - RM

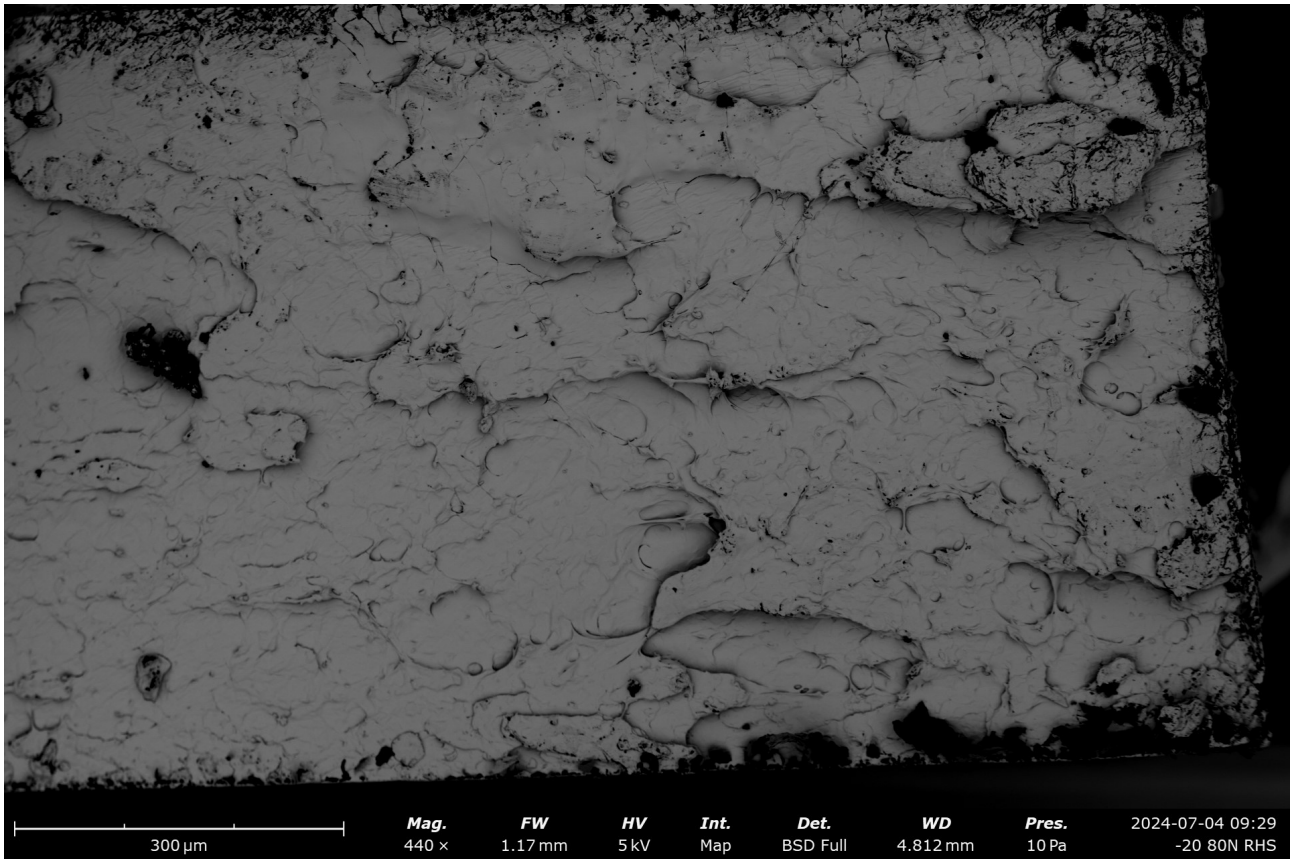

Figure 10.30: SEM image of sample tested at -20 ^{o}C and 80N - RHS

PAPER NAME

High_Strain_Rate_Characterization_of_Polymeric_Material_Properties_by_Low_Temperature_Testing_6-9.pd

AUTHOR

Mats Olde Dubbelink

WORD COUNT

31247 Words

CHARACTER COUNT

161366 Characters

PAGE COUNT

84 Pages

FILE SIZE

31.2MB

SUBMISSION DATE

Sep 6, 2024 10:27 AM GMT+2

REPORT DATE

Sep 6, 2024 10:29 AM GMT+2

14% Overall Similarity

The combined total of all matches, including overlapping sources, for each database.

- 11% Internet database
- 10% Publications database
- Crossref database
- Crossref Posted Content database
- 1% Submitted Works database

Excluded from Similarity Report

- Bibliographic material
- Quoted material
- Cited material
- Small Matches (Less then 8 words)